National Technical University of Athens

Laboratory of Steam Boilers and Thermal Plants (LSBTP)

Director: Emmanuel Kakaras

Diploma Thesis in Mechanical Engineering

Name: Loukianos Korovesis

Student ID : 02102026

Supervising Professor: Emmanuel Kakaras

Date : 01/10/2008

"Parametric analysis of the hydrodynamics of a Dual Fluidized Bed system for post-combustion capture of CO2 through a scaled cold model"

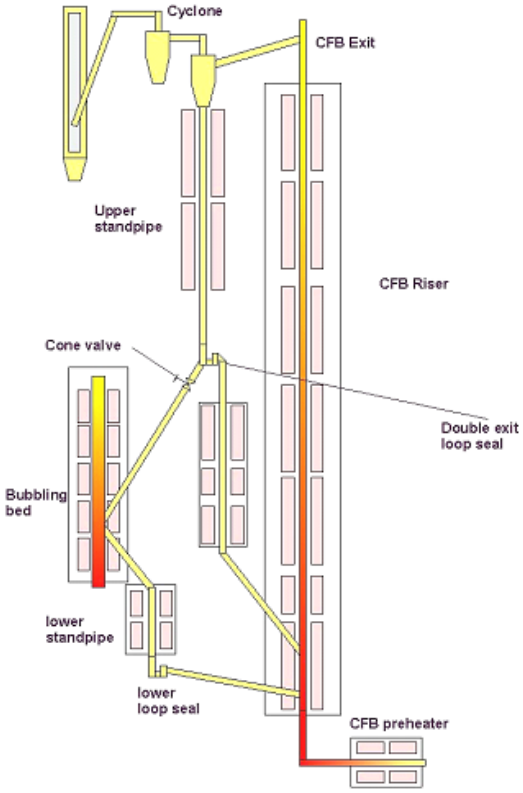

Prologue

With the present thesis entitled "**Parametric analysis of the hydrodynamics of a Dual Fluidized Bed system for post-combustion capture of CO2 through a scaled cold model**", I proudly complete my studies in the National Technical University of Athens (N.T.U.A.) and graduate as a mechanical engineer.

With this prologue I would like to thank Mr. Emmanouil Kakaras, for supervising me in account of N.T.U.A. and Mr. Alexander Charitos and Prof. Dr. techn. G. Scheffknecht for doing so in account of I.V.D. (Institute of Process Engineering and Power Plant Technology) in Stuttgart Germany, as part of the Erasmus exchange program.

In addition I would like to thank Mr. Ajay Bidwe, Mr. Craig Hawthorne and Mr. Senthoorselvan Silva for their help, supervision and support and everyone in I.V.D. for hosting me during all this time I was completing my thesis.

This work is dedicated to my family.

"I don't want to achieve immortality through my work. I want to achieve immortality through not dying."

Woody Allen

Loukianos Korovesis
Athens, Greece
26 – 09 – 2008

Diplomarbeit/ Master Thesis

Parametric analysis of the hydrodynamics of a Dual Fluidized Bed System (DFB) for the post combustion capture of CO2 through a cold model.

Motivation: CO_2 capture is a big problem of our times, which has to be tackled from science and industry. A lot of methods to separate CO_2 from flue gases coming from combustion are being explored. This technology has the benefit that it utilises equipment (fluidised beds) that are well established in power production (450 MWe fluidised bed combustor under construction) and other chemical processes. Furthermore, CaO is one of the most cheap and widely distributed material in the world. This two unmatched advantages make this technology very promising and this is why there are currently in Europe and world wide a lot of effort to make the process commercial

Process description: Power plant combustion flue gases (15% CO_2 by volume) enter the carbonator at 650 °C. The carbonator is a circulating fluidised bed. There CaO will react with CO_2 to form $CaCO_3$. The $CaCO_3$ will be circulated to a bubbling fluidised bed reactor. There CaO will be regenerated producing a pure CO_2 stream. The CaO than will be transported back to the carbonator for further CO_2 capture.

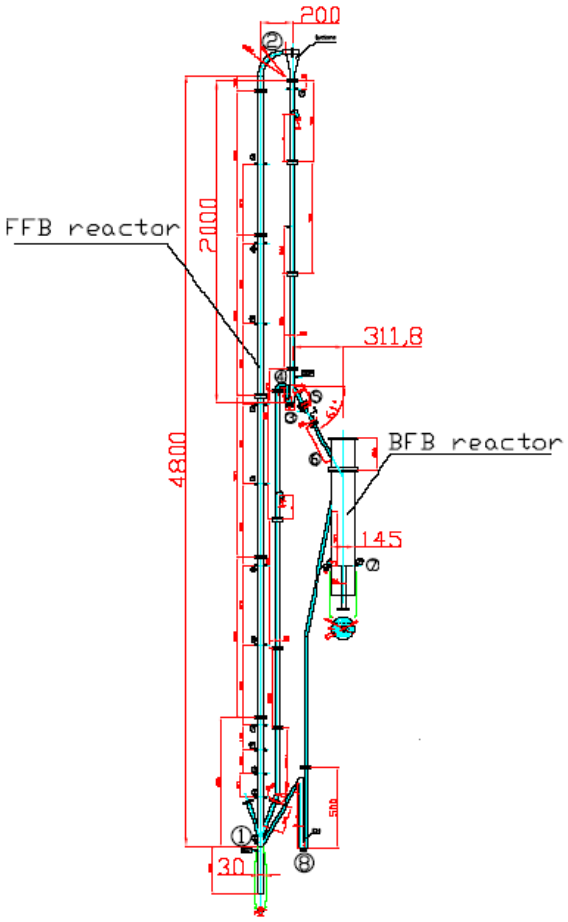

Goal of this thesis:

- To continue the work done in IVD for predicting the real operation of the coupled fluidised bed facility through the cold model . This can be done by running the cold model at conditions defined by scaling laws. If these scaling laws are met than one can extrapolate hydrodynamic results from the cold model that are valid for the hot facility. The effect on hydrodynamic parameters influencing efficiency of all the operational variables an operator can change (particle size, velocity, loop seal aeration etc.) must be defined.
- To provide operating experience from the cold model operation and suggest changes that will lead to smoother operation of the system and serve process objectives. Such improvements must be implemented and tested
- To provide a formula which will predict the solid flow through conical valve.

IVD research on this topic: IVD is coordinating a European project which has as a goal to prove the feasibility of this technology and is currently building a pilot scale facility to realise this process

Abstract

Carbonate looping is a post combustion route for power generation with CO_2 capture. The technology comprises of a Dual Fluidized Bed (DFB) system with continuous sorbent looping between the two beds. The sorbent utilized is CaO. The system consists of a CFB carbonator operating at temperatures of 600- 700 °C and a regenerator operating at temperatures above 900 °C. At IVD, University of Stuttgart, a 15 KW Dual Fluidized bed system has been designed and is in the first stages of operation. A major novelty of this facility is the use of a cone valve to control the sorbent looping rate between the beds. This study presents the results of tests conducted at a scaled cold model of this facility. The suitability of the pilot plant for the carbonate looping process is proved in terms of meeting the process boundary conditions, namely solid looping rate and carbonator inventory. This is done under hydrodynamically scaled conditions at the cold model. Furthermore the effect of all operating variables, namely the Total Solid Inventory (TSI), carbonator superficial velocity, loop seal aeration, regenerator pressure, cone valve opening and particle size on parameters affecting the CO_2 capture efficiency of the CFB carbonator is discussed. Moreover, design decisions regarding the plant geometry are analyzed and possible design improvements are suggested. Cold model operation aside proving a valuable design tool also provided valuable expertise in handling and operating the 15KW DFB pilot facility.

Character Index

NAME	EXPLANATION	VALUE
AER	Absorption Enhanced Reforming	
BFB	Bubbling Fluidized Bed	
CFB	Circulating Fluidized Bed	
CLC	Chemical Looping Combustion	
DFB	Dual Fluidized Bed	
DIVA	Dual zIrkulierende versuchsAnlage	
ELWIRA	Elektrische WIRbelschicht Anlage	
FB	Fluidized Bed	
FICFB	Fast Internally Circulating Fluidized Bed	
LEGS	Lime Enhansed Gasification of Solids	
LSD	Loop Seal Down	
LSU	Loops Seal Up	
TSI	Total Solid Inventory	
Δp	Pressure drop	[mbar]
Δu	Velocity	[m/s]
ε	Voidage	
ρ	Density	[Kg/ m^3]
Φs		
A	Surface	[mm^2]
Ar	Archimedes Number	
D	Diameter	[mm]
dp	Particle Size	[μm]
F	Opening of cone valve times the cone valve opening	[m^2Pa]
F_{CO2}	Moles of CO2 entering the carbonator with flue gas	[moles/sec]
Fo	Molar flow of fresh sorbent entering the system	[moles/sec]
g	Earth's gravity	[m/s^2]
Gs	Riser Entrainment	[Kg/ m^2s]
h	Height	[mm]
L	Length	[mm]
P	Pressure	[mbar]
Re	Reynolds Number	
U	Superficial velocity	[m/s]
W	Weight	[Kg]

Contents

1. Introduction

It is common knowledge that CO_2 emissions result in deteriorating the "green-house" effect, which causes multiple changes in our planet, with the most significant one being the rise of the mean temperature throughout the world. Therefore, the science nowadays seeks for more environmental friendly solutions in controlling the emissions of CO_2 that are created from industrial activities. The main concern of these solutions is to separate these emissions from the rest of the products of the combustions in use, so as to produce flu gases free from CO_2 components.

In this field, the technology of fluidized beds was introduced. This technology has the benefit that it utilises equipment (fluidised beds) that are well established in power production (450 MWe fluidised bed combustor under construction) and other chemical processes. In order to separate CO_2 from the rest of the components of the post-combustion gases, CaO (which is both cheap and widely distributed) is used as a "CO_2 carrier" between a carbonator (circulating fluidized bed) and a regenerator (bubbling fluidized bed). In the carbonator the incoming stream of 15% CO_2 by volume gases enter, the CO_2 reacts with CaO to form $CaCO_3$. Then the $CaCO_3$ will enter the regenerator and the exact opposite chemical reaction will take place, so as to generate a pure CO_2 stream. The CaO then will be transported back to the initial carbonator, so as to close the cycle and initiate once again the CO_2 capture.

In order to study the real operation of a dual fluidized bed facility, a cold model was designed by I.V.D., at conditions defined by scaling laws. By running this cold model through meeting these scaling laws, one can extrapolate hydrodynamic results from the cold model that are valid for the hot facility of 15 kW, currently under construction. Furthermore, there was a vast need of knowledge of parametrical analysis of this model's behaviour, with the parameters being various and pre-defined by the operators. The change of these parameters effect the CO_2 capture efficiency in the CFB carbonator. These parameters are: the particle size, the velocity of the riser, the upper loop seal aeration, the BFB pressure, the Total Solid Inventory (T.S.I.) and the opening of the orifice of the cone valve. Furthermore, the operation on the cold model provided useful results in operating experience, results that were noted to be taken into consideration when running the actual hot facility. During the experimental work, all these parameters where singled out, changed exclusively and the effects in the output parameters of the cold model, and hence its efficiency, where noted.

At this point it should be stated that for the purposes of the present thesis, the know-how, the experimental results and the operating experience of previous work in the field for the account of I.V.D. were needed and therefore used. This previous work had resulted in an operating routine for running the cold model in an appropriate way and thus, this routine was in use in the present work as well. Furthermore, this earlier work resulted in designing an operating window for the facility, for the particle size in use. In order to broaden the spectrum of the particle size, a different particle size was used for the purposes of this thesis and all the results are presented in the following chapters. This work tried to explore the possibility of a design improvement for the cold model in use, and hence a piece was redesigned, replaced another one and the experimental results of this alternation in the installation where measured, noted and analysed in the following chapters, as well.

2. Fundamentals And Description Of Experimental Facilities

2.1 Review on cold models applied for Dual Fluidized Bed processes

CO_2 capture and storage and the utilization of biomass are ways to reduce CO_2 emissions produced by carbonaceous fuels in power generation. Dual Fluidized Bed Systems are used in a number of promising novel energy production technologies. Hence, DFB systems are found in chemical looping processes, gasification processes with or without CO_2 capture and in the carbonate looping process under consideration.

The process scheme for chemical looping combustion (CLC) is shown in fig. 2.1 below. A chemical looping system consists two fluidized beds, namely a fuel reactor and an air reactor. Proof of principle of demonstration of chemical looping combustion has been performed for gaseous [1, 2] and solid fuels [3, 4]. Gaseous fuels CLC combustion provides no significant problems while for solid fuels full conversion has not yet been demonstrated.

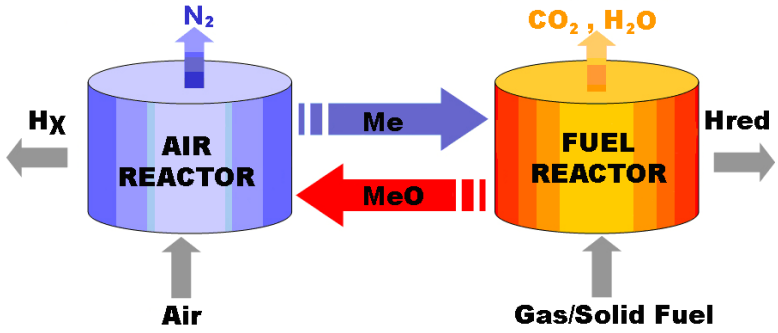

Figure 2.1: Principle of chemical looping combustion

The chemical reactions that are taking place in the fuel and air reactor are shown in eq. 2.1 and 2.2 for a gaseous fuel. Metal oxides are used as oxygen carriers for fuel combustion. Metal oxides are reduced in the fuel reactor and provide the necessary oxygen for fuel combustion producing reduced metal oxide particles and a mixture of CO_2 and water vapor. The water vapor is condensed, leaving pure CO_2 which can be sequestered. Reduced solid metal oxide particles are oxidized again in the air reactor in circular loop. This process can be carried out at atmospheric pressure. A number of metal oxides [5] have been investigated thermodynamically and NiO/Ni, Mn_3O_4/MnO, Fe_2O_3/Fe_3O_4, Cu_2O/Cu were found to be suitable oxygen carriers [5].

$$(2n+m)MeO + C_nH_{2m} \rightarrow (2n+m)Me + mH_2O + nCO_2 \quad \Delta H_{red} \quad \textbf{(2.1)}$$

$$Me + 1/2O_2 \rightarrow MeO \quad \Delta H_{O\chi} \quad \textbf{(2.2)}$$

A number of chemical looping facilities have been designed and operated. The scale of these facilities varies from 300 W [6], to 10 kWth for combustion of gaseous [1. 2] and solid fuels [3. 4]. Most recently a 120 kWth Process Demonstration Unit has been built at the TU Wien [7] for CLC. A number of cold models of CLC combustors have been built and operated in the past years. A detailed cold model study aiming at the study of the fluid dynamics of the above mentioned 120 kWth gaseous fuel CLC combustor has been recently published [8] demonstrating the effect of various parameters on the operation of the facility. Cold model studies have been conducted also for the 300 W reactor mentioned above, for a 60 kWth pressurized CLC combustor and for a 2 MW CLC combustor plant all using syngas as a fuel [9]. These studies aimed in proving that process boundary conditions can be met by proposed designs. Another cold model study [10] has been previously preformed to optimize the design of a 10 kWth CLC gaseous fuel combustor which resulted in the optimization of reactor geometry

in respect to solid circulation rate, gas leakage, bed mass and solid residence time. The potential problem of gas leakage between reactors, which has been demonstrated to be rather low in CLC combustors, has been also investigated in a 30 kWth cold model [11]. Some studies have been also performed in the field of chemical looping reforming processes (CLR) [5].

Gasification processes, which are CO_2 lean, are also carried out in DFB systems. The gasifier fuel is coal or biomass. Gasification takes place with use of steam. The gasifier is normally a Bubbling Fluidized Bed (BFB). The heat to sustain the endothermic gasification reactions is provided by the combustion of char in a second FB. the combustor. This reactor is normally a CFB. In the case of biomass gasification no CO_2 stream ready for storage is produced. This happens because biomass is a rather decentralized fuel and because biomass is CO_2 neutral. In the case of coal, which is a centralized fuel, a production of a CO_2 stream for storage is necessary so as for the process to contribute to the mitigation of CO_2 emissions. In the case of biomass the bed material is olivine or limestone. When using olivine as a bed than this type of gasification represents the FICFB (Fast Internally Circulating Fluidized Bed) technology. as found in [12]. A schematic of this process is shown in fig. 2.2.

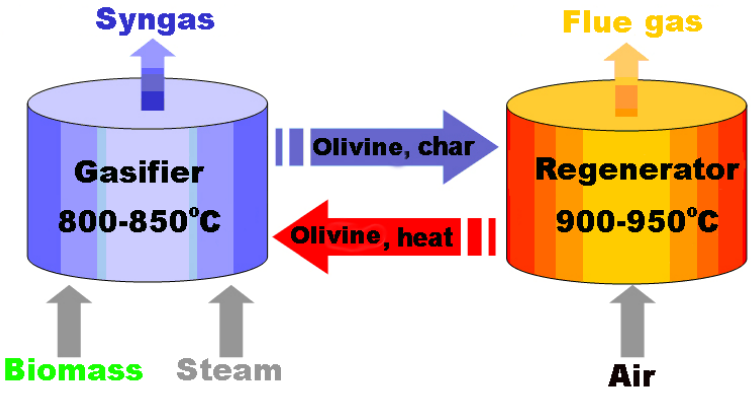

Figure 2.2: Schematic of Fast Internally Circulating Fluidized Bed (FICFB)

Gasification of biomass in a DFB system using olivine is demonstrated at the 8MW facility of CHP Guessing and has been a research topic for the last decades. Biomass gasification experiments with limestone as a bed have been presented in a 100KWth DFB facility [13]. These experiments have been performed in preparation for large scale experiments to be conducted in CHP Guessing. CaO reacts with CO_2 in the gasifier at 600- 700 °C. The absorption of CO_2 results in the shift of the overall gasification reaction towards H_2 rich gas production, through eq. 2.3-2.5. Due to this characteristic gasification of biomass with use of lime as bed material is called **AER (Absorption Enhanced Reforming)** process [14]. [41]. A schematic of the AER process is shown in fig. 2.3.

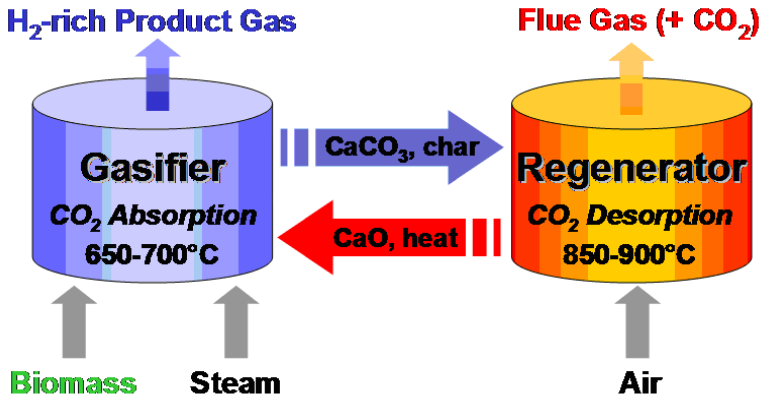

Figure 2.3: Schematic of Absorption Enhanced Reforming

The CFB combustor has two roles in the AER process [41]: first is to provide the heat for the endothermic gasification and second is to regenerate the $CaCO_3$ by the reverse reaction of eq. 2.5. Since producing a pure CO_2 stream is not an issue for the AER process the combustor is fluidized with air. H_2 rich gas production can be achieved through the same route for coal gasification and a lime/ limestone bed. This process is feasible at pressurized conditions. This process is called **LEGS (Lime Enhanced Gasification of Solids)** and work performed is well described in [15]. A schematic of the LEGS process is shown in fig. 2.4.

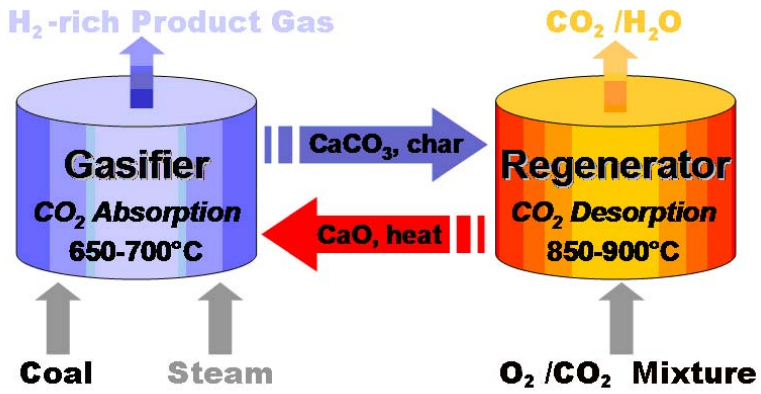

Figure 2.4: Schematic of LEGS (Lime Enhanced Gasification of Solids)

Since CO_2 capture and storage is an interest for the LEGS process the combustor/ regenerator CFB would bed fluidized with an O_2 and CO_2 mixture. The CO_2 would be provided through recirculation of the flue gas of the CFB combustor. Cold model studies have played a major role in the development of the FICFB gasification process. Cold flow models have been used so as to develop suitable and secure designs for 10 kWth, 100 kWth pilot plants and for the scale up to the 8 MWth CHP Guessing plant as shown in [12. 16]. Moreover, cold model prediction proved to be sufficiently accurate when compared to real plant data [12]. Regarding the same plant also recent cold model studies have been published [17. 18]. Above studies aimed in determining the effect of different operational and geometrical parameters at examining the control of the circulation rate between the two beds. the residence times of olivine and biomass particles in the different bed compartments and gas leakage. Cold model testing on the same apparatus has been used so to validate models describing the CFB combustor hydrodynamics [19], the solid circulation rate and the pressure loop of the DFB plant [20].

$$C_mH_nO_o + (m-n)H_2O \rightarrow mCO + (m+\frac{n}{2}-o)H_2 \quad \textbf{(2.3)}$$

$$mCO + mH_2O \rightarrow mCO_2 + mH_2 \quad \textbf{(2.4)}$$

$$CaO + CO_2 \rightarrow CaCO_3 \quad \textbf{(2.5)}$$

Equation 2.3 is called steam reforming reaction, eq. 2.4 is called water shift reaction, eq. 2.5 is called carbonation reaction and the reverse equation of eq. 2.5 is called calcination reaction [27]. Cold model testing has also applied in another process for biomass utilization, namely biomass pyrolysis [21, 22]. Novel process left aside cold model testing has also been applied to BFB and CFB combustors. Recently, it was used for determining spots that are particularly vulnerable to erosion due to collision of particles in a CFB combustor [23] and solid backflow issues in the distributor nozzles of a 235 MWe combustor [24]. Finally cold model, studies are used very frequently used so as to study the more basic aspects of fluidization science, such as the study demarcation of new hydrodynamic regimes [25, 26].

2.2 Carbonate looping

Carbonate looping is a post combustion route for power generation with CO_2 capture. It is an economically feasible and advantageous technology when compared to alternatives as shown in [27,28]. The technology comprises of a Dual Fluidized Bed (DFB) system with continuous sorbent looping between the two beds. The sorbent utilized is CaO. Shimizu was the first to propose this process [29]. The system consists of a CFB carbonator operating at temperatures of 600- 700 °C and a regenerator operating at temperatures above 900 °C. The basic principle of operation is shown in fig. 2.5. CO_2 is absorbed through CaO (eq.2.5). Therefore CO_2 lean flue gas is produced and released to the atmosphere.

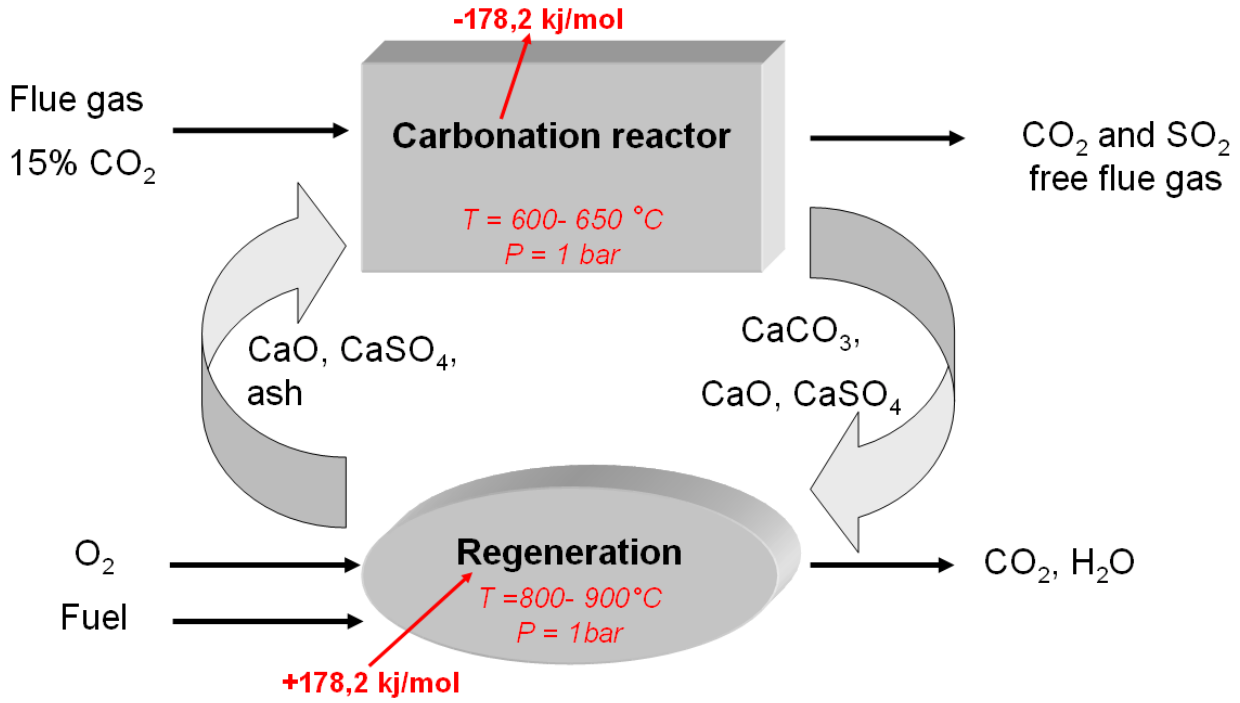

Figure 2.5: Carbonate looping

The partially carbonated sorbent is than transferred to the regenerator where the CO_2 is released from the sorbent particles utilizing the reverse reaction of eq. 2.5. The energy input required to heat the solids to calcination temperatures and to provide energy for the endothermic calcination is provided by the oxy- combustion of a carbonaceous fuel. Thereby, a stream of CO_2 and steam is produced from the regenerator. After condensation of the steam a "pure" CO_2 stream is available for compression and storage. The regenerated sorbent is returned to carbonator for subsequent CO_2 capture thereby closing the solid loop. Due to the deactivation of the sorbent CO2 carrying capacity over multiple full carbonation- calcination cycles [30]. [44]. as shown in fig. 2.6. a make- up flow and purge of limestone is necessary.

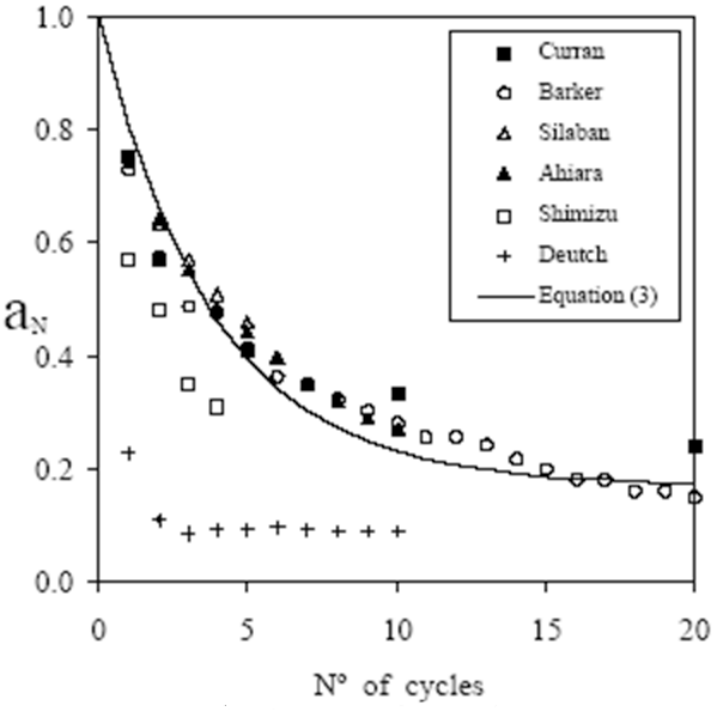

Figure 2.6: Decay CaO-CO_2 carrying capacity

In the last decade a vast number of TGA studies [30. 31] have been performed along with limited batch FB experiments [32]. Pilot scale experimentation is underway and quite a number of facilities in Canada. Spain. France and Germany have commenced operation. Until now promising results have been published from the pilot facility in Canada which utilizes a moving bed carbonator and a CFB regenerator [33]. In all other countries initial experimental campaigns are ongoing. At I.V.D. a 15 kW Dual Fluidized Bed (DFB) carbonate looping facility has been built utilizing a 12.4 m high. 7 cm diameter CFB carbonator riser and a 11.4 cm diameter BFB regenerator. Major novelty of this rig in comparison to most existing DFB systems is the control of the solid looping rate between carbonator and regenerator with use of a cone valve.

The definition of process boundary conditions, namely the solid looping rate, fresh sorbent make-up flow, carbonator inventory, riser velocity and carbonator temperature was essential for designing the pilot DFB system and is listed in Table 2.1. A detailed analysis of the CFB carbonator model leading to the calculation of theses figures can be found in [34]. This model was based on the one hand on existing sorbent kinetic information [31, 35], system particle population balances [36] and on the other hand on existing hydrodynamic models describing the different regions of a CFB riser [37, 38]. This study aims to prove that the design concept of the 15 kW DFB pilot plant is suitable for the carbonate looping process in terms of meeting process boundary conditions. This is done through cold model experimentation under hydrodynamically scaled conditions. Preliminary results of cold model experimentation for this pilot plant can be found in [39]. Investigations are conducted in terms of defining hydrodynamically stable operating conditions that would lead to high CO_2 capture efficiencies. Moreover, operating parameters are defined and their effect on the overall operation of the DFB system is investigated in a parametric manor. In addition issues regarding the CFB carbonator

geometry and the geometry of the solid circulation system are discussed with implication to the overall DFB reactor performance. Finally possible design improvements are proposed.

Table 2.1 Boundary conditions for 15 kW DFB pilot plant

Carbonator riser velocity (m/s)	4-6
Sorbent looping rate (F_R/F_{CO2}= 2-8) (kg/h)	20- 80
Sorbent make up flow(F_o/F_{CO2}= 0.01-0.05) (kg/h)	0.15- 0.70
Carbonator pressure drop (mbar)	70- 130
Carbonator Temperature °C	600- 700

Where F_R is the moles of sorbent circulating between the two beds, $F_{CO2\ is}$ the incoming moles of CO_2 entering the carbonator with the flue gas and F_o is the molar flow of fresh sorbent entering the system.

2.3 Description of the 15 kW carbonate looping facility at IVD

The synthetic flue gas consisting of 15% CO_2 is preheated to a desired temperature before entering the windbox at the bottom of the CFB. In continuance gas enters the CFB and fluidizes a mixture of CaO and $CaCO_3$ (mainly CaO).

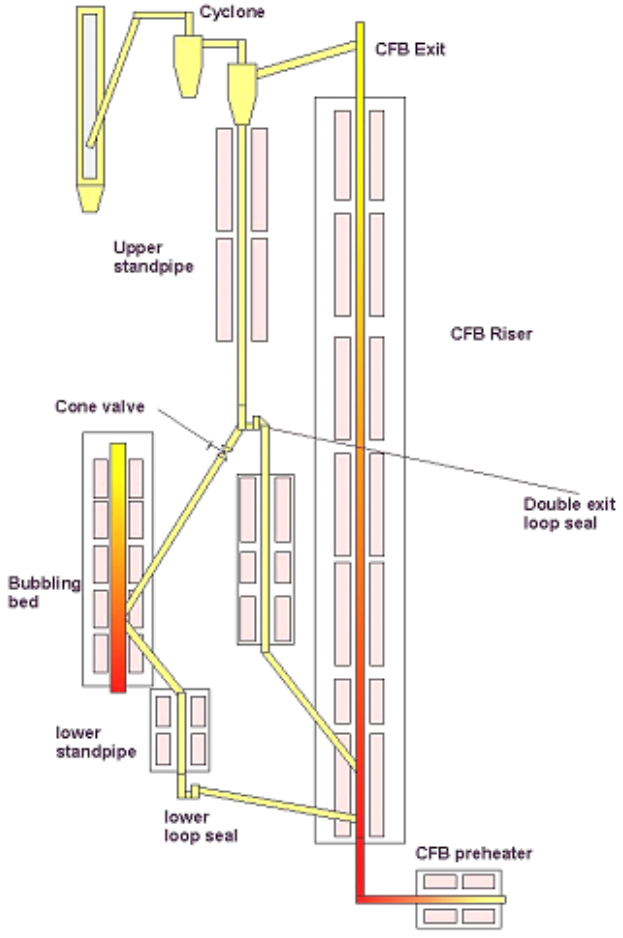

Figure 2.7: Schematic of the 15 kW DFB carbonate looping facility (DIVA- ELWIRA) at IVD

CO_2 reacts quickly with CaO to form $CaCO_3$. The CO_2 lean gases. $CaCO_3$ and unreacted CaO then leave the reactor through the riser exit and the solids are separated from the gas in the cyclone. The gas is further filtered through a second cyclone and a candle filter and released to the atmosphere. Solids from the cyclone fall into the loop seal standpipe. The loop seal consists of two exits: one back to the riser and the other towards the bubbling bed controlled by a cone valve. This phenomenon is called 'Split' and will be referenced as such in the future. The split is controlled so as for 20 to 50 % of the solids to proceed to the BFB and the remaining 50 to 80 % to return to the riser. The split is controlled by changing the cone valve opening and the pressure in BFB. Solids which now enter BFB undergo temperature rise up to 900 °C and the reaction of eq. 2.5 is reversed. The heat required is supplied from the heaters and by natural gas combustion in the bubbling bed.

$CaCO_3$ is calcined into CaO and CO_2 leaves the facility through BFB top. This CO_2 stream would be highly concentrated, if steam was to be condensed. (>90% CO_2) and would be ready for storage. Regenerated CaO overflows to a second loop seal. This loop seal is also fluidized so as to transfer regenerated CaO back to riser, thus completing the loop. To design and learn to operate this plant a scaled cold model has been considered a necessity.

The CFB riser has been named as DIVA (Dual zIrkulierende VersuchsAnlage) and the BFB calciner has been named as ELWIRA (ELektrische WIRbelschicht Anlage).

2.4 Cold model of the 15 kW Dual Fluidized Bed carbonate looping facility at IVD

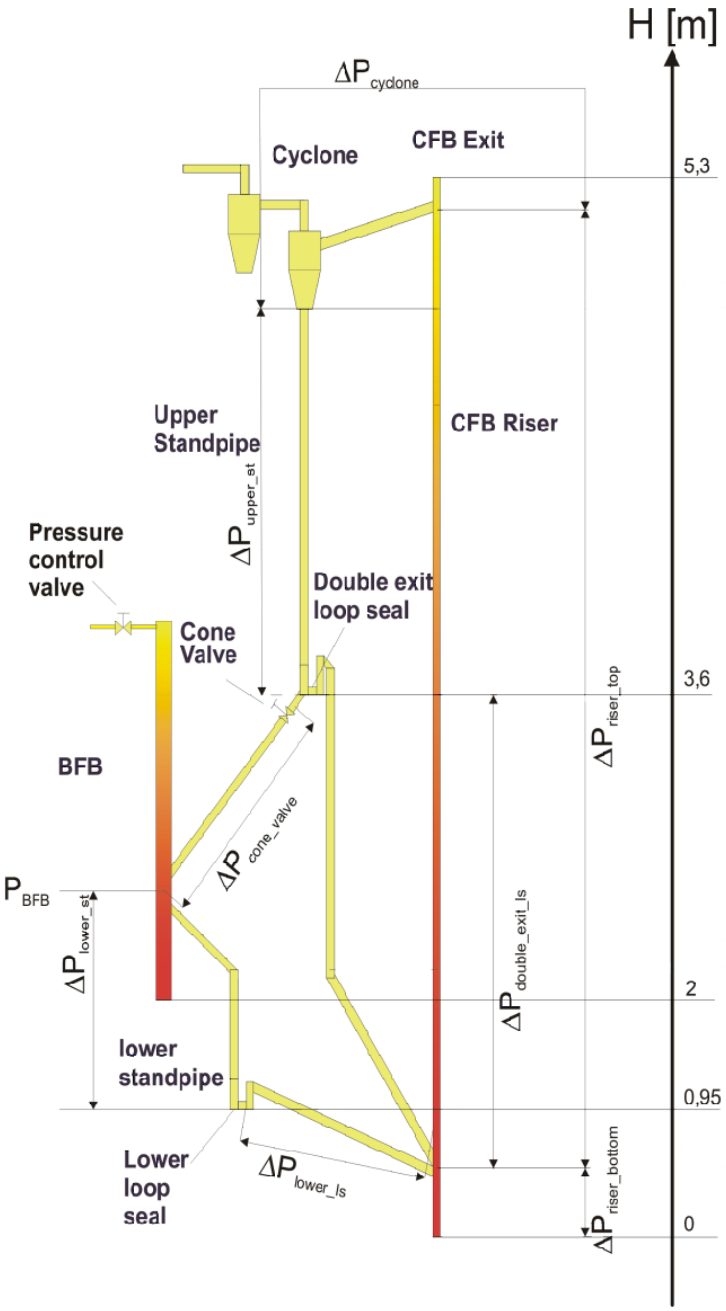

Figure 2. 8: Cold model of the 15 kW DFB carbonate looping facility (DIVA- ELWIRA) at IVD

The cold model is built in the same scheme as the pilot plant. Of course there is no occurrence of reactions and no heating zones.The cold model is 2.33 times downscaled and operates with ambient air at atmospheric pressure. Solids are chosen as per scaling laws [49-54]. Figure 2.8 shows the schematic of cold model. The height. Diameters and other geometric aspects are scaled down by the ratio of 2.33. The whole cold model facility is made of plexi-glass. The cold model is a tool to study the hydrodynamics of the pilot plant. The relevancy of the cold model hydrodynamics [42].[43] to the pilot plant hydrodynamics is ensured from the use of appropriate scaling laws [46]. The most useful theoretical tool used to determine the effect of various operating parameters on the DFB hydrodynamic behavior is the pressure balance which is also analyzed below.

2.5 Fluidized bed scaling

2.5.1 Introduction

Scaling has been used extensively in solving fluid mechanics and heat transfer problems and has been applied to general chemical engineering applications. Scaling implies the construction of a geometrically similar model or component to be tested. Obtained values can be extrapolated to the real component. Scaling is particularly useful if it is difficult or expensive to carry out experimentation on a real prototype. For example dynamic modelling of flow over an airplane is performed using a scaled model in a wind tunnel [24] [28].As long as the certain dimensionless parameters are matched such as the Reynolds number, mach number etc. the performance of the scaled model and modelled component or prototype will be same if expressed in proper dimensionless form such as the drag coefficient. In general scaling has helps to increase understanding about fluidized beds. Scaling also helps in predicting and tackling operational problems in large and small facilities [12]. Furthermore, scaling promotes understanding at smaller scale and can help to improve large scale design [12].

2.5.2 Scaling in fluidized bed

Scaling [49-54] is quite a known tool in the field of fluidized beds but is not as familiar as in fluid mechanics problems such as pipe flows, impellers, heat exchangers etc. According to Matsen [29] success in scaling of a fluidised bed lies not in increasing exactitude of calculations but rather in the recognition and management of uncertainties. Inexact scaling may affect overall performance, especially the anticipated reaction kinetics. Therefore following scaling laws are very important. Fair amount of literature is available on scaling. Most widely used is the work done by L.R. Glicksman. He developed a set of scaling laws in a series of publications [49-54] and this series contains the systematic derivation of laws, experimental validation and further simplification of laws for more easy use. The laws of Glicksman are also verified by other authors like Chang and Louge et al. [54].

2.5.3 Scaling laws

On the basis of governing equations of conservation of mass and motion of fluid and particle phase, Glicksman derived a set of non-dimensional parameters to be matched in order to obtain similarity between cold model and the actual “hot” fluidized bed. Glickmann’s full set of scaling equations are as follows [30]:

$$\left(\frac{\beta L}{\rho_s U_0}, \frac{gL}{U_0^2}, \frac{L_1}{L_2}, \frac{\rho_f}{\rho_s}, \frac{P}{\rho_s U_0^2} \right) \qquad \textbf{(2.6)}$$

Glicksman further simplified the above laws so as to make their application in cold model experimentation easier. The simplified scaling laws are presented below [31]:

$$\left(\frac{U_0^2}{gL}, \frac{\rho_f}{\rho_s}, \frac{U_0}{U_{mf}}, \frac{L_1}{L_2},, \frac{Gs}{\rho_s U_o}, \phi, Particle\_size\_distribution(PSD) \right) \qquad \textbf{(2.7)}$$

In this work it is very important to compare the axial mass distributions between the cold model riser and the actual carbonator riser. Therefore, the term $\frac{p}{\rho_s gD}$ from Chang. Louge et al [34] has been added. Hence, the complete set of scaling laws is:

$$\left(\frac{U_0^2}{gL}, \frac{\rho_f}{\rho_s}, \frac{U_0}{U_{mf}}, \frac{L_1}{L_2}, \frac{Gs}{\rho_s U_o}, \frac{p}{\rho_s gD}, \phi, Particle\_size\_distribution(PSD)\right) \quad \textbf{(2.8)}$$

2.5.4 Application of the scaling laws at the 15 kW Dual Fluidized Bed carbonate looping cold model

- *General methodology*

Using the scaling laws described in eq. 2.6 – 2.8 it is possible to arbitrarily choose the values of two measures. As a result, the value of every other measure is automatically set. In this case the geometrical ratio and the cold model gas (ambient air) were chosen. Since flue gas and calcium oxide particles are used in the actual riser carbonator and ambient air is used in the cold model for simplicity, it was important to match the **Error! Bookmark not defined.** $\frac{\rho_f}{\rho_s}$ ratio by using a solid with appropriate solid density. The particle diameter of the cold model was determined so as to match $\frac{U_0}{U_{mf}}$ ratio. $\frac{L_1}{L_2}$ ratio is matched in every geometrical aspect between the two beds, i.e. Length, diameter etc of the bed. The above method is also described by Kehlenbeck [55].

In the following table geometrical measures and operating conditions of the 15 kW DFB carbonate looping facility (DIVA- ELWIRA) are presented:

Table 2. 2 -Details of hot pilot plant facility DIVA- ELWIRA

Geometry		
DIVA CFB diameter	70.3	mm
DIVA CFB length	12.463	m
ELWIRA BFB diameter	114	mm
Operational conditions		
DIVA CFB temperature	650	° C
ELWIRA BFB temperature	900	° C
Pressure	Atmospheric	
Gas properties (DIVA)		
Gas	Flue gases 15 %vol. CO2	
Gas density	0.369	kg/m^3
Gas viscosity	3.9 E-5	PaS
Gas velocity	3-6	m/s
Particle properties		
Particles	Calcium oxide	
Density	1800	kg/m3
Size	419 μm & 687 μm	μm

- *Geometric similarity*

Since geometrical similarity is met:

$$\left(\frac{L_1}{L_2}\right)_{hot} = \left(\frac{L_1}{L_2}\right)_{cold} \quad \textbf{(2.9)}$$

The main geometric considerations are length and diameter, therefore:

$$\left(\frac{D}{L}\right)_{hot} = \left(\frac{D}{L}\right)_{cold} \quad \therefore \left(\frac{D_{hot}}{D_{cold}}\right) = \left(\frac{L_{hot}}{L_{cold}}\right)_{cold} \quad \textbf{(2.10)}$$

A 30 mm Plexiglas riser on which previous cold model experimentation [58] has been performed was used [56]. Since D_{cold} is 30mm and since D_{hot} is 70.3mm this yields a geometric ratio of '2.33'. This ratio was matched for all dimensions of the cold model thus the length of cold model riser was chosen as 5326 mm and the diameter of bubbling bed as 49 mm.

- *Determination of particle density*

Since the density ratio has to be met it is concluded that:

$$\left(\frac{\rho_f}{\rho_s}\right)_{hot} = \left(\frac{\rho_f}{\rho_s}\right)_{cold} \quad \textbf{(2.11)}$$

Using data above from table 2.1 the density ratio in the CFB carbonator DIVA is:

$$\frac{\rho_f}{\rho_s} = 2.05\text{x}10^{-4} \quad \textbf{(2.12)}$$

As far as the cold model is concerned, ambient air with a density of 1.188 kg/m^3 is used as found from Perry's handbook [57].Through the density ratio, particle density of $\rho_{s,cold}$ = 5795 kg/m^3 is obtained. This density is very close to the density of zirconium dioxide (5850 kg/m^3) [57]. However the particles purchased were Zirconium dioxide and had density of 5700 kg/m^3 as found in the laboratory experiments.

- *Determination of the cold model riser velocity*

The Fr number is also a scaling ratio. Therefore:

$$\left(\frac{U_o^2}{gL}\right)_{cold} = \left(\frac{U_o^2}{gL}\right)_{hot} \quad \textbf{(2.13)}$$

Consequently

$$\frac{U_{0,hot}}{U_{0,cold}} = \sqrt{\frac{L_{hot}}{L_{cold}}} = 1{,}53 \quad \textbf{(2.14)}$$

Thereby when using a certain superficial velocity in the cold model riser, the hydrodynamic situation of the pilot plant facility is simulated at a velocity that is 1.53 times greater than the velocity of the cold model riser.

- *Determination of the cold model particle size*

This relationship is established from the $\frac{U_0}{U_{mf}}$ ratio. So:

$$\left(\frac{U_o}{U_{mf}}\right)_{hot} = \left(\frac{U_o}{U_{mf}}\right)_{cold} \quad \textbf{(2.15)}$$

The relationship between cold model and pilot plant facility has already been established above by eq.(2.13). The minimum fluidization velocity is a function of particle size and is calculated here with use of the following equation:

$$\mathrm{Re}_{mf} = \frac{d_p u_{mf} \rho_g}{\mu} = (\mathrm{C_1}^2 + \mathrm{C_2 Ar})^{0.5}\ \mathrm{C_1} \quad \textbf{(2.16)}$$

Where:

$$Ar = \frac{\rho_g(\rho_p - \rho_g) g d_p^3}{\mu^2} \quad \textbf{(2.17)}$$

C_1 and C_2 can be taken as 27.2 and 0.0408 respectively.

Using the above methodology the minimum fluidization velocity can be calculated for both systems. With combination of the equations (2.9-2.14) the relationship between the particle size and the pilot plant is established. In the study of Bidwe [40] a mean ZrO_2 particle size of 142 μm was used to simulate a mean lime particle size of 419 μm. In this study a 230μm ZrO_2 particle size was used so as to simulate a mean lime particle size of 687 μm.

- *Extrapolating cold model data to the pilot facility*

The following scaling ratios allows for the extrapolation of cold model results to the pilot facility.

$\frac{Gs}{\rho_s U_o}, \frac{p}{\rho_s g D}$. These ratios obtained allow the extrapolation of the cold model riser entrainment. cone valve discharge and measured pressure drop to pilot plant data. These are:

$$\frac{Gs_{hot}}{Gs_{cold}} = 0.475 \textbf{ where Gs is kg/(time. area)} \quad \textbf{(2.18)}$$

$$\frac{Gs_{hot}}{Gs_{cold}} = 2.61 \textbf{ where Gs is in kg/time} \quad \textbf{(2.19)}$$

$$\frac{\Delta p_{hot}}{\Delta p_{cold}} = 0.726 \quad \textbf{(2.20)}$$

The above data is summarized for cold model as in Table 2.3.

Table 2. 3: Details of cold model

Geometry		
riser diameter	30	mm
riser length	5.32	m
BFB diameter	48	mm
Operational conditions		
BFB temperature	20	°C
ELWIRA temperature	20	°C
Pressure	Atmospheric	
Gas properties cold model		
Gas	Atmsopheric air	
Gas density	1.188	kg/m3
Gas viscosity	1.8 E-5	PaS
Gas velocity	2.3-3.5	m/s
Particle properties		
Particles	Zirconium dioxide	
Density	5700	kg/m3
Size	142 & 230	µm

- *Limitations of scaling*

As mentioned in the literature the scaling laws are only valid as far as the governing set of equations is concerned. Both literature references and the present analysis conclude that the following parameters provide limitations to the application of the scaling laws in the system:

- Influence of intra-particle forces: This factor is not taken into consideration while deriving the laws. In the system there have been some electrostatic phenomena. Electrostatic forces can alter fluid dynamics. [30]
- Particle attrition is not being considered by the scaling laws. It is well known that calcium oxide particles do undergo attrition, while zirconium dioxide particles didn't show so much of attrition.
- The change in solid and gas density due to reaction can not be considered in scaling. This is important because matching the solid to gas density ratio is very important in scaling.

The BFB temperature is 900 ^{o}C and its gas composition is much different than the one of the carbonator. Therefore it can not be considered scaled with the use of same solids in the cold model. Since the focus is mainly on the riser carbonator no other hydrodynamic studies in the BFB have been carried out.

2.6 Pressure balance analysis at the 15 kW Dual Fluidized Bed carbonate looping facility for the Dual Fluidized Bed system

The basic principle behind the pressure balance [47,48] is that for a closed circuit system the algebraic sum of the pressure drop across each section of the circulation loop should be equal to zero [3. 23]. The fluidized bed system used in this case i.e. DIVA- ELWIRA DFB has been explained in detail earlier. The figure 2.8 below is the representation of DIVA- ELWIRA DFB

that will be used for explaining the pressure balance [47,48] in DIVA- ELWIRA DFB and its cold model.

Horio as well as Basu and Cheng [23] have presented the pressure balance of CFB taking the loop seal into consideration [45]. Their work mainly aimed at the performance of the loop seal but it also explains the methodology and many aspects of bed hydrodynamics.

In the system it is very clear that its system is running on two loops:

- The **upper loop** consisting of the following: the cyclone, the upper standpipe, the upper loop seal loop and the riser loop **(d-f-g-b-c-d)**.
- The **lower loop** consisting of the following: the atmosphere, the cyclone, the riser, the lower loop seal, the lower standpipe, the BFB freeboard and the atmosphere loop **(atmosphere-d-c-b-h-i-j-k- atmosphere)**.

The pressure balance will be explained with the use of the Fig 2.8

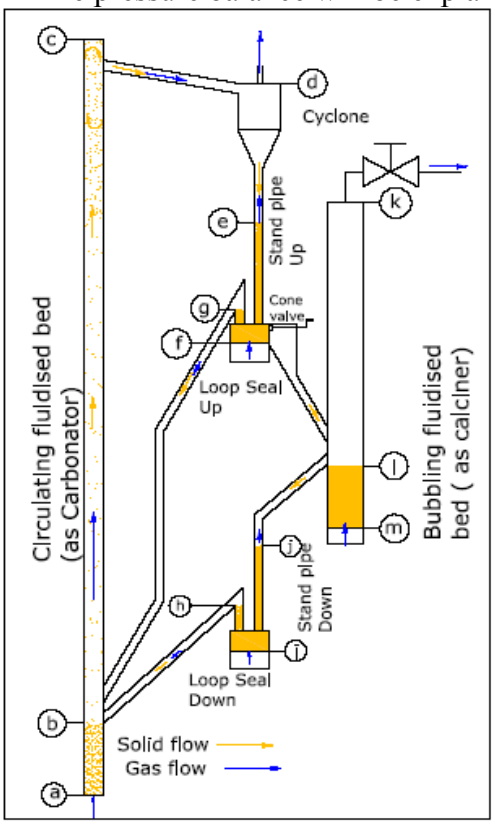

a	Distributor
b	Point of both loop seals inlet- It can be termed as secondary air inlet. It has been observed that above this point bed is dilute and below dense.
c	Top of riser- exit
d	Cyclone exit
e	Upper standpipe particle bed height
f	Bottom of upper loop seal
g	Top of recycle chamber of upper loop seal
h	Top of recycle chamber of lower loop seal
i	Lower loop seal down bottom
j	Top of loop seal down solid height
k	BFB freeboard
l	Top of BFB free board
m	Bottom of BFB

Figure 2.8: Schematic of the 15 KW carbonate looping DFB facility

2.6.1 The upper loop pressure balance equation

The above pressure loop is written, considering point f as highest pressure point.

$$(P_f - P_e) + (P_e - P_d) = (P_f - P_g) + (P_g - P_b) + (P_b - P_c) + (P_c - P_d) \quad \textbf{(2.21)}$$

In section d-e solids are free- falling and therefore no pressure drop occurs. For the same reason pressure drop in the discharge line g-b can be neglected too. Therefore, $(P_d - P_e) = (P_g - P_b) = 0$. $(P_f - P_g)$ is the pressure drop in the loop seal [45] and recycle chamber and can be considered as double exit loop seal pressure drop.

In general symbols the pressure balance [47,48] is written as:

$$\Delta P_{upper\_stp} = \Delta P_{double\_exit\_LS} + \Delta P_{riser\_top} + \Delta P_{cyclone} \quad \textbf{(2.22)}$$

2.6.2 The lower loop pressure balance equation

The above pressure loop is written, considering point 'i' as the highest pressure point. Since the BFB is overflowing it does not contribute to the pressure balance.

$$(P_i - P_j) + (P_j - P_k) + (P_{BFB} - P_{atm}) = (P_i - P_h) + (P_h - P_b) + (P_b - P_c) + (P_c - P_d) \quad \textbf{(2.23)}$$

Similar to the upper loop seal section j-k doesn't contain any solid so its pressure drop due to solids is neglected. The BFB can be pressurized at will. So the pressure above the particle bed height in the lower standpipe is always the same as in the BFB freeboard, namely $P_{BFB.}$ Also the pressure drop in the discharge line h-b can be neglected too, therefore, $(P_j - P_k) = (P_h - P_b) = 0$. $(P_i - P_h)$ is the pressure drop in the loop seal [45] and recycle chamber and is considered as the lower loop seal pressure drop.

In general symbol pressure balance is written as [47,48]

$$\Delta P_{lower\_stp} + (P_{BFB} - P_{atm}) = \Delta P_{lower\_LS} + \Delta P_{riser\_top} + \Delta P_{cyclone} \quad \textbf{(2.24)}$$

The above equations do agree with some of the derived equations for pressure balance for similar CFB reactors and combustors. [26] [27].

2.6.3 Pressure drop analysis in the riser

From fig. 2.8 it is clear that the pressure drop through the riser is [23]

$\Delta P_{riser} = (P_a - P_b) + (P_b - P_c)$ i.e. sum of dense bottom and dilute top pressure drops **(2.25)**

$$(P_a - P_b) = (1 - \varepsilon_{den})\rho_s g h_{ab} = \Delta P_{riser\_bottom} \quad \textbf{(2.26)}$$

$$(P_b - P_c) = (1 - \varepsilon_{dil})\rho_s g h_{bc} = \Delta P_{riser\_top} \quad \textbf{(2.27)}$$

In reality, the total riser pressure also includes frictional loss including acceleration loss so:

$$\Delta P_{riser} = (1 - \varepsilon_{den})\rho_s g h_{ab} + (1 - \varepsilon_{dil})\rho_s g h_{bc} + \Delta P_{ac} \quad \textbf{(2.28)}$$

Here ε_{den} and ε_{dil} are the voidages of bottom dense and top dilute regions respectively. The part of the above term $(1-\varepsilon)\rho_s h$ can be written as $\frac{actual\_mass}{Area * h} h$ Thus eq. 2.25- 2.27 can be modified to eq 2.29 with the consideration that the cross sectional area of the dense and the dilute sections are equal.

$$\Delta P_{riser} = \frac{(W_{ab} + W_{bc} = W_{riser})g}{A_{riser}} + \Delta P_{ac} \quad \textbf{(2.29)}$$

A frictional loss is assumed, which contributes 20 % of the total pressure drop. Thus:

$$\Delta P_{riser} = \frac{1.2 W_{riser}\, g}{A_{riser}} \quad \textbf{(2.30)}$$

2.6.4 Pressure drop analysis in the upper standpipe

Solids fall from the cyclone into the upper loop seal standpipe. The standpipe is either kept bubbling or at moving bed conditions. The condition at which the upper standpipe is a bubbling or a moving bed will be discussed later in the results and discussion chapter.

2.6.5 Moving bed regime standpipe conditions

In moving bed conditions particles move downwards in the standpipe, as a moving packed bed. Voidage values in the standpipe and supply chamber of the loop seal resemble voidage values between a fixed bed and an incipiently fluidised bed. Supply and recycle chambers of a loop seal are shown in figures in the next chapter. The pressure drop is calculated as per the modified Ergun equation [26], [23].

$$\frac{P_f - P_e}{h_{upper\_stp}} or \frac{P_i - P_j}{h_{lower\_stp}} = 150\frac{(1-\varepsilon_s)^2}{\varepsilon_s^3}\frac{\mu_g(\Delta u)}{\phi_s d_p^2} + 1.75\frac{(1-\varepsilon_s)\rho_g}{\varepsilon_s^3}\frac{(\Delta u)^2}{\phi_s d_p} \quad \textbf{(2.31)}$$

Here Δu is the relative velocity of gas with respect to the down flowing solids [23], [26]. εs is the solids fraction in standpipe. Superficial velocity through standpipe is small, since most of aeration gas escapes to the riser through recycle chamber due to less resistance.

The equation shows the important fact that pressure drop across the standpipe is a combined result of solids height and relative velocity between the solids and the gas. The latter is very much dependant on the value of loop seal aeration. As a result, different standpipe heights can show same pressure drop and vice versa. This fact makes difficult to estimate bed inventory which is easier in case of bubbling standpipe conditions as explained later.

2.6.6 Bubbling bed regime standpipe conditions

For a bubbling standpipe, aeration rate is maintained higher than moving bed conditions so that the loop seal supply chamber and recycle chamber are both in bubbling condition. The fraction of aeration gas leakage through the standpipe is much larger than for moving bed standpipes. In this case the pressure drop in the standpipes is:

$$(P_f - P_e) or (P_i - P_j) = (1-\varepsilon_b)\rho_s g h_{stp} \quad \textbf{(2.32)}$$

Similar to equation (2.31) the above equation can be written for the upper as well as the lower standpipe as

$$\Delta P_{upper\_stp} = \frac{W_{upper\_stp}\, g}{A_{upper\_stp}} \quad \textbf{(2.33)}$$

$$\Delta P_{lower\_stp} = \frac{W_{lower\_stp}\, g}{A_{lower\_stp}} \quad \textbf{(2.34)}$$

For optimum operation of the system, the standpipe height should be enough so as to avoid leakage from the carbonator gas to the loop seals and the calciner or vice versa. Standpipe may exhibit slugging if the riser exhibits even mild slugging due to operation of the riser in the turbulent regime and small scale of the facility.

2.7 Estimation of inventory deriving from the pressure balance

It is clear from the CO_2 capture requirement that to achieve higher efficiency in the riser the mass within it should be enough. The required mass is mainly a function of superficial gas velocity and the molar ratios of the sorbent looping rate to incoming moles of CO2 in the carbonator ($\frac{F_R}{F_{CO2}}$) and of the fresh make up flow of sorbent to the incoming molar flow of CO2

($\frac{F_O}{F_{CO2}}$). It is convenient to be able to estimate the Total Solid Inventory (TSI) from the required mass in the riser in advance. A co-relation which can estimate inventory for bubbling standpipe conditions has been developed. For moving bed conditions this will be subject of further work.

For bubbling standpipes: Considering equation 2.33, 2.34 and assuming pressure drops in cyclone and loop seals as negligible it is concluded:

$$\Delta P_{upper\_stp} = \Delta P_{riser\_top} \quad \textbf{(2.35)}$$

$$\Delta P_{lower\_stp} + (P_{BFB} - P_{atm}) = \Delta P_{riser\_top} \quad \textbf{(2.36)}$$

incorporating equation 2.33 and 2.34 in eq.2.35 and 2.36 directly it is obtained:

$$\frac{W_{upper\_stp}}{A_{upper\_stp}} = \frac{W_{riser\_top}}{A_{riser\_top}} \quad \textbf{(2.37)}$$

$$\frac{W_{lower\_stp}}{A_{lower\_stp}} + \frac{(P_{BFB} - P_{atm})}{1.2g} = \frac{W_{riser\_top}}{A_{riser\_top}} \quad \textbf{(2.38)}$$

Mass quantities contained in the BFB, the recycle and supply chambers of the loop seals are constant since components mentioned are in bubbling conditions. The sum of the above mass will be referred to in this work as constant mass W_{const}.

By making the assumption that W_{riser_top} = *40%* of the W_{riser} and using the mass balance equation below the system TSI is obtained:

$$TSI = W_{riser} + W_{upper\_stp} + W_{lower\_stp} + W_{const} \quad \textbf{(2.39)}$$

Finally. the 2.35 with the combination of (2.32) – (2.34) results in the following equation:

$$\text{TSI} = W_{Riser} + \left(\frac{0.4W_{Riser}}{A_{Riser\_top}} - \frac{(P_{BFB} - P_{atm})}{1.2g} \right) * A_{Lower\_stp} + \left(\frac{0.4W_{Riser}}{A_{Riser\_top}} \right) * A_{Upper\_stp} \quad \textbf{(2.40)}$$

2.8 Cone valve pressure drop analysis

Solids from the supply chamber flow to the recycle chamber through an opening slit. The pressure drop across this opening can be calculated by Cheng and Basu et al [23].

$$(P_{f2} - P_{f1}) = 0.66(A_s / A_{sc})^{-1.2} G_s \quad \textbf{(2.41)}$$

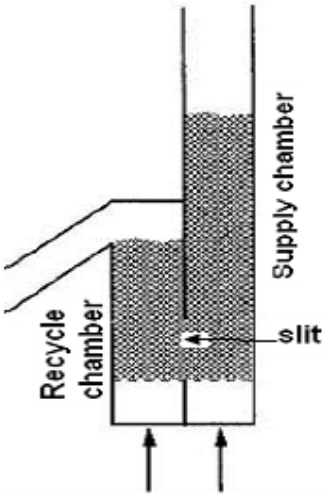

Figure 2.9: Loop seal schematic

This equation is very important since the flow rate balance is necessary for the system to achieve a steady state. A loop seal should be able to pass the same amount of mass as it is receiving from the riser. This flow rate is governed by the pressure difference (P_{f2}-P_{f1}) and this difference is governed by other factors discussed later.

3. Experimental Set Up

3.1 Introduction

In order to complete the experiments, a scaled down model was designed and constructed out of Plexi-glass. & He [56] carried out cold model experimentation in a similar scheme using sand as solid and ambient air as gas. Their experience is valuable in conducting cold model experiments. Previous work in the field also was conducted for IVD by Ajay Bidwe [40]. Bidwe used the same cold model installation with a material of different particle size in order to study its behaviour and design an operational window for this particular particle size and did a preliminary evaluation of different operating parameters on the hydrodynamics of the system. The same set up although modifying some dimensions. It is a main concern to maintain the same geometric ratio in every part of the facility. The basic design as per the e laws will be explained later on.

3.2 Cold model set up

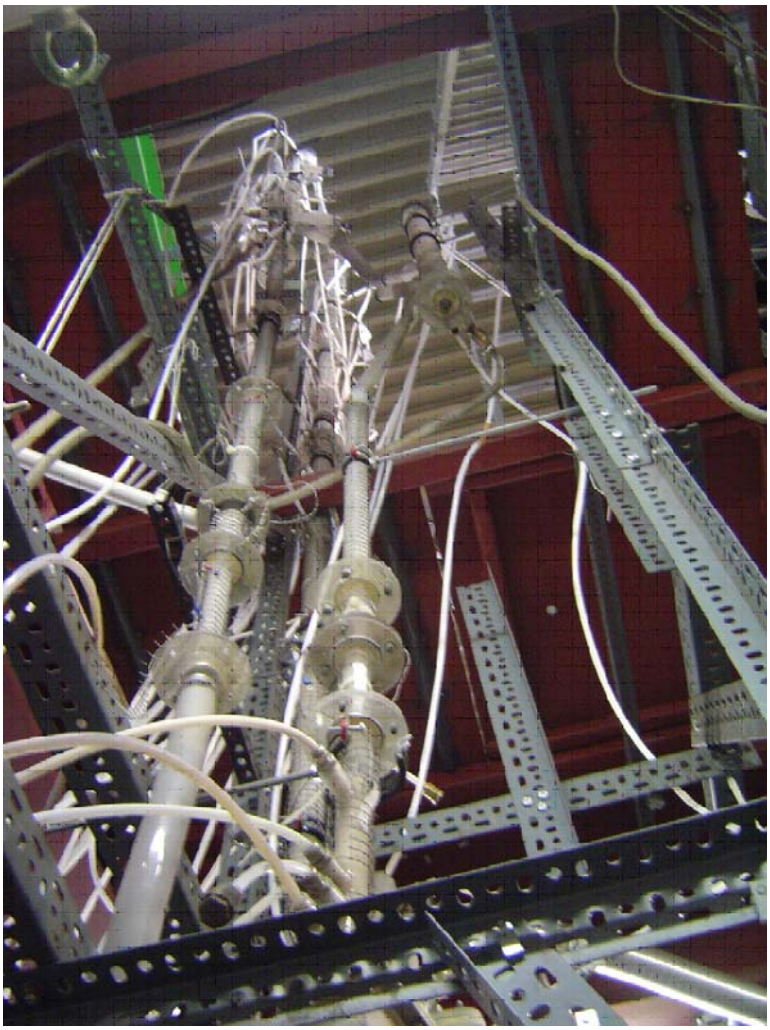

Figure 3.1: Cold Model As Built

The Figure 3.1 below shows the picture of cold model as built. As seen the facility is mounted on an angled structure. The main riser (ø30 x 5320 mm) is divided into 5 parts joined by flanges. The bottom part consists of inlets for both loop seal at different heights. Due to previous experience with electrostatics [24]. [46]. most part of the cold model is covered with mesh wire just to minimize the electrostatic effects and is grounded at regular intervals. The pressure measurement nozzles were fabricated wherever required. The list of pressure transducer nozzles is given in Table 3.1.

Air supply is provided at 6 locations as shown in the Table 3. 1. with separate pressure regulating valves (PRV´s) and rotameters. PRV's were set to 1.2 bar pressure. Rotameters were calibrated before the start-up of the experiments. The Table 3. 1 below shows the list of all air supply points with their rotameter range and calibration equation.

Table 3. 1: List of Air Supply Locations in Cold Model

Sr no	Location	Rotameter range	Rotameter calibration equation for flowrate in Nm3/h
1	Riser bottom	2-25 Nm3/h	1.1256x-0.286
2	BFB bottom	0.8 – 3.5 Nm3/h	0.1948x+0.4191
3	Upper loop seal bottom air	0-3 Nm3/h	0.001x
4	Upper loop seal side air	0-150 LPM	(0.35x-0.6)0.06
5	Lower loop seal bottom air	0-3 Nm3/h	1.2636x-0.0258

x – reading shown on Rotameter.

3.3 Measurement of pressure drops

When the location of the pressure transducers on the DIVA- ELWIRA DFB was finalized Bidwe marked the location of pressure transducer nozzles on the cold model at geometrically similar distances. Each nozzle is filled with a fine mesh wire and glass wool to keep transducer safe from malfunctioning and from the incoming fine particles.

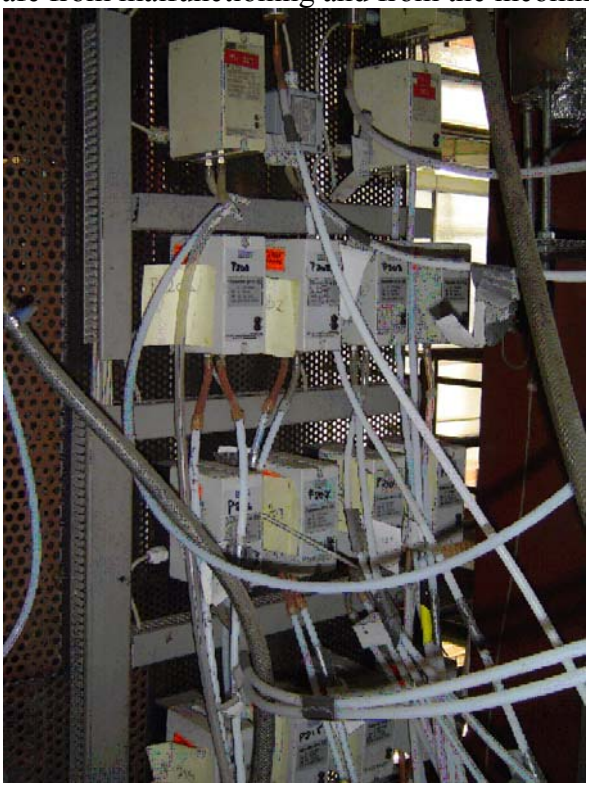

Figure 3.2: Pressure transducers panel at cold model IVD

In total 15 transducers were used. Pressure transducers were available in different ranges like 0-10, 0-50, 0-100, 0-200 mbar. Transducers were placed according to their range in the places where the maximum pressure drops where expected to be present. Pressure transducers used were diaphragm type differential pressure transducers, with 4-20 mA digital output. The respective signals are sent to the computer (see Index) which senses the signal using LabView ® software, converts the digital signal into the calibrated value and displays the value on the screen as shown in **Error! Reference source not found.**b. The displayed value is often checked for calibration using a manometer which can be attached in parallel to the transducer. Values are recorded with sampling period of 1 Hz. The list of the traducers is shown in the following table.

Table 3. 2: List of pressure transducers on cold model

Sr no	Location	Transducer name	Range mbar
1	Riser- 21 - 333 mm from distributor	P-201	0-100
2	Riser- 333 – 2621 mm from distributor	P-202	0-100
3	Riser- 2621 – 4328 mm from distributor	P-203	0-100
4	Riser- 4328 – 5090 mm from distributor	P-223	0-200
5	Riser-21 – 5090 mm from distributor (for quality check)	P-215	0-200
6	After cyclone - loop seal up stand pipe	P-217	0-200
7	Loop seal up stand pipe - Loop seal up box	P-206	0-50
8	Loop seal up box – 333 mm from distributor	P-205	0-50
9	Loop seal up box - BFB top (cone valve pressure)	P-225	0-100
10	Loop seal down box – Top of BFB	P-207	0-100
11	5090 mm - After cyclone	P-224	0-10
12	Loop seal down box - Top of BFB	P-204	0-100
13	Loop seal down box - 333 mm from distributor	P-210	0-50
14	BFB absolute pressure	P-218	0-400
15	Cyclone absolute pressure	P-219	0-400

3.4 Initial pre experiments

Following pre experiments were carried out:

- To calibrate all rotameters
- Particle size distribution of ZrO_2 particles.
- Density measurement, using pychnometer.
- Voidage measurement.
- To find leakages in the cold model and repair. since solids are very costly.
- To find out a range of good operating conditions. good methods of operation and prepare a standard operating procedure for carrying out proper experiments.

For the experiments two different particle-sized materials were used. For Bidwe's work [40], the particle size of the Zirconium dioxide was 142 μm and its density was 5700 kg/m^3, while for the present thesis the particle size of the Zirconium Dioxide was 230 μm and its density was 5700 kg/m^3 as well.

3.5 Experimental procedure

Carrying out a successful experiment involves following activities: The procedure is constantly getting upgraded. In the experiments experimental procedure is highly influenced by the previous works of Ling and Zenteno [56] and Nikolopoulos [46] and is the same as in Bidwe [40].

First task is that the computer has to get started, along with the Lab View Measurement software and the recording data. The system should be totally empty (no solids at all). In continuance the amount of solids should be weighted (say 2 kg). The BFB should be filled till the overflow level and the supply and recycle chambers of both loop seals. Next the solids should be weighted again and the difference should be noted as $W_{const.}$

As a next step the rest of the mass intended to be loaded to the system should be weighted (termed as moving mass) and be divided into two halves. Next, the first half of solids should be filled into the upper standpipe through a valve provided below the cyclone and the lower standpipe by pouring into the BFB through a valve at the BFB top. Following, all rotameters should be checked if they are properly closed and the air supply valve should be open for all rotameters.

As a next stem the BFB should be started at approximately $\frac{U}{U_{mf}}$ = 3 to 5 and the solids should be let to overflow into the lower loop seal. Next, the air supply should be started in the riser until velocity becomes approximately 50% of U_t. In continuance, the air supply should be started slowly at the upper loop seal. The upper loop seal soon will fluidize and will start pushing solids into the riser. As soon as this happens, the air supply in the riser can be increased to a little more than U_t.

As a following activity, the loop seal flow should be increased till the standpipe starts slightly bubbling. The circulation will begin in the upper loop seal riser loop. Then, slowly the riser velocity should be increased till the desired value. The loop seal may stop bubbling due to higher entrainment. so please try to keep it bubbling by increasing upper loop seal side air or bottom air. Next, slowly the upper loop seal will become steady. Slowly the air flow should be started in the lower loop seal in the same manner as in the upper loop seal till it starts bubbling. Since the riser has received more solids pressure drop in the riser and the cyclone entrainment rate will increase. Next, the upper loop seal standpipe height will have risen and can be again adjusted by adjusting the upper loop seal bottom and side air. Then you have to wait for system to get balanced.

Now slowly open the cone valve to a predecided number of rounds and see the cone valve flow rate. If the cone valve flow rate is higher than the cyclone entrainment rate and the upper standpipe solid particle bed height levels are falling below satisfactory level (level at which leakage may be caused) then an increase in the BFB pressure will reduce this flow. Always be sure that some solids may return through the loop seal recycle chamber to the riser. At the same time adjust the lower loop seal flow rates so as to keep its height constant and wait for the system to get balanced.

A system is balanced when it shows constant pressure drops in riser, the upper loop seal and the lower loop seal, with a definite range of fluctuations. A good sign to be sure is to see if the upper standpipe height and the lower standpipe particle bed heights are constant or not. A constant standpipe height is an indication of equal entrainment coming in and returning through recycle chamber and cone valve. a perfectly balanced system.

Once the system is balanced, the time at which it is balanced should be noted and the data should get recorded for 10 minutes and the flow values of riser. BFB upper loop seal and lower loop seal etc should be recorded as well. Also please note the loop seal heights and standpipe condition whether it's bubbling, slugging or moving bed.

Now once the 10 minutes are over, the lower loop seal flow should be stopped without disturbing other flows and the time required to accumulate a certain volume of solids should be noted. This will give us the cone valve flow rate. Immediately after recording start the LSD bottom air to the original value, wait for 3 minutes for the next reading, take 3-5 readings as per requirement and deviation .(if higher deviation observed then wait longer for more stabilization and more readings with more volume).

Next step is to close the valve below cyclone and record the time for accumulation of 3 to 4 cm of solids and immediately open it, wait for 3 minutes again, repeat the procedure for 3 to 5 times. This procedure will give us the value of the Riser entrainment rate, Gs.

Should the actual masses in the riser, upper standpipe and lower standpipe be noted, the air flow from all rotameters should be stopped at once. Then the masses are taken out, weighted and notes concerning their weights should be kept.

Charge the mass again to upper standpipe and lower standpipe equally to find the performance at different conditions of velocity, BFB pressure or cone valve opening. One can use the same mass or other, according to his experimental plan.

4. Previous Results At Cold Model

4.1 Introduction

In this chapter the previous work done in the field by IVD [40] and [46] will be discussed. The main objective of this work was to operate a Dual Fluidized Bed scaled cold model, study its behaviour and state its operating parameters, so as to create know-how in the field. This previous information and expertise was of vital importance for the thesis presented here. The two most important breakthroughs were the design of the operating window of the facility for the particle size in use (142 μm) and furthermore the initial validation of the design of the 15 kW carbonate looping DFB facility (DIVA- ELWIRA).

4.2 Operating Window

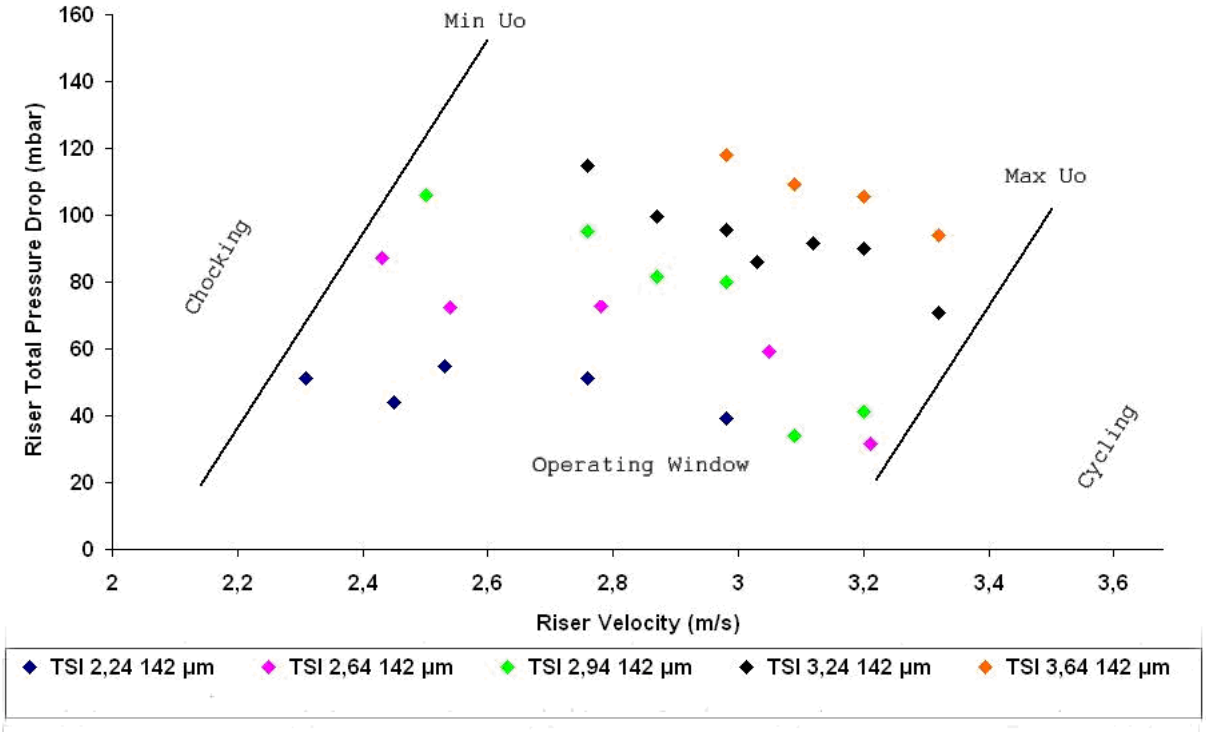

Figure 4.1: Operating Window for particle size of 142 μm

The above operational window depicts the pressure drop through the riser against the riser superficial velocity for all runs conducted in [40]. The previous undergone research on the subject resulted in the operating window above, which depicts clearly the three operational zones for the particle size in use in the cold model. Certain experiments were carried out, with different TSI (Total Solid Inventory) and riser velocities which resulted in plotting this graph. In the far left zone (for lower riser velocity (Uo)) the cold model has many difficulties lifting up the mass provided in the riser and as a result 'chocking' appears. This condition is considered highly unstable, the entrainment of the mass is not enough to achieve a smooth and constant flowrate, therefore the operation in this spectrum of lower riser velocities is not recommended and unacceptable due to high pressure fluctuations. The standard deviation of the pressure fluctuations divided by the mean pressure drop in the bed can reach 30% and therefore this main problem is making this region unacceptable. In the second (middle) zone, there is the normal operating window for the cold model. where all experimental runs are quite stable and the ratio of the standard deviation of the pressure fluctuations to the mean pressure drop of the riser is in

the range of 5- 10%. Therefore this is the region of TSI and riser velocities that the cold model operates. In the far right zone, (for higher TSI and riser velocities) the cold model is not able to run properly, due to a phenomenon termed “cycling”, which was an astonishing finding from previous work and is analysed thoroughly in 4.3. Another useful finding concerning the operating window is that as showed in the graph, the minimum and maximum operating riser velocity for each TSI, is increasing, with increasing TSI as stated in Figure 4.1.

4.3 Cycling

4.3.1 The phenomenon

The effect was first observed at 2.98 m/s with atmospheric pressure for a TSI of 2.24 kg and at 3.09 m/s for a TSI of 2.64kg. When this phenomenon occurs the upper and lower loop seal stops delivering solids to the riser, till a sufficient standpipe height is built up. Then mass starts pouring into riser from the loop seals. at much higher rate than normal and again stops. This happens at regular pulse and in cyclic manner. During this time the pressure drop varies from min to max which means the mass in the riser increases and decreases. This phenomenon was hence called ‘cycling’, due to its cyclic occurrence. In order to depict the differences between a normal run and a run where the cycling phenomenon takes place, two distinct runs have been chosen. Run 14 is a normal run while in Run 19 cycling occurs. The operating conditions for both runs appear in the following table.

Table 4.1: Operating Conditions for Runs 14 and 19

No. of Run	TSI	CFB (m/s)	BFB (m/s)	LSU Bottom (m/s)	LSD Bottom (m/s)	LSU Side (m/s)	Cone Valve Opening (mm)
14	2.64	2.54	0.18	0.08	0.04	0.01	5.26
19	2.64	3.05	0.18	0.05	0.05	0.03	5.26

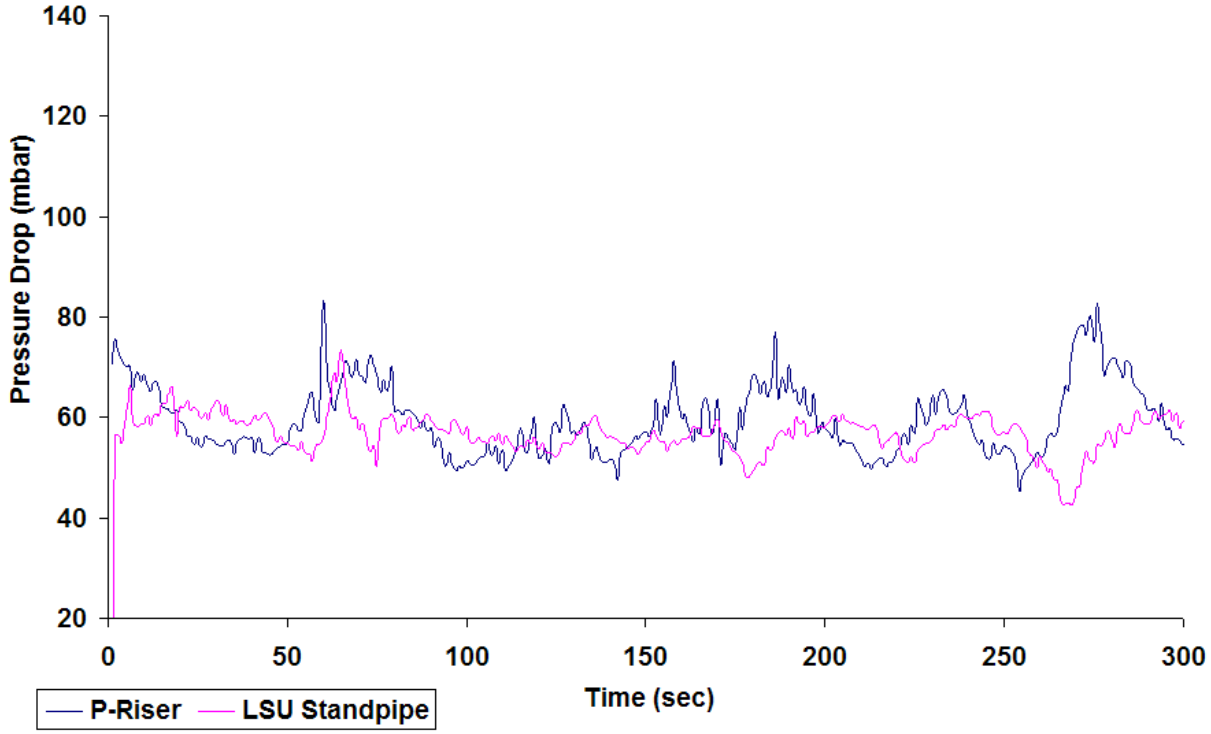

Figure 4.2 : System with cycling phenomenon

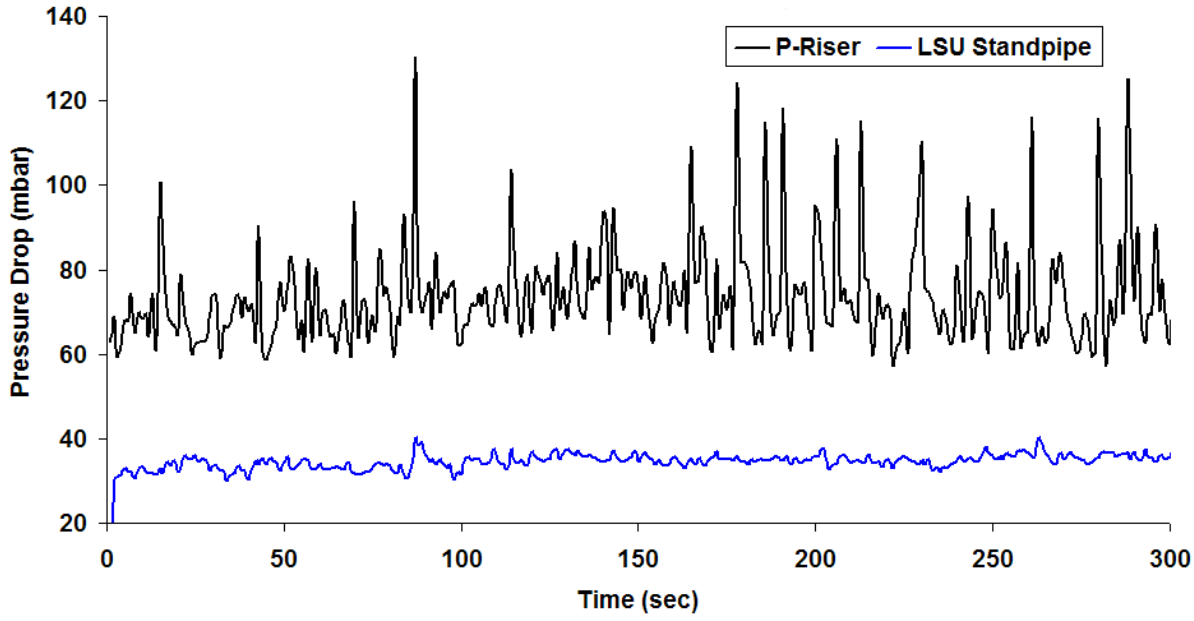

Figure 4.3 : System with balanced run

The figure 4.2 shows a typical run with cycling phenomenon while figure 4.3 shows a normal perfectly balanced run. The main differences are basically the following:

- **Patterns of the riser pressure fluctuations**: During the cycling phenomenon the riser fluctuations are showing a sinusoidal function while during normal runs riser pressure fluctuations are purely due to the turbulent nature of fluidized bed. This indicates that in cycling phenomenon the riser inventory increases and decreases (as already discussed) while in normal runs it remains relatively constant. Both behaviours were visually observed while watching the cold model in function.
- **Loop seal pressure fluctuations:** In normal runs the loop seal pressure is almost constant but in cycling it also follows a sinusoidal function. The sinusoidal function of pressure variation follows a typical rhythm. Riser pressure drop reaches maximum just after the pressure drop through the loop seal reaches minimum because as already mentioned the mass is discharged to the riser abruptly (riser maximum. standpipe minimum) and than mass accumulates in the standpipes. Before mass is again discharged to the riser there is a minimum pressure drop in the riser and maximum in the standpipes.

4.3.2 Theoretical background of cycling

Cycling mainly occurs at higher velocities when entrainment rates are higher. In every situation, in order to maintain the system under balance, the loop seals must deliver at the same rate as the riser. Loop seal flow rate is a function of the pressure drop through the slit of the loop seal standpipe pressure. From the Basu, Cheng equation, as found in [45], it is derived:

$$(P_{f2} - P_{f1}) = 0.66\left(A_s / A_{sc}\right)^{-1.2} G_s \qquad \textbf{(4.1)}$$

The P_{f1} is the pressure at the supply side and P_{f2} is the pressure on the delivery side of the loop seal which is influenced by the loop seal recycle chamber and riser top pressure drop. Loop seals will fail to deliver when they will not have enough $(P_{f1} - P_{f2})$. In the case presented in this chapter (TSI 2.24 kg), the standpipe could not generate more pressure to have higher $(P_{f1} - P_{f2})$ for higher G_s above 3 m/s (Run 19). In that case solid height builds up in the stand pipe so as to create enough $(P_{f1} - P_{f2})$ by in the meantime, the riser empties. Thus $(P_{f1} - P_{f2})$ increases even more and therefore loop seal vigorously delivers solids into the riser.

The behaviour of the cycle is as follows: First, the solids enter the bottom part of the riser, which doesn't take part in the pressure drop closed circuit, and hence, its equations. As the flow continues, the solids move upwards, towards the riser top. In the mean time, since the riser top has less resistance (meaning pressure drop), the loop seal continues to pour solids into the riser. While this pouring towards the riser occurs, the flow continues to push the mass towards the upper parts of the riser and therefore the mass in the standpipe reduces. Therefore the pressure drop through the loop seal slit $(P_{f1} - P_{f2})$ is drastically reduced and at some point the loop seal flow stops. When the flow from the loop seal stops, the mass from the upper part of the riser accumulates in the standpipes. Therefore the pressure drop through the slit $(P_{f1} - P_{f2})$ increases again. The flow from the upper part of the riser towards the loop seal diminishes and the flow for the loop seal to the lower part of the riser starts once more. The phenomenon, as mentioned, happens in repetitive manor.

In order to avoid this phenomenon, higher TSI in the riser is suggested for higher velocities. Higher TSI will create higher pressure drop in the riser as well as the standpipe and this will allow higher $(P_{f1} - P_{f2})$ to create higher Gs through the loop seal slit. This is proved by fig. 4.1 by the observation that cycling occurs at higher velocities for increased TSI. Secondary measures so as to hinder cycling are to increase loop seal aeration and the absolute pressure of the BFB. This happens because increase of both result into less requirements of solids in the standpipes as shown by the pressure balance equations.

Cycling is not a desirable mode to operate in the pilot plant facility since it would cause fluctuations in CO2 capture efficiency. This is a possibility for two reasons:

- The flow rate of solids coming from the BFB regenerator is not constant during cycling. Therefore, at one point the CFB carbonator will have a high flow rate of freshly calcined active solids entering and at another point no such flow will be present.
- The carbonator inventory follows a sinusoidal function. Therefore the amount of sorbent that captures CO2 in the carbonator varies.

4.4 Effect of the riser velocity on riser entrainment

These circulation rates were measured after the cyclone. The following graph shows the plot of riser entrainment against the superficial velocity of the riser for all runs conducted in [40].

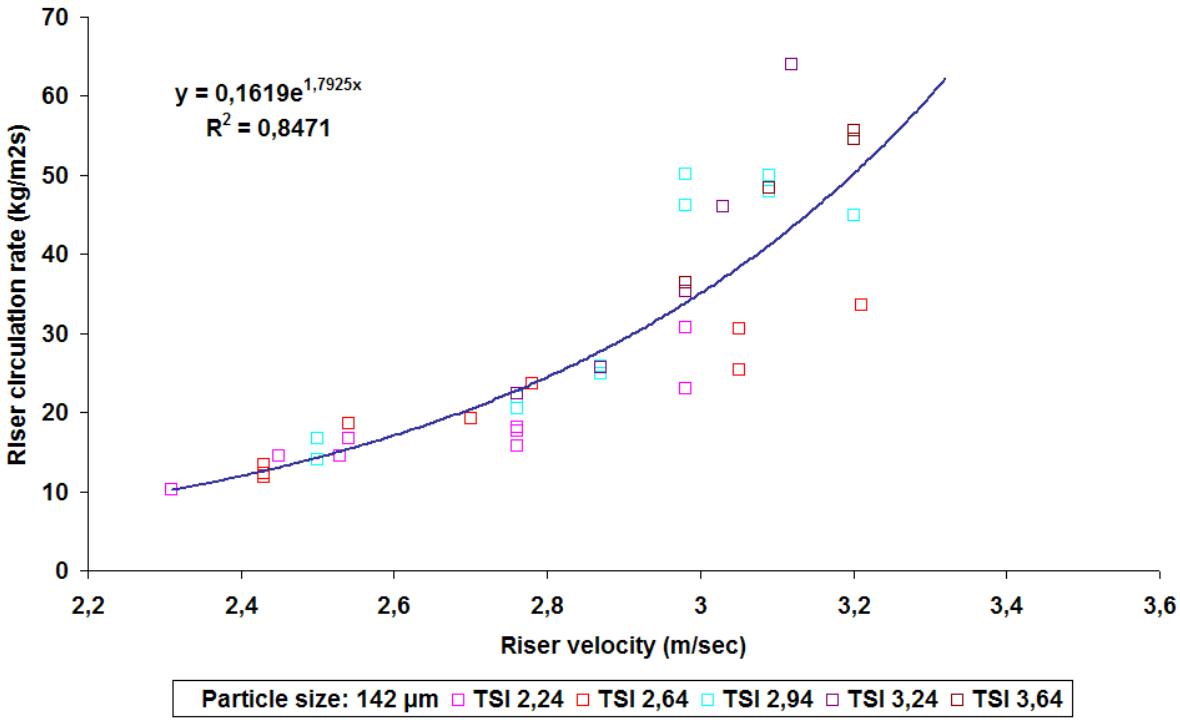

Figure 4.5: Riser entrainment against superficial velocity

As observed in the graph. for lower velocities (below 3 m/s) circulation rate is only a function of velocity u_o but with higher velocity Gs seems to be dependant on the TSI too. Therefore it is concluded:

$$Gs = f(u_0, W_{riser}) \qquad \textbf{(4.2)}$$

The empirical equation is plotted for the experimental values in with the help of excel. yields a best fit of exponential equation of

$$Gs_{cyclone} = 0.1619e^{1.7925U_0} \text{ with } R^2 = 0{,}85 \qquad \textbf{(4.3)}$$

Where $G_{scyclone}$ is in kg/m2s and U_o is in m/s.

The fact that equation 4.3 has such a good fit when plotted against riser velocity only shows that the riser superficial velocity is the primary parameter influencing riser entrainment. Also during the study it was observed that pressure drop in the top section on the riser has

influence on the circulation rates. Therefore riser pressure drop at 4328 mm and respective Gs at every TSI are plotted below. With rise in pressure drop at top section Gs values also raised accordingly.

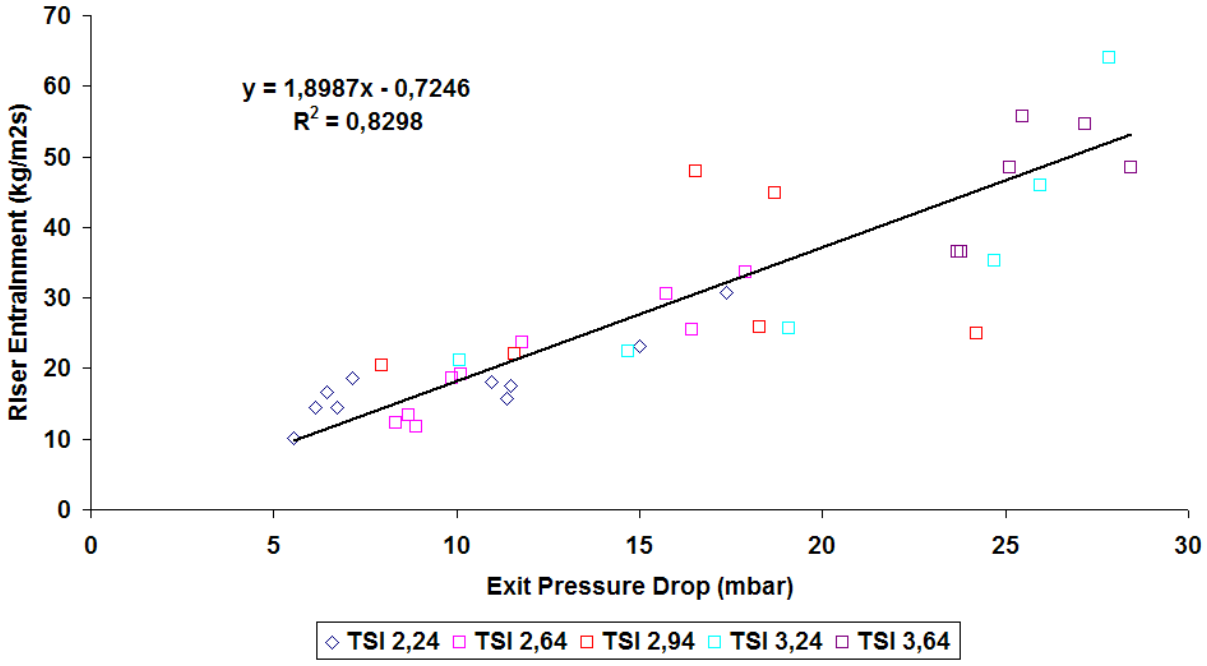

Figure 4.6: Riser entrainment against pressure drop at the exit part of the riser

The empirical equation is plotted for the experimental values in with the help of excel. yields a best fit of linear equation of

$$Gs_{cyclone} = 1.8987 P_{exit} - 0.7246 \quad \text{with } R^2 = 0{,}83 \qquad \textbf{(4.4)}$$

Where $G_{scyclone}$ is in kg/hr and and P_{exit} is in mbar.

4.5 Flow rate and pressure drop through the cone valve

Previous studies in the field showed that the cone valve discharge is mainly controlled by the product of the pressure drop through the valve and the opening of the valve (F. measured in m2Pa). The pressure drop through the cone valve is a result of the operating parameters of the system and will be discussed in the following chapter. At this point it can be statet that the results of this work have showed that this very pressure drop can be controlled by charging manually the BFB absolute pressure, in the installation. An increase in the BFB pressure results in decreasing the flow rate and a decrease in the BFB pressure, has the exact opposite effect. Figure 4.6 depicts the relationship between the cone valve discharge and the product of the pressure drop through the cone valve and its opening. F.

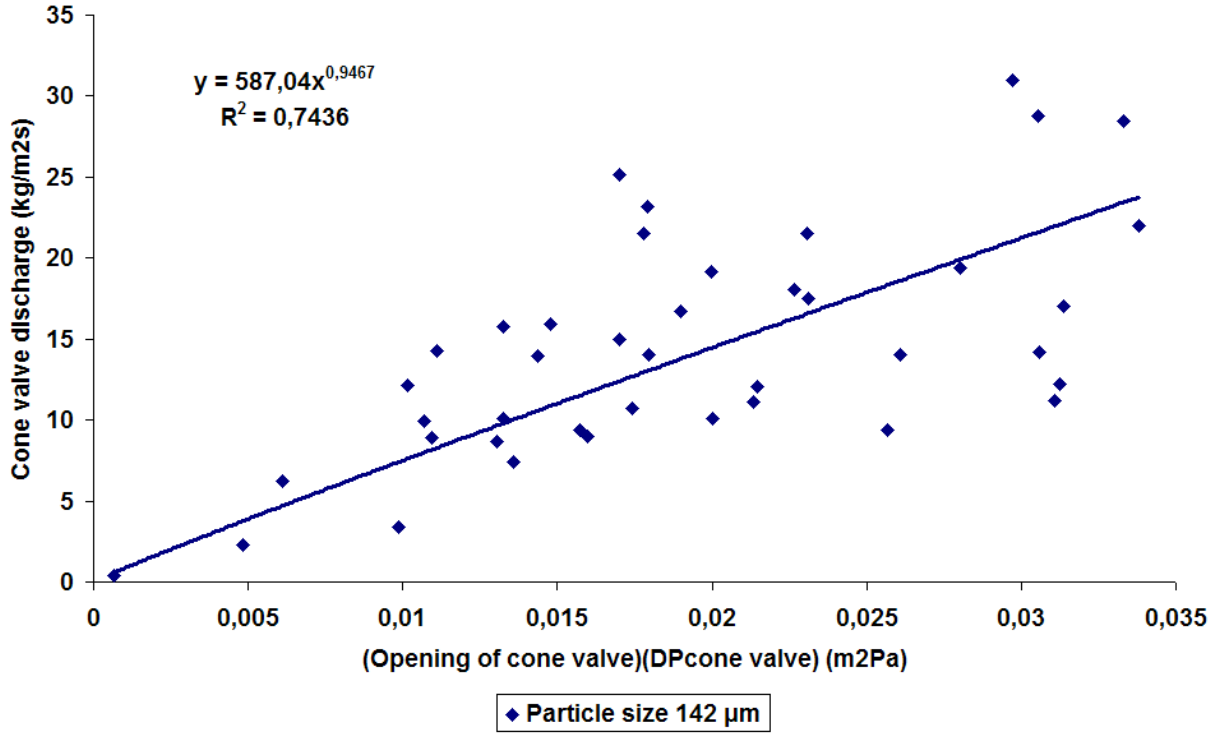

Figure 4.7: Cone valve discharge versus F for a particle size of 142 µm

$$CV_{discharge} = 587.04F^{0.9467} \qquad \textbf{(4.5)}$$

Where $F = A_{cv}\Delta P_{cv}$. with $R^2 = 0{,}74$

Where Cone Valve discharge is measured in kg/m^{2}s and F is expressed in m^{2}Pa.

With the increase of the TSI in the system, there is an increase in standpipe heights and standpipe pressures. Furthermore, Gs from cyclone is more dependant on the velocity than on W_{riser}. Therefore to control the flow at higher TSI's, higher P_{BFB} is required. This higher P_{BFB} would decrease the $\Delta P_{cone\ valve}$ and thus control the flow. During initial phases of the experiments, small values of P_{BFB} caused problems such as the emptying of the loop seal up through the cone valve, because with low P_{BFB} there was no opposing power, to stop this flow. Finally, it was understood that in order to control the flow, someone has to adjust the P_{BFB} manually.

5. Results And Discussion

5.1 Input and output experimental parameters and their effect on efficiency

The operational input parameters which have been adjusted according to the experiments' purposes were the following:

- Total solid inventory (TSI): the mass that is loaded in the installation
- BFB pressure: the absolute pressure in the Bubbling Fluidized Bed
- Loop seal aeration: the aeration through the both loop seals
- Cone valve opening: the opening of the orifice in the cone valve
- Particle size: the size of the particles of the solid in use
- Riser velocity: the velocity of the Circulating Fluidized Bed

In order to specify the behaviour of the system and analyze it in depth, a series of experiments were made. In these experiments all the parameters were kept constant, except for one, which was the parameter in question for analysis. Through this simple scheme, the effects of each and every of these parameters to the output parameters of the system were depicted.

The output parameters which were affected by the experimental procedure were the following:

- Riser pressure drop: the total pressure drop of the Circulating Fluidized Bed
- Axial pressure profile: the axial pressure profile through the CFB riser
- Riser entrainment: the flow rate of the riser
- Cone valve discharge : the amount of solids through the cone valve per second

All the undergone research was made so as to optimize the installation and increase its efficiency. The factors that affect it are clearly the output parameters because:

- **The riser pressure drop:** It defines the total mass in the riser. Generally more mass means better CO_2 capture efficiency.
- **The axial pressure profile:** It is important because it shows the distribution of the mass between the different hydrodynamic regions of the CFB riser carbonator. Different regions represent different gas- solid contacting modes. The dense region has generally a high solid fraction but poor contacting due to formation of bubbles. The core- annulus region has low solid fraction but good solid contacting. The exit region shows intermediate solid fraction values and intermediate contacting.
- **Riser entrainment**: The flow rate of the riser is of high importance because it it represents the maximum possible sorbent looping rate between the beds.
- **Cone valve discharge**: The function of the cone valve dictates the sorbent looping rate between the beds.

5.2 Operating Window

In this chapter the operating conditions and the hydrodynamics for the experiments carried out (as already stated) for higher particle size (mean dp 230 μm), as well as the effect of the particle size will be discussed. For the analysis, the data merging from the present results were crossed checked with those of the data from Ajay D. Bidwe's Thesis [40]. Furthermore the possibility of a design improvement, its behaviour and its effect on the experimental parameters

will be discussed. In Annex 1 there are all the experimental conditions for all runs conducted in this thesis.

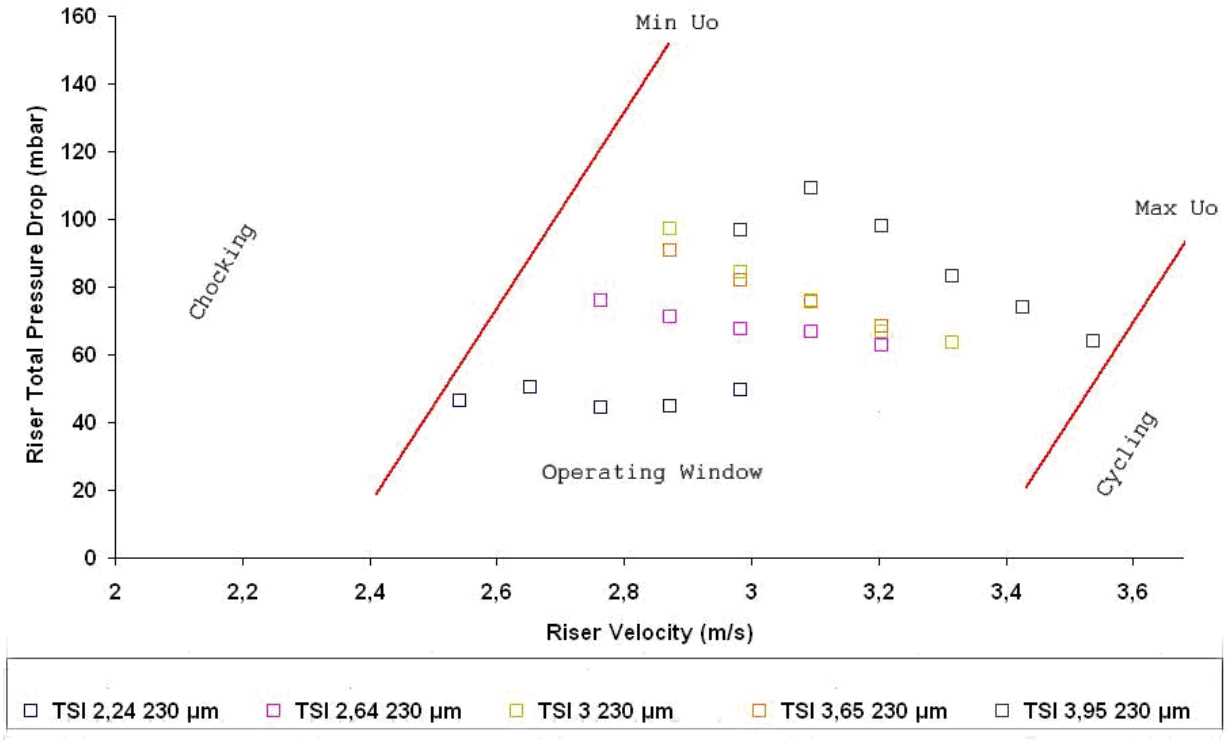

Figure 5.1: Operating Window for particle size of 230 μm

During the experimental work for the thesis, the cold model was operated with different TSI (Total Solid Inventory) values and for several different velocities, so as to create the operational window of the facility. as shown in Figure 6.1, for the particle size of 230 μm. For 5 different values of TSI, namely 2.24 kg. 2.64 kg. 3.00 kg. 3.65 kg and 3.95 kg experiments were carried out with the operating conditions as shown in table in Annex 1. The main objective of the runs was to find out the operating window for the facility for the higher particle size. The minimum riser velocity (U_o) for each TSI was noted when the riser couldn't lift the given mass and the phenomenon of chocking appeared, whereas the maximum riser velocity for each TSI was noted when the cycling phenomenon appeared. P_{BFB} pressure, LSU (Loop Seal Up) aeration and LSD (Loop Seal Down) aeration were dictated so as to achieve bubbling conditions in both loop seals and so as to achieve pressure balance and constant and smooth flow rate, through the whole facility. Cone valve opening was kept constant (as shown in Annex 1).

When increasing TSI more mass is available in the CFB riser. As a result, higher TSI creates higher pressure drops. as clearly shown in the graph. Furthermore, in the operating window above the three operational zones (chocking-normal-cycling) as expected and as discussed in previous chapter describing previous work can be seen. Please note that the occurring phenomena both for lower riser velocities and higher riser velocities where the same as in as or the lower particle size of 142 μm tested previously. Another notable fact that can be seen is that when the riser superficial velocity increases the total pressure drop in the riser seams to decrease. This is due to a rapid increase of the pressure drop through the cyclone with increase of velocity and the effect it has on the pressure balance. This "cyclone effect" is discussed later in detail.

5.3: Flow structure of CFB carbonator

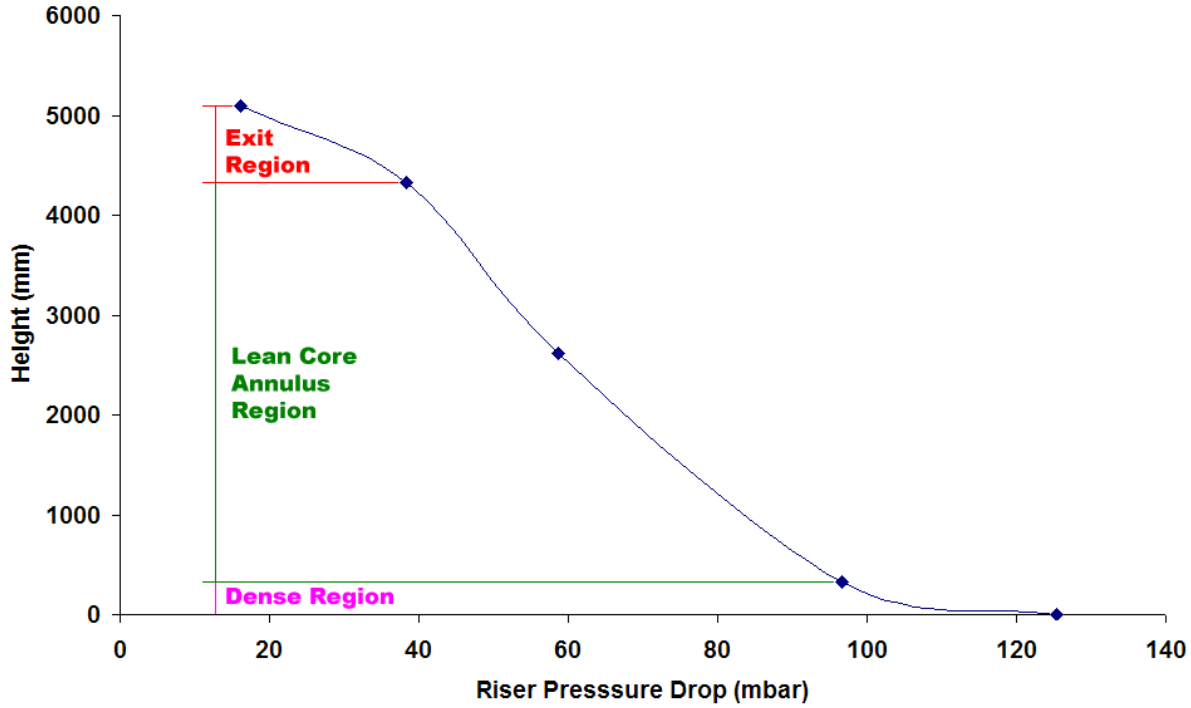

Figure 5.2: Flow Structure along the riser height. Run 40

In fig. 5.2 there is a typical pressure drop profile of the riser. The specifications of this particular Run 40 are shown in the table below.

Table 5.1: Operating Conditions of Run 40

Run No.	u_o	TSI	P_{BFB}	A_{cone_valve}	LSU bottom air	LSU side air	LSD bottom air	Standpipe status
	m/s	kg	mbar	mm^2	m/s	m/s	m/s	up-down
40	3.09	3.95	65	5.26	0.38	0	0.08	bubbling-bubbling

In fig. 5.2 three distinctive and characteristic areas for a typical pressure drop profile can be witnessed. At the bottom part of the riser there is a **'dense region'** (noted in pink) where the solid fraction is 0.1-0.21. The dense phase consists of a bubble phase and an emulsion phase. Hydrodynamics here have some resemblance to those of a bubbling bed. In the middle of the riser there is the **'lean core- annulus region'** (noted in green), with a solid fraction of 0.01-0.025. Solids here move upwards from the center of the riser and downwards from the side. Finally at the top- exit region of the riser there is the **'exit region'** (noted in red) with a solid fraction of 0.03- 0.1. This happens because of the abrupt riser exit used. The riser exit is located 189mm below the riser top and has a 20° inclination. Due to the solids inertia it is difficult for them to achieve this "bend". Hence they collide with the top of the riser and each other and form a "denser" recirculation zone at the top of the riser as compared to the core- annulus region.

The flow structure of a CFB carbonator is a lot different than that of a CFB combustor. Due to the inventory needed the flow is much "denser". This note has to be taken into account in reactor design and modeling of such a system.

5.4 Effect of Total Solid Inventory on the pressure drop profile of the riser

As is shown in fig. 5.3 higher TSI results in higher pressure drop in the riser due to the higher availability of mass. In fig. 5.3 the riser pressure drop profile of runs with different TSI and same other operational parameters (shown in table 5.2) are plotted. The added mass, resulting in increased pressure drop when increasing TSI, is gathered mainly in the bottom part of the riser. The pressure drop at the exit of the bed does not change significantly for the different TSI with the exception of Run 53. A certain velocity in the riser has a certain solid carrying capacity. In the case of runs 36, 39 and 53 this carrying capacity is fully used. For Run 53 there is not enough inventory in the system so as for the flow to reach this maximum carrying capacity. Hence, the pressure drop at the exit of the riser is lower than the other runs of fig. 5.3. The fact that the exit of the riser exhibits a slightly increased value for Run 36 in comparison to Run 39 and 53 can be attributed to the increment of riser superficial velocity at the upper part of the riser caused by the higher aeration of the upper loop seal. Difference in loop seal aeration have no significant effect in the mass distribution between riser and standpipes since standpipes are in bubbling conditions and the therefore have a constant pressure drop gradient.

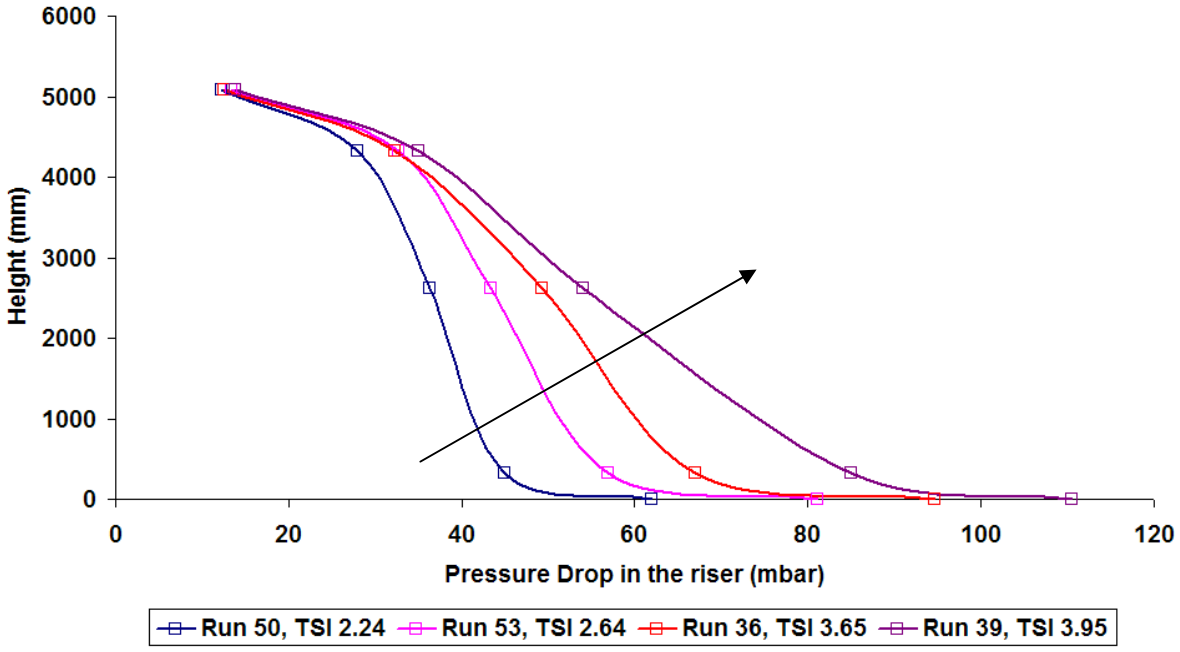

Figure 5.3: Effect of TSI on the riser pressure drop profile

Table 5.2: Operating Conditions of Runs 36. 39. 50 and 53

Run No.	u_o	TSI	P_{BFB}	A_{cone_valve}	LSU bottom air	LSU side air	LSD bottom air	Standpipe status
	m/s	kg	mbar	mm^2	m/s	m/s	m/s	up-down
36	2.98	3.65	40	5.26	0.31	0	0.09	bubbling-bubbling
39	2.98	3.95	30	5.26	0.35	0	0.07	bubbling-bubbling

50	2.98	2.24	35	5.26	0.24	0.02	0.07	bubbling-bubbling
53	2.98	2.64	35	5.26	0.35	0	0.08	bubbling-bubbling

5.5 Effect of upper loop seal aeration on the pressure drop profile of the riser

In fig. 5.4 the pressure drop profile is plotted. The set of the runs in use had the exact same operating conditions, with the parameter of upper of loop seal aeration changing from lower values (Run 33) towards higher (Run 35). In Run 35 the upper standpipe is in bubbling conditions, while in Runs 33 & 34 it is in moving bed conditions. In order to achieve bubbling conditions in the upper standpipe, one should keep increasing the upper loop seal aeration. As shown clearly in the figure, this increase in the aeration results in increasing the total pressure drops of the riser, through increasing the amount of the mass that is gathered in its lower dense area. Increasing aeration means that more air is pumped through the loop seal. Hence, as noted from equations 3.26 the pressure gradient of the upper standpipe increases. This means that lesser mass is needed to sustain the seal of the standpipe. Therefore mass is discharged from the upper standpipe to the riser. Furthermore it should be noted that the increase of the upper loop seal aeration increases only the mass at the bottom part of the riser and causes no other deviation in the upper part of the riser as noted in Figure 5.4. This happens because increasing the loop seal aeration does not increase significantly the carrying capacity of a given flow. The effect of increasing loop seal aeration is similar to increasing the TSI as shown above.

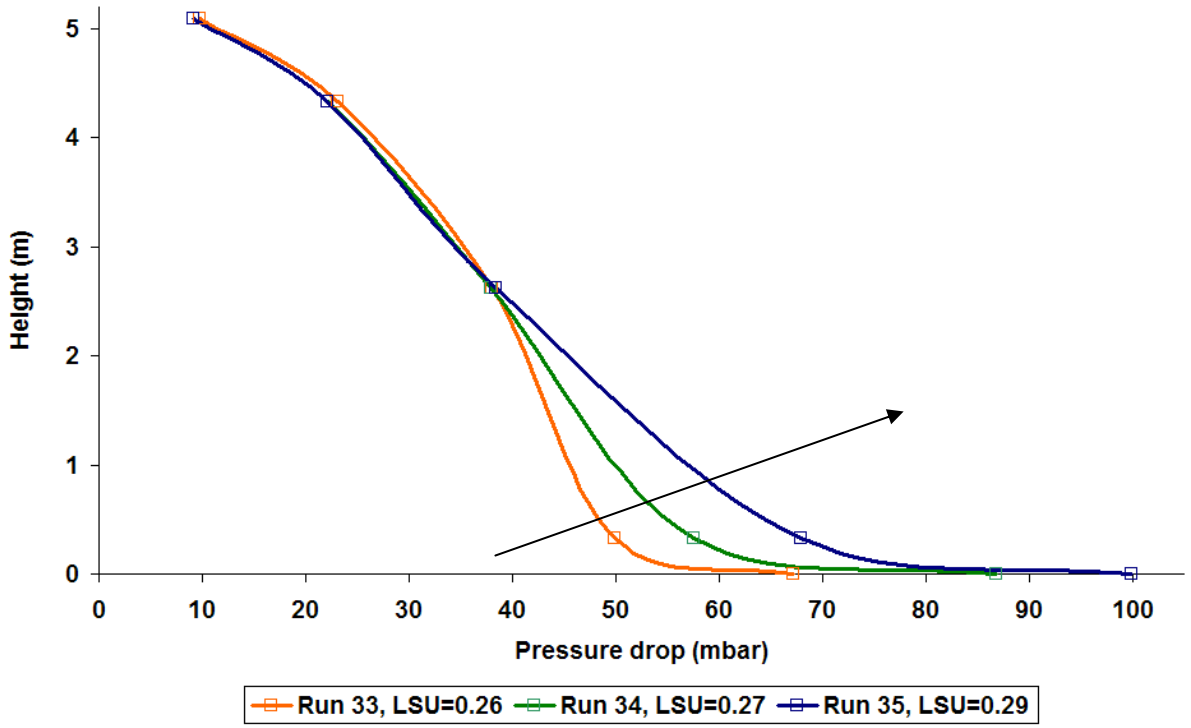

Figure 5.4: Effect of upper loop seal aeration on the pressure drop profile of the riser

Table 5.3: Operating Conditions of Runs 32. 33. 34. 35

Run No.	u_o	TSI	P_{BFB}	A_{cone_valve}	LSU bottom air	LSU side air	LSD bottom air	Standpipe status
	m/s	kg	mbar	mm^2	m/s	m/s	m/s	up-down
33	2.87	3.65	36.51	5.26	0.26	0	0.08	moving-bubbling
34	2.87	3.65	36.04	5.26	0.27	0	0.08	moving-bubbling
35	2.87	3.65	38.19	5.26	0.29	0	0.08	bubbling-bubbling

5.6 Effect of BFB pressure on the pressure drop profile of the riser

In fig. 5.5 the riser pressure drop profile for two runs that have the same operating conditions is plotted against the riser pressure drop. Differences in loop seal aeration are considered not to be significant in regard to mass distribution since the standpipes are in both cases in bubbling conditions and due to the explanation provided above. The significant parameter that changes is the BFB pressure. In Run 2 the BFB pressure was increased so as to study its results. The increase of BFB pressure results in pushing more mass through the lower standpipe into the riser. As a result, the mass loading of the riser increases, hence its pressure drop increases. This increase happens because the pressure drop of the bottom part increases. The pressure drop at the upper part remains the same as shown in fig. 5.5. The increase of mass in the CFB carbonator with increasing BFB overpressure can be explained theoretically from the pressure balance of equations (2.21 and 2.22). According to this equation when increasing the BFB pressure less mass is required in the lower standpipe so as to maintain a seal. Therefore mass from the lower standpipe is discharged to the riser.

Furthermore, it should be mentioned that the BFB overpressure plays a role on the sorbent looping rate, because through its adjustment, the cone valve discharge can be forced to take any value between 0 and the riser entrainment.

Table 5.4: Operating Conditions of Runs 1 and 2

Run No.	u_o	TSI	P_{BFB}	A_{cone_valve}	LSU bottom air	LSU side air	LSD bottom air	Standpipe status
	m/sec	kg	mbar	mm^2	m/s	m/s	m/s	up-down
1	2.45	2.24	0	5.78	0.09	0.03	0.06	moving-moving
2	2.45	2.24	20	5.78	0.09	0.01	0.07	moving-moving

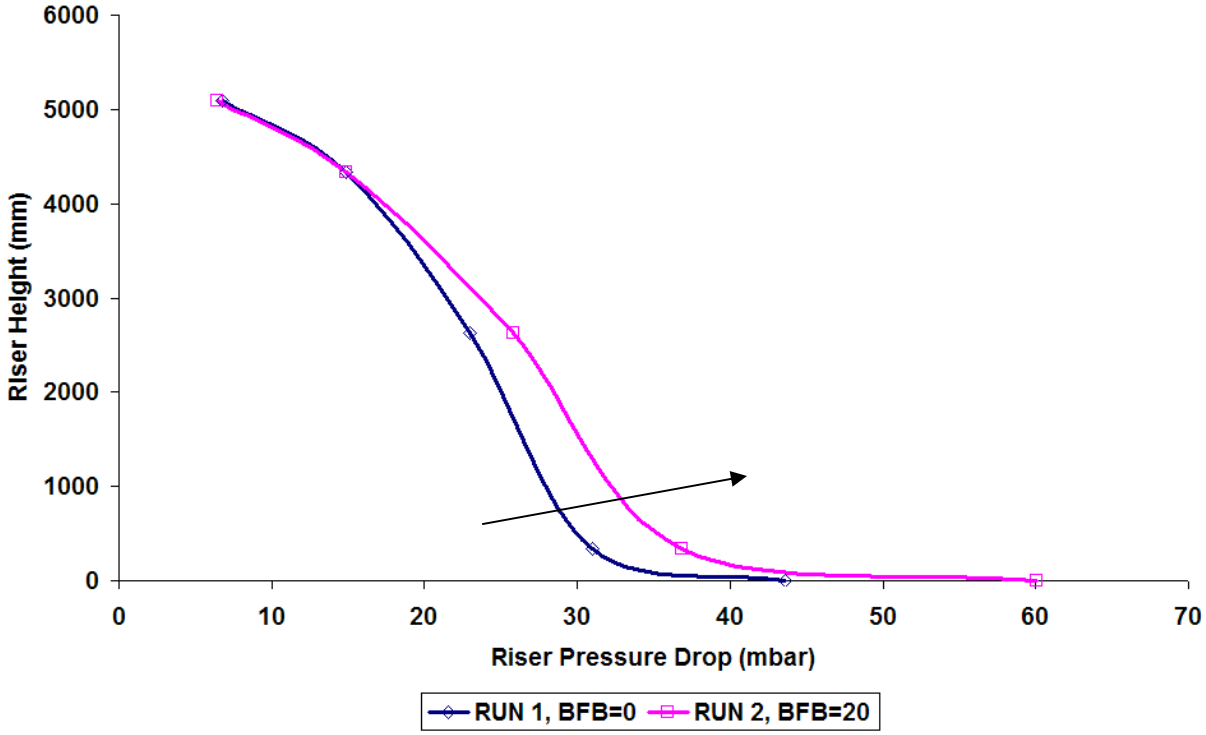

Figure 5.5: Effect of BFB pressure on the pressure drop profile of the riser

5.7 Effect of cone valve opening on the pressure drop profile of the riser

In fig. 5.6 and fig. 5.7 the cone valve discharge is plotted against the opening of the cone valve times its pressure drop. There is a linear relation for both particle sizes of the cone valve discharge Gs_cyclone and the product of the cone valve area and the pressure drop through the valve. Hence the cone valve discharge can be controlled through closing or opening the cone valve and by increasing or decreasing the absolute pressure of the BFB.

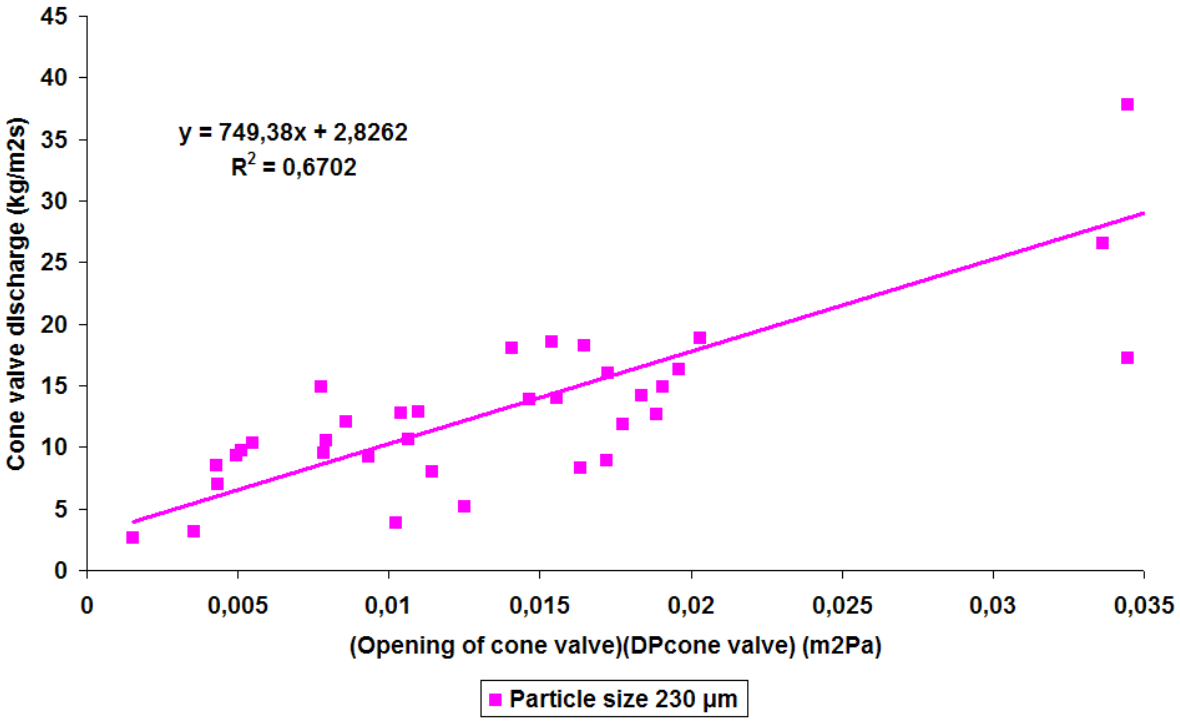

Figure 5.6: Cone valve discharge against opening of the cone valve for particle size of 230 µm

$$G_{s\_cyclone} = 749.38F + 2.8262 \text{ . with } R^2 = 0.67 \quad \textbf{(5.1)}$$

$G_{s\ cyclone}$ in (kg/m2s) and F ($A*\Delta P_{cone\ valve}$) in (m^2Pa).

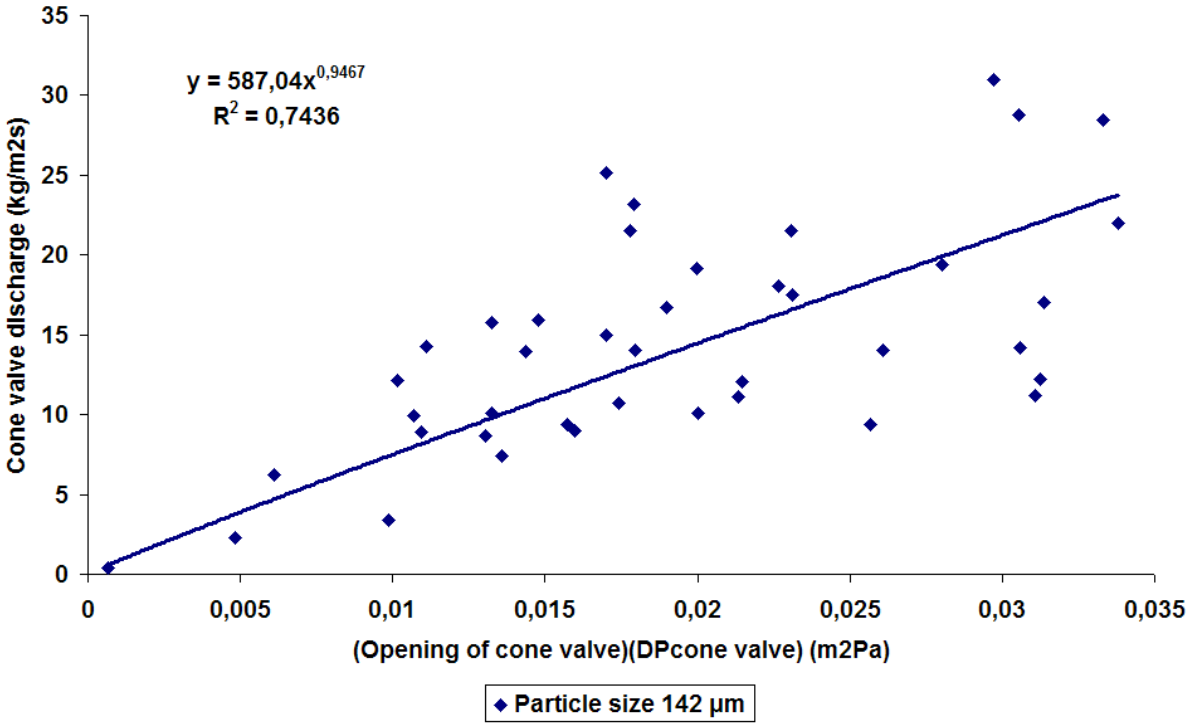

Figure 5.7: Cone valve discharge against opening of the cone valve plot for particle size of 142 µm

$$G_{s\_cyclone} = 587.04F^{0.9467} \text{ . with } R^2 = 0.74 \quad \textbf{(5.2)}$$

$G_{s\_cyclone}$ in (kg/m2s) and F ($A*\Delta P_{cone\_valve}$) in (m^2Pa).

5.8 Effect of riser velocity on riser entrainment

The parameter that has the greatest effect on the system is the riser velocity. Riser velocity affects the pressure balance of the whole system. the shape of the riser pressure profile and riser entrainment. While carrying out the experiments, the circulation rate of the cold model had to be measured. Previous work in the field has showed that there is an exponential equation connecting the riser superficial velocity and the flow rate of the cyclone. The experimental data of the higher particle size showed exactly the same behaviour and the trendline that resulted. has very nice fit. Hence, it can be stated that the riser velocity is the primary parameter affecting the riser entrainment. The secondary effect of the riser inventory on the riser entrainment can be shown by the elevated riser entrainment values depicted for higher TSI. The effect of the TSI on the riser entrainment is small for lower velocities and is amplified at higher velocities. All of the above are clearly shown in the figure 5.8 and 5.9 for both particle sizes.

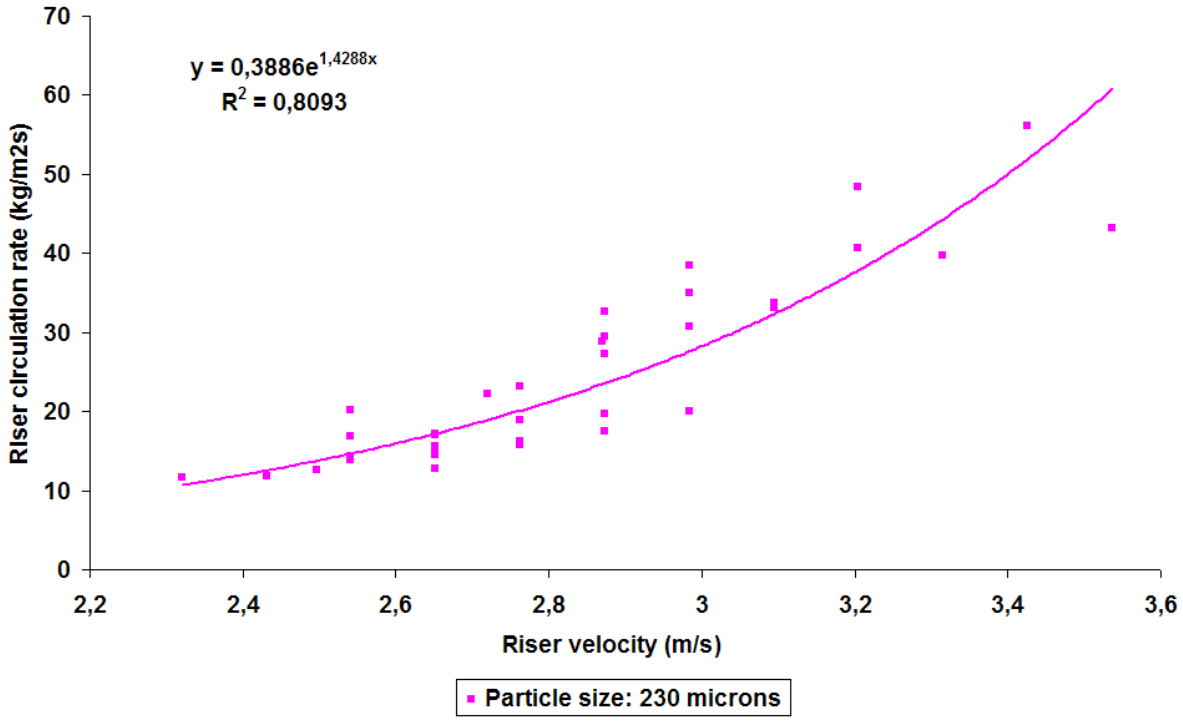

Figure 5.8: Riser circulation rate versus riser velocity for particle size of 230 µm

$$G_{s\_cyclone} = 0.3886e^{\,1.4288U_o} \text{ with } R^2 = 0.81 \qquad \textbf{(5.3)}$$

$G_{s\_cyclone}$ in (kg/m^{2}s) and Uo in (m/s).

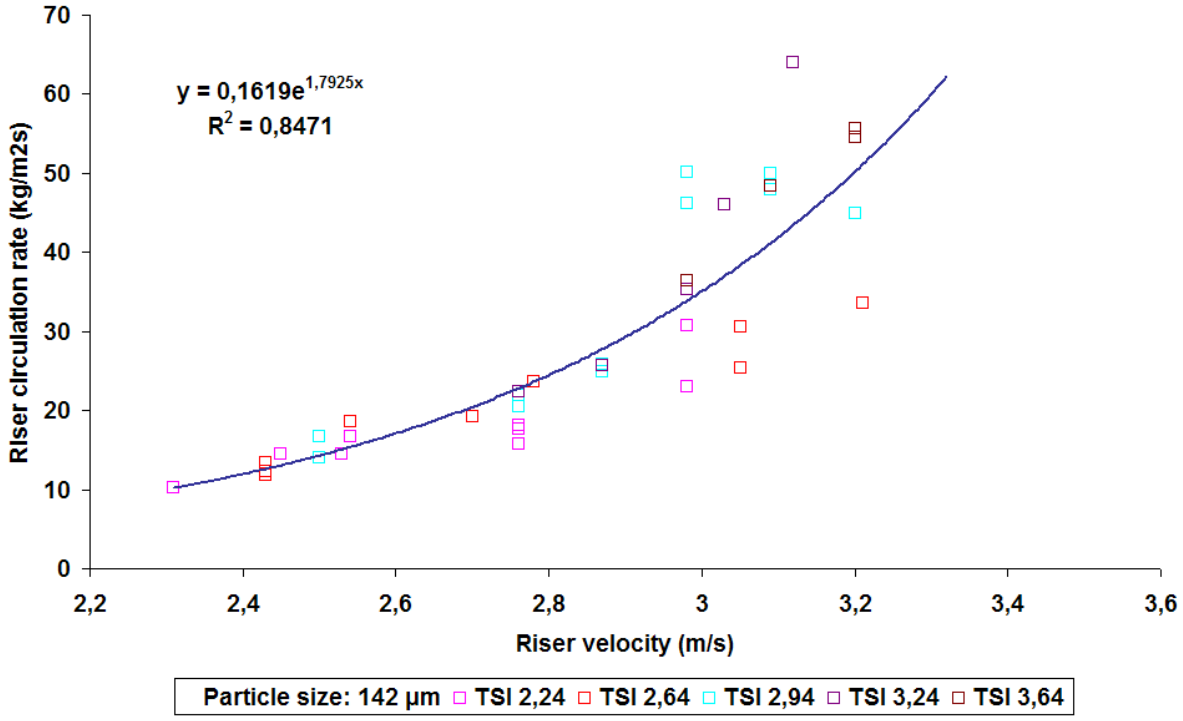

Figure 5.9: Riser circulation rate versus riser velocity for particle size of 142 µm

$$G_s = 0.4804e^{\,1.7397U_o} \text{ with } R^2 = 0.85 \qquad \textbf{(5.4)}$$

$G_{s\_cyclone}$ in (kg/m^{2}s) and Uo in (m/s).

5.9 Effect of riser velocity on the pressure drop through the cyclone

As already stated, the pressure drop in the cyclone takes part in closing the pressure drop loop balance, according to the know pressure balance equations 2.21 and 2.22.

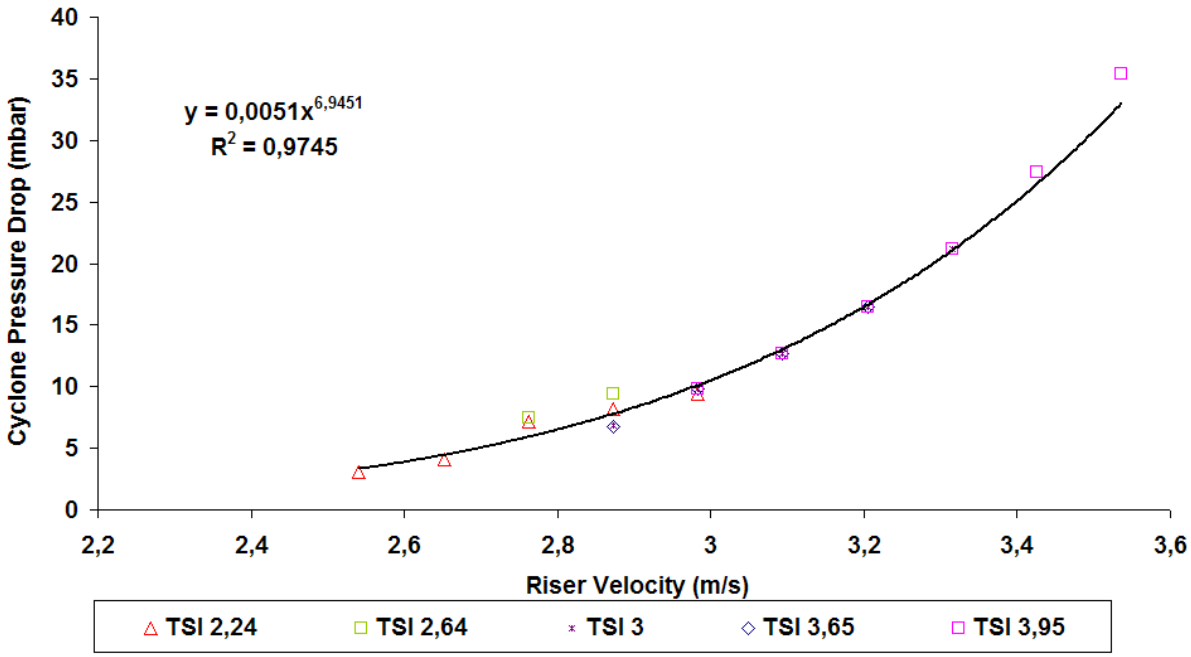

Figure 5.10: Cyclone pressure drop against riser velocity for particle size of 230 µm

$$\Delta P_{cyclone} = 0.0051 U_o^{6.9451} \text{ with } R^2 = 0.97 \quad \textbf{(5.5)}$$

ΔP in mbar. Uo in m/s.

To begin with, the results for higher particle size showed (as shown in fig. 5.10) that there is a strong relationship between the pressure drop in the cyclone and the velocity of the riser. For velocities lower than 3m/s. the values of the cyclone pressure drop are relatively low (reaching 10 mbars maximum), whilst for a range of values from 3 m/s to 3.5 m/s. this value rises up to 40 mbars, resulting in an increase of 450%. The experimental work showed that when the boundary velocity of the 2.8- 3m/s is exceeded the cyclone starts to show significant pressure drop. When fitting the cyclone pressure drop against the superficial velocity, the equation of 5.5 is obtained. When plotting the cyclone pressure drop against superficial riser velocity of the riser for the 142 µm a similar graph and a similar equation are obtained as shown in fig. 5.11 and eq. 5.6. However, the pressure drops through the cyclone seem milder for the lower particle size.

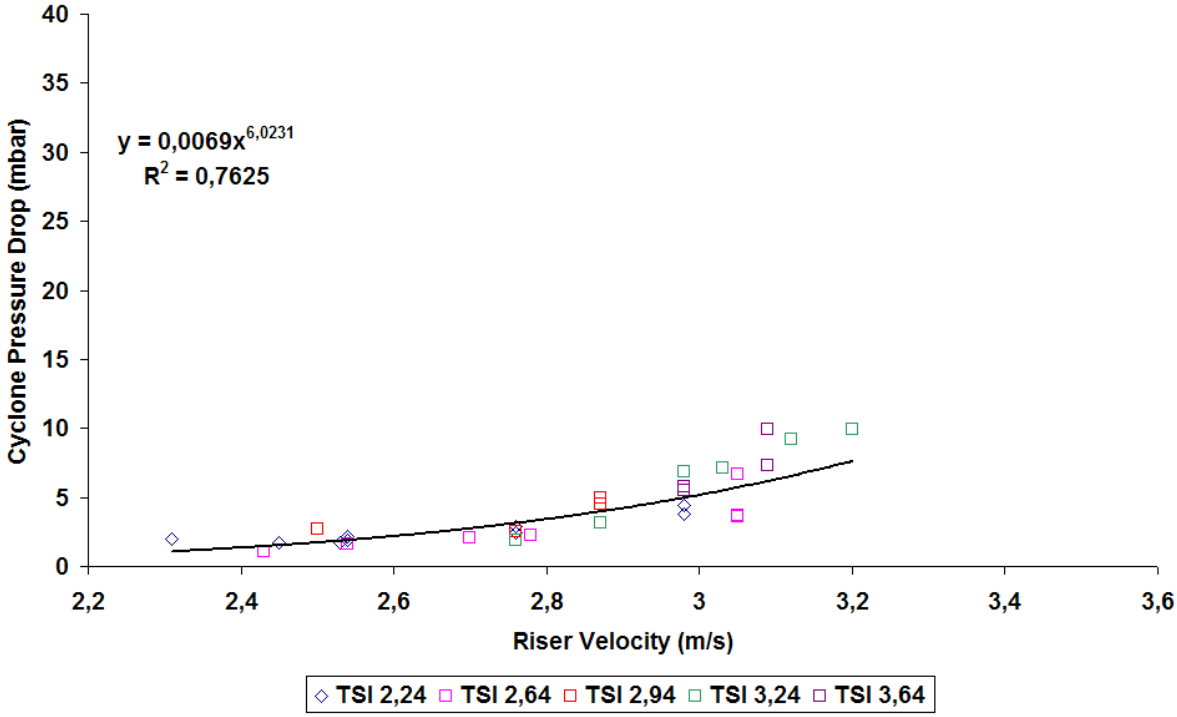

Figure 5.11: Cyclone pressure drop against riser velocity for particle size of 142 µm

$$\Delta P_{cyclone} = 0.0069 U_o^{6.0231} \text{ with } R^2 = 0.76 \quad \textbf{(5.6)}$$

ΔP in mbar. Uo in m/s.

The cyclone pressure drop is included in the right hand side of the pressure balance equations (eq.2.17. 2.19). This means that increasing cyclone pressure drop leads to a mass distribution of the given mass in the pressure balance loops that is less favourable for the riser. In other words higher cyclone pressure drops for a given situation results in lesser inventory for the carbonator.

5.10 Effect of upper loop seal aeration on upper loop seal pressure drop

In fig. 5.12 and 5.13 the upper loop seal pressure drop is plotted against its aeration. With increasing riser velocity, the upper loop seal aeration has to be increased in order to maintain a high standpipe pressure drop gradient. For most of the runs with 230 µm particle size this means bubbling conditions in the standpipes, while for most of the runs with 142 µm particle size this means short standpipes. For the particle size of 230 µm in fig. 5.12 it is stated that with increasing upper loop seal aeration the pressure drop through the loop seal decreases. This happens because more and more mass is led out of the recycle chamber of the loop seal, resulting in lowering the mass in the recycle chamber and hence the pressure drop through the loop seal. When plotting the same pressure drop for this particle size with the riser superficial velocity it is produced a very similarly shaped plot as showed in Annex 2. This is because the riser velocity and loop seal aeration are interconnected. On the other hand when plotting the pressure drop through the upper loop seal against aeration for particle size of 142 µm, if fig. 5.13 is checked, a scattered profile is witnessed there. However, most of the data is located between 15- 20 mbar. That can be attributed to the fact that while conducting the experiments for the particle size of 142 µm the loop seal aeration was much less than for the experiments conducted for the particle

size of 230 µm. Therefore for the 230 µm a very dilute loop seal recycle chamber existed in contrast to the 142 µm particle size where a bubbling bed existed in the recycle chamber.

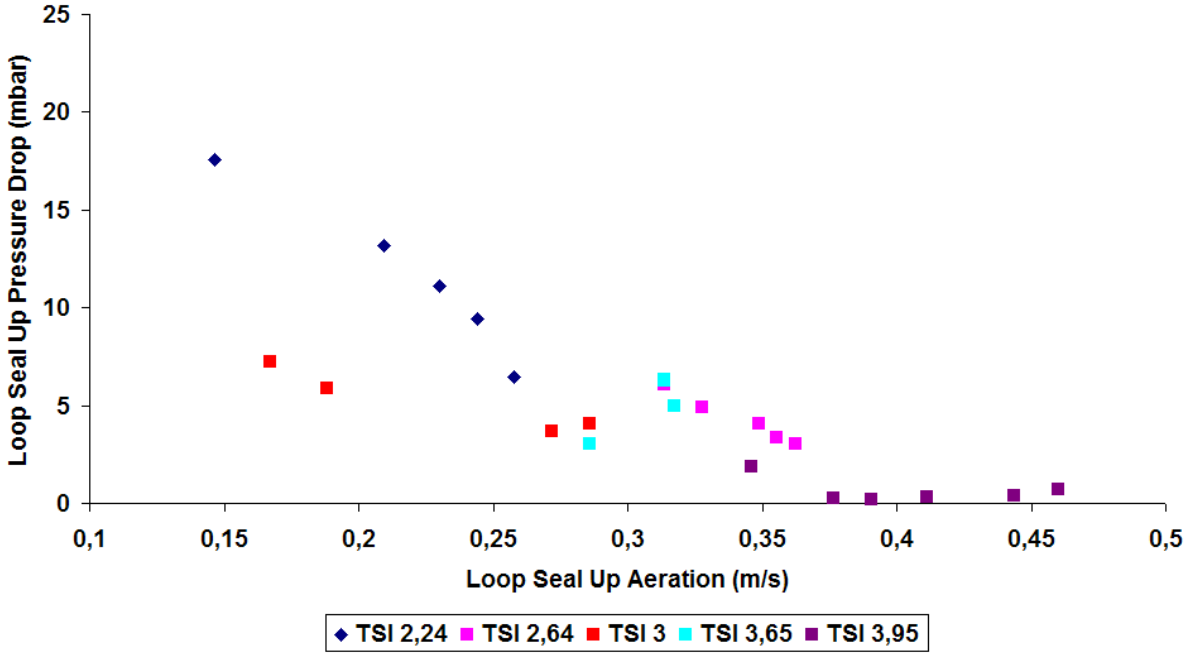

Figure 5.12: Upper Loop Seal pressure drop versus Upper Loop Seal Aeration for particle size of 230 µm

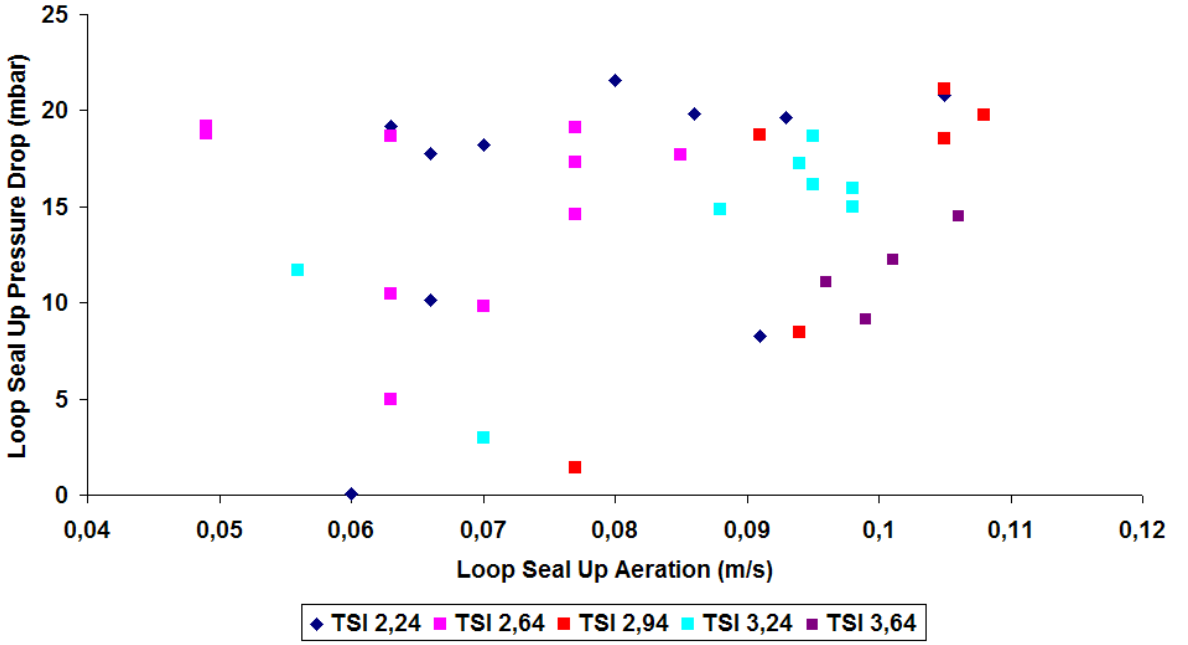

Figure 5.13: Upper Loop Seal pressure drop versus Upper Loop Seal Aeration for particle size of 142 µm

5.11 Effect of lower loop seal aeration on lower loop seal pressure drop

In 3 and 4 of the annex the loop seal down pressure drop is plotted against the riser velocity for both particle sizes. For both particle sizes, it can be stated that the loop seal down pressure drop is more or less constant since it ranges generally from 8- 16 mbars. Solid flows through the lower loop seals are never as high as those from the upper loop seal. Therefore the loop seal aeration and pressure drop through the loop seals are not interconnected with the riser velocities. Hence, the recycle chamber of the lower loop seal is for both particle sizes are in mild bubbling conditions.

5.12 Effect of riser velocity on the pressure drop of the riser bottom part

The lowest part of the riser (0mm – 333 mm) is called riser bottom. This region mainly exhibits a dense bed flow structure with bubble phase and emulsion phase. This region is below the entrance of the loop seals and therefore the pressure drop of this part does not participate in the pressure loop. However it can function as a mass source or sink for the pressure balance loops, when altering conditions. Firstly, the pressure drop in the bottom region is firstly dependant on the TSI, hence the available mass. Furthermore, for velocities before the critical velocity of 3m/s there is generally a mild decrease of pressure drop, with increase of velocity. A possible explanation maybe that increased velocity leads to lower solid fraction in the dense region, as predicted by the K-L two phase model [14] and because of the ability of the flow due to its higher velocity to entrain more mass to the upper region of the riser. For higher velocities it is more than obvious that the riser bottom starts emptying more rapidly (decrease of mass happens at higher slope). This can be explicitly seen for both particle sizes. The added reason causing this phenomenon maybe the increased pressure drops produced by the cyclone when increasing velocity as described in the section above. When increasing the velocity in the range above 3m/sec. increasingly more mass is needed in the standpipe so as to cope with the increased cyclone pressure drops. Part of this mass is supplied by the decrease of mass in the bottom. In large TSIs where the spectrum of velocities consists of really high velocities, this behaviour is so intense, that the dense bed almost got empty, as it is shown in the chart (pressure drop that close to 0 mbars means that the dense bed is almost empty). This behaviour is exhibited in fig. 5.14 and 5.15.

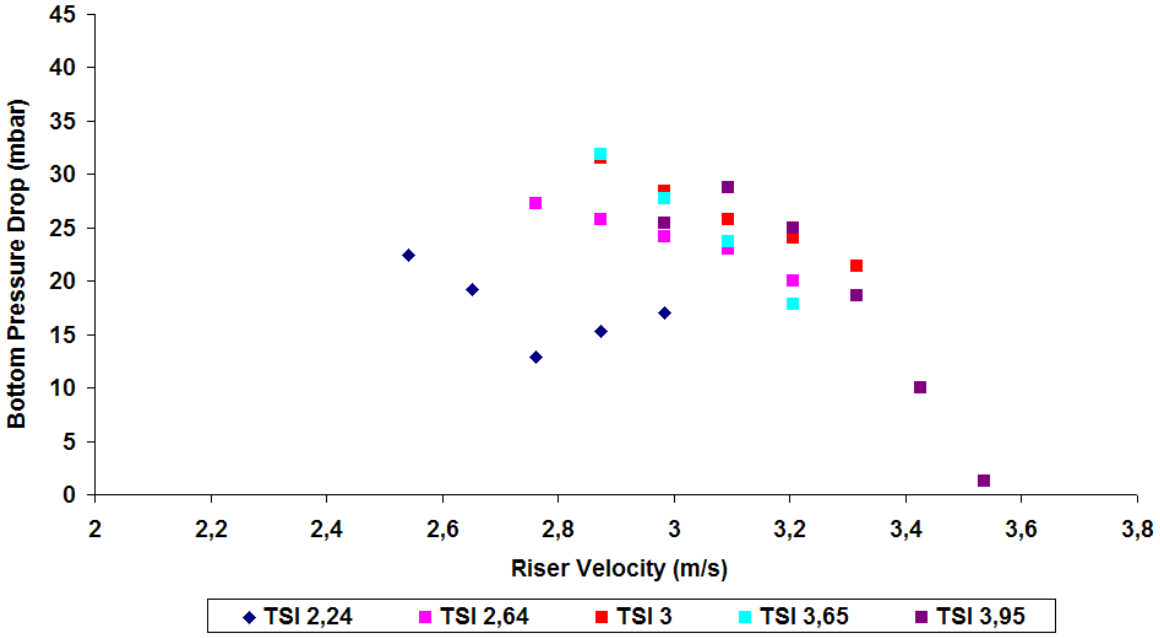

Figure 5.14: Bottom pressure drop versus riser velocity for particle size of 230 µm

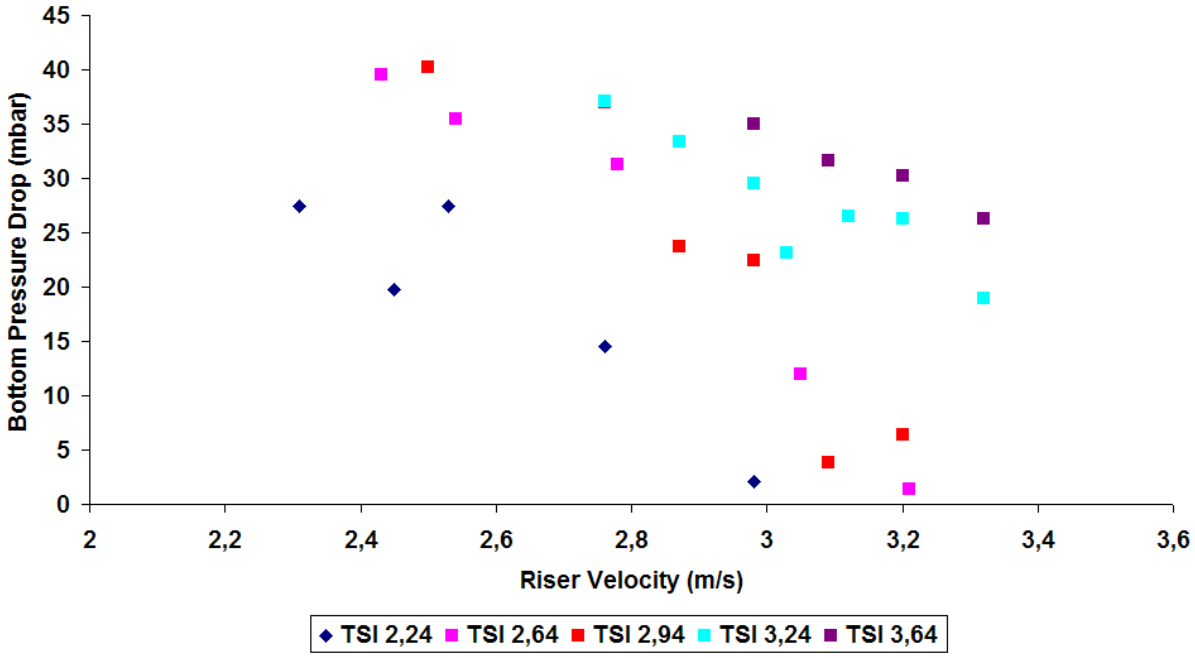

Figure 5.15: Bottom pressure drop versus riser velocity for particle size of 142 µm

5.13 Effect of riser velocity on the pressure drop of the riser upper part

In fig. 5.16 and 5.17 the riser top pressure drop is plotted against the riser velocity for both particle sizes. Also here the most important parameter for this pressure is the TSI. However velocity plays also a significant role. For the particle size of 142 µm it is witnessed that for velocities below the critical 3m/s. the total mass which is gathered in the riser top increases with

the increase of the riser velocity, because (as already stated in previous chapter) the mass moves from the bottom part, towards the upper part. The increase of the pressure drop of the cyclone is below 3 m/s insignificant and therefore mass from the bottom region is distributed between the upper region and the standpipe. That is the case for the particle size of 230 μm only for the few runs conducted with velocities below 2.8 m/s. On the other hand, when 3 m/s is exceeded, the cyclone pressure drop become significant and hence the riser top pressure drop starts decreases while mass is accumulated in the standpipes so as to counterbalance the cyclone pressure drop, as described in equations 2.21 and 2.22.

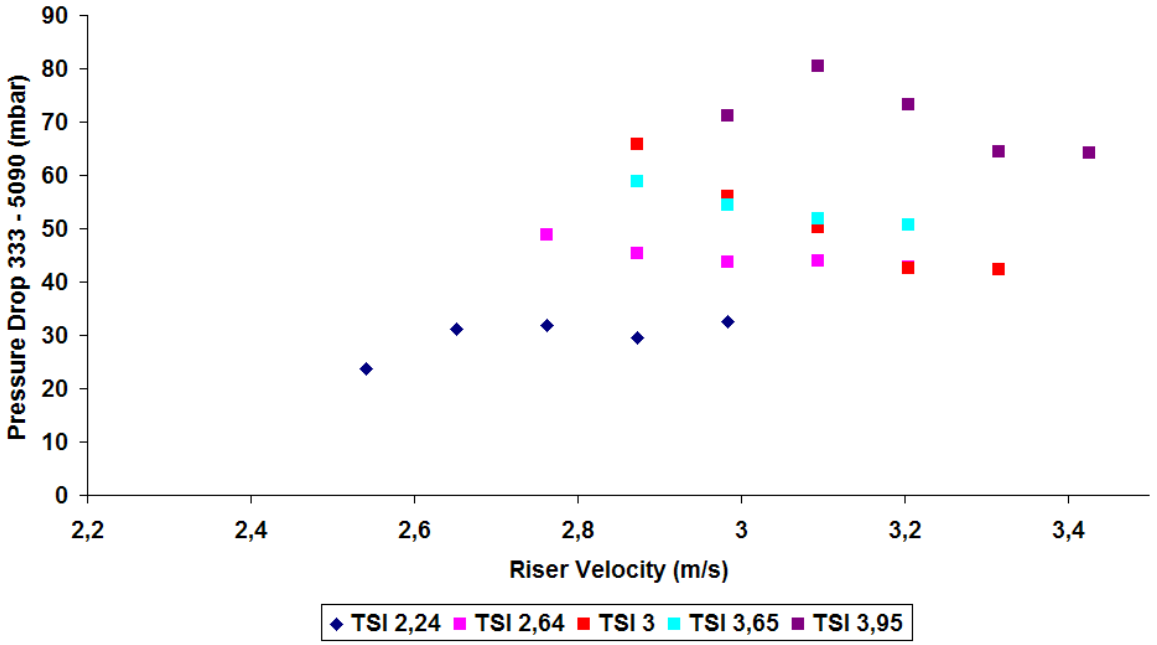

Figure 5.16: Pressure Drop Riser Top versus Riser velocity for particle size of 230 μm

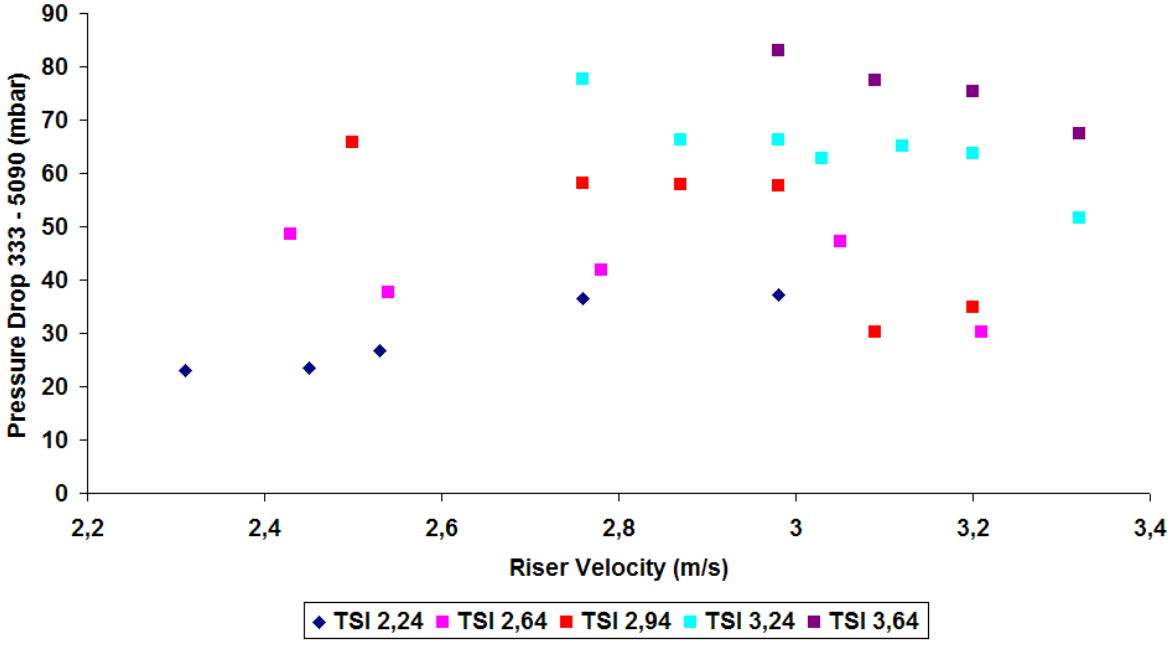

Figure 5.17: Pressure Drop Riser Top versus Riser velocity for particle size of 142 μm

5.14 Effect of riser velocity on the pressure drop of the riser exit part

As shown in fig. 5.18 and 5.19, the pressure drop in the riser exit increases with the increase of riser velocity. This happens because the carrying capacity of the flow increases when increasing velocity. For the highest velocities of operation the pressure drop at the exit of the riser seems to be rather constant or even decrease a little. The reason here may either lay in that the exit region is saturated or in the high pressure drops through the cyclone. In the first case, the exit region has reached the maximum solid voidage it can take under these conditions, while in the second this would mean that the increased mass needed in the standpipes so as to overcome the increased cyclone pressure drops is enough so as to reduce the mass in this section also. Empirical equations describing the dependence of pressure drop at the exit of the riser and riser superficial velocity have been already given in previous chapters.

The pressure drop at the exit of the riser is a strong indicator of riser entrainment. This is shown also by own data. A "valve like" behaviour of the riser exit is observed in the sense that more pressure drop in this region leads to higher riser circulation rates, as shown in Fig. 5.20 and Fig. 5.21 for the 230 μm and 142 μm respectively. The empirical equation describing this behaviour for the 230 μm particle size is already given in previous chapter.

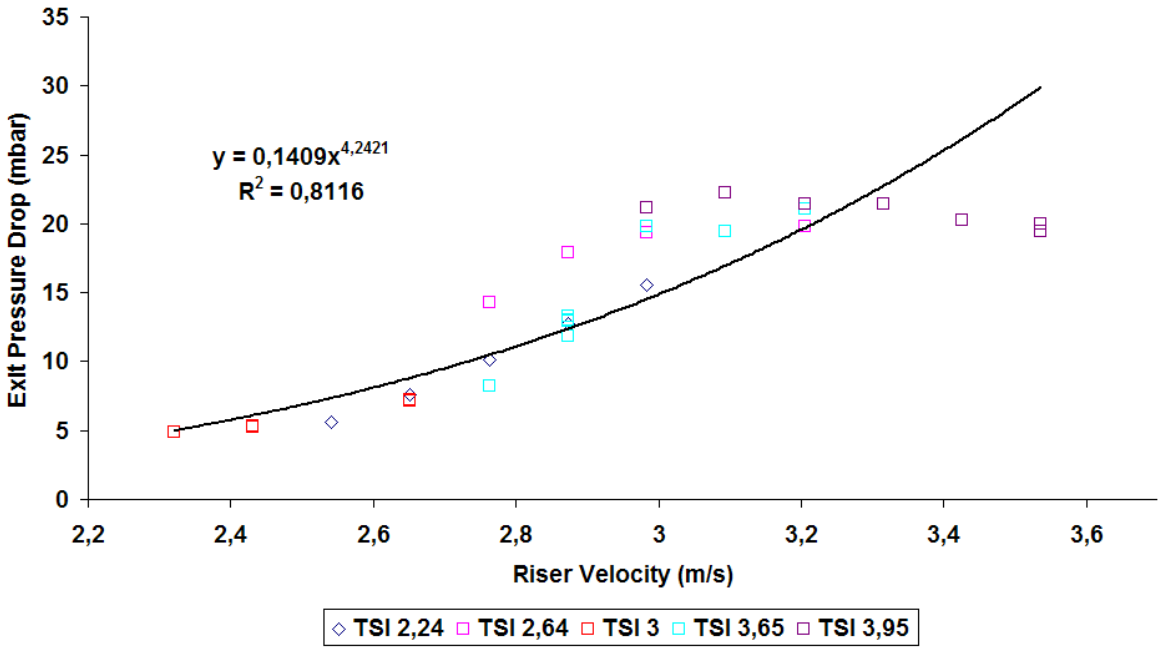

Figure 5.18: Exit pressure drop versus riser velocity for a particle size of 230 μm

$$\Delta P_{exit} = 0.1409 U^{4.2421} \text{ with } R^2 = 0.81 \quad \textbf{(5.7)}$$

ΔP in mbar and U in m/s.

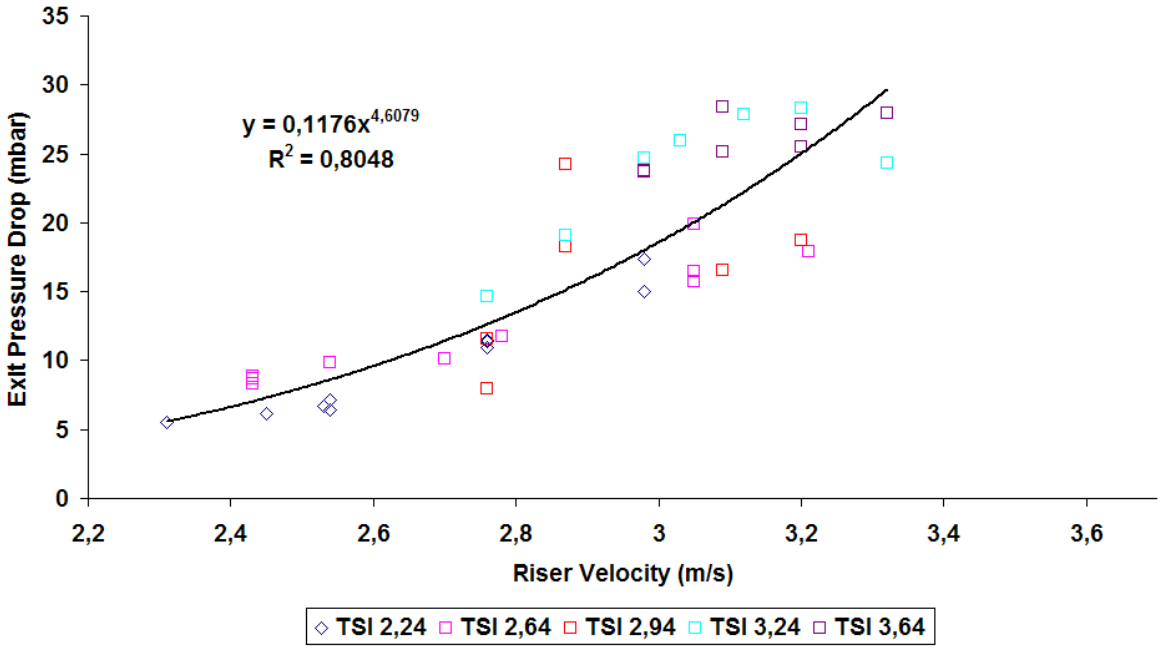

Figure 5.19: Exit pressure drop versus riser velocity for a particle size of 142 µm

$$\Delta P_{exit} = 0.1176U^{4.6079} \text{ with } R^2 = 0.80 \quad \textbf{(5.8)}$$

ΔP in mbar and U in m/s.

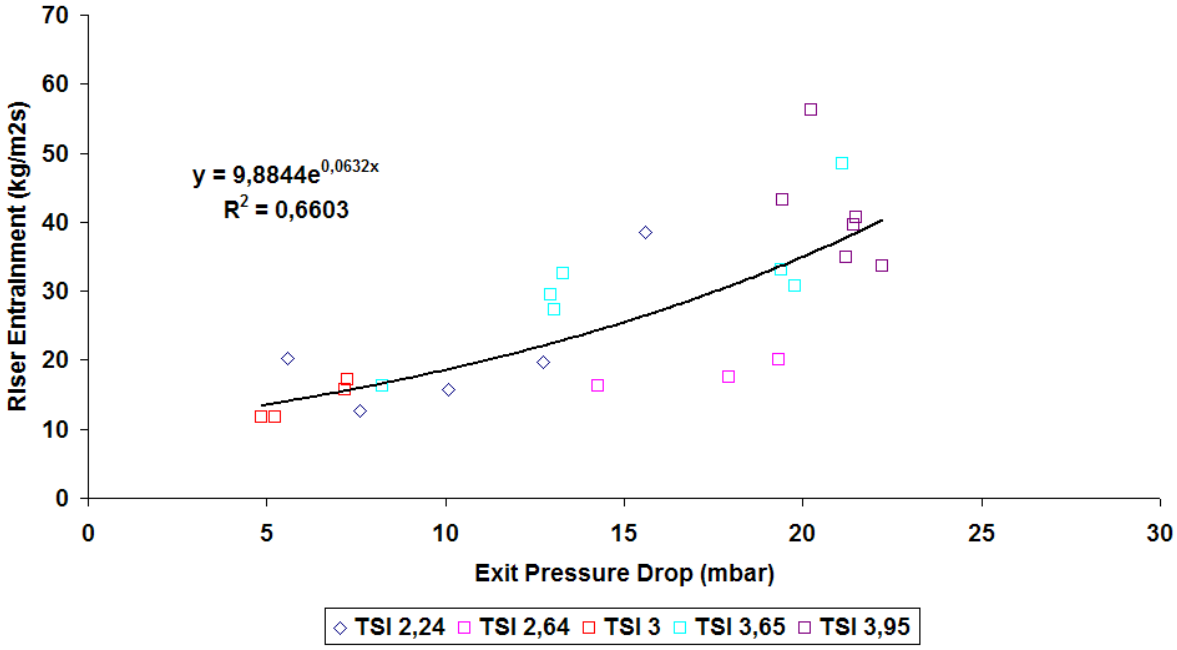

Figure 5.20: Riser Entrainment versus exit pressure drop for particle size of 230 µm

$$G_{s\_cyclone} = 9.8844e^{0.0632\Delta P_{exit}} \text{ with } R^2 = 0.66 \quad \textbf{(6.9)}$$

Gs in kg/m2s and ΔP in mbar.

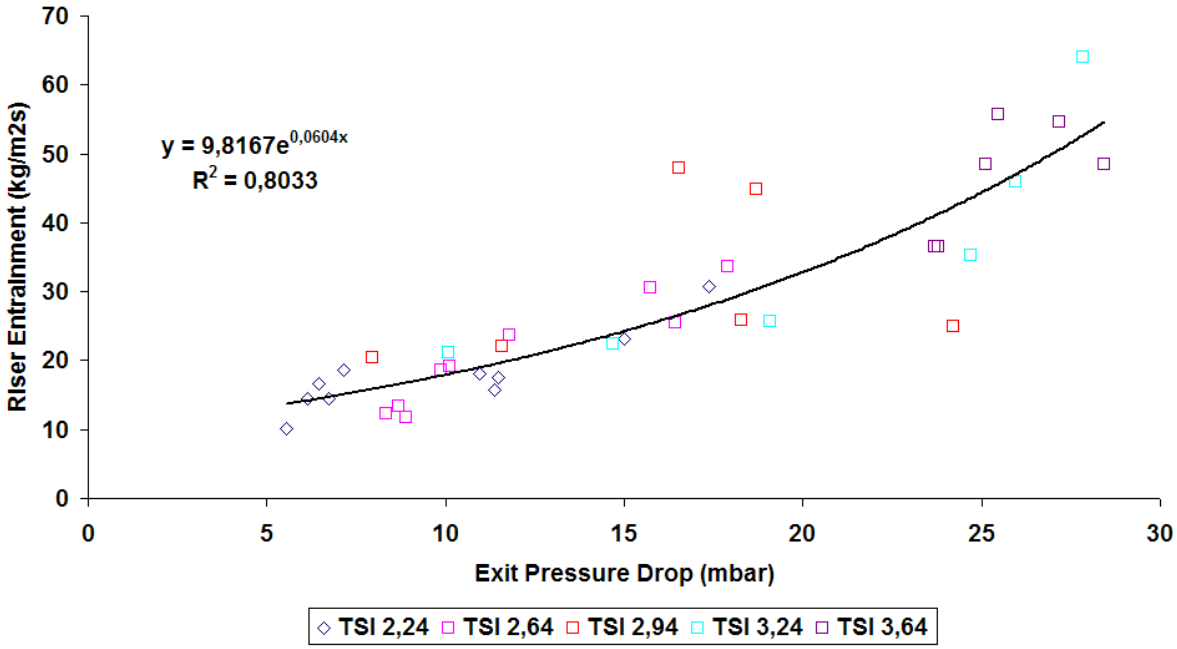

Figure 5.21: Riser Entrainment versus exit pressure drop for particle size of 142 µm

$$G_{s\_cyclone} = 9.8167e^{0.0604\Delta P_{exit}} \text{ with } R^2 = 0.80 \quad \textbf{(6.10)}$$

Gs in kg/m2s and ΔP in mbar.

5.15 Upper and lower pressure balance equilibrium

Earlier pressure balance equations are formulated as eq. 2.21 and 2.22. In order to prove that the pressure balance "closes" according to these equations, the right hand side and left hand side of these equations have been plotted in the same graph. Hence in fig. 5.22 and 5.23 it is witnessed that for both particle sizes, as far as the upper pressure balance equilibrium is concerned, the circuit "closes", and the left part of the equation matches the right part, noted with "R" and "L" in the graph. Small deviations can be attributed to measurement errors. The pressure drops of the different parts of the facility is presented for all runs and for experiments conducted for both particle sizes in tabular form in table 2 and table 3 of the Annex 7-8. In all cases the experimental data is in accordance with the pressure balance equations. Same behaviour applies for the lower pressure balance equilibrium, and the corresponding graphs can be found for both cases inn 5 and 6 of the Annex. In all graphs and cases it is noted that the left part of the pressure balance equilibrium equations, matches its corresponding right.

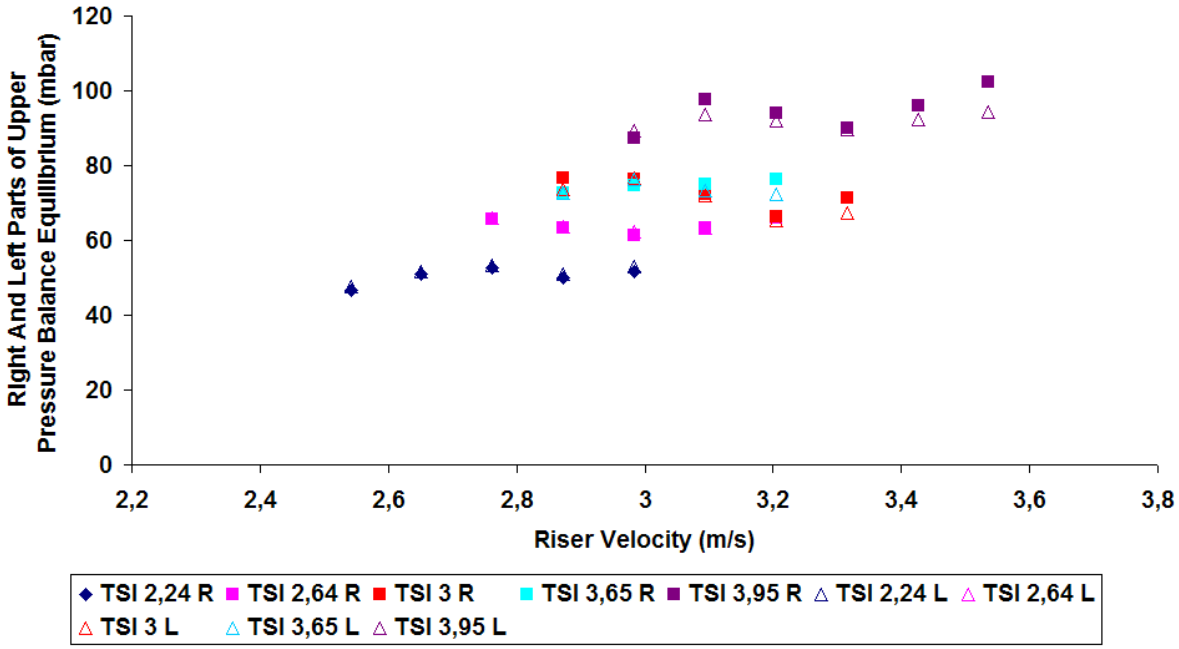

Figure 5.22: Upper pressure balance equilibrium for a particle size of 230 µm

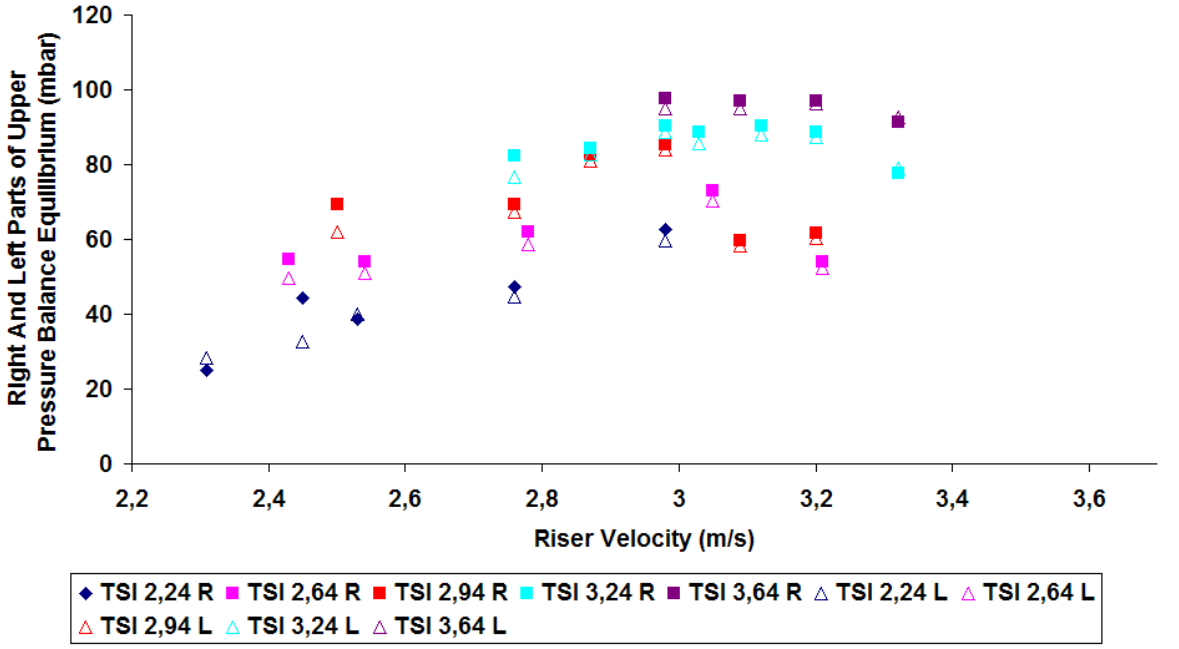

Figure 5.23: Upper pressure balance equilibrium for a particle size of 142 µm

5.16 Summary of hydrodynamic behaviour versus riser superficial velocity

In fig. 5.24 the pressure balance of different parts of the installation is plotted, against the riser superficial velocity, so as to summarize conclusions made for system hydrodynamic behaviour made in earlier section.

With increasing velocity:

- **the sum of the pressure drops of the upper loop seal plus the cyclone pressure drop always increase**. Same behaviour applies for increasing velocity for the sum of the pressure drops of the lower loop seal plus the pressure drop of cyclone. This is shown in fig. 5.24.
- **pressure drop of the bottom part of the riser decreases**. as shown in fig. 5.24. This means that increasing velocity leads to transfer of mass away from the bottom part of the riser.
- **The pressure drop of the upper part of the riser for most of the runs decreases** since the corresponding rise of the pressure drop through the cyclone is for velocities above 2.8- 3 m/s significant. This is the case in Fig. 5.24. This means the mass reduced from the bottom region and additional mass from the upper region are transferred to the standpipes. However, for velocities where the cyclone contribution is insignificant an increase in velocity leads to an increase of the pressure drop and hence the mass in the upper part of the riser as shown in fig.5.16 and 5.17 for velocities below 2.8- 3m/s.
- **Increases entrainment and pressure drop at the riser exit.** (This is demonstrated in fig. 5.18, 5.19). It is a result of the increased solid carrying capacity of the flow with increasing velocity.

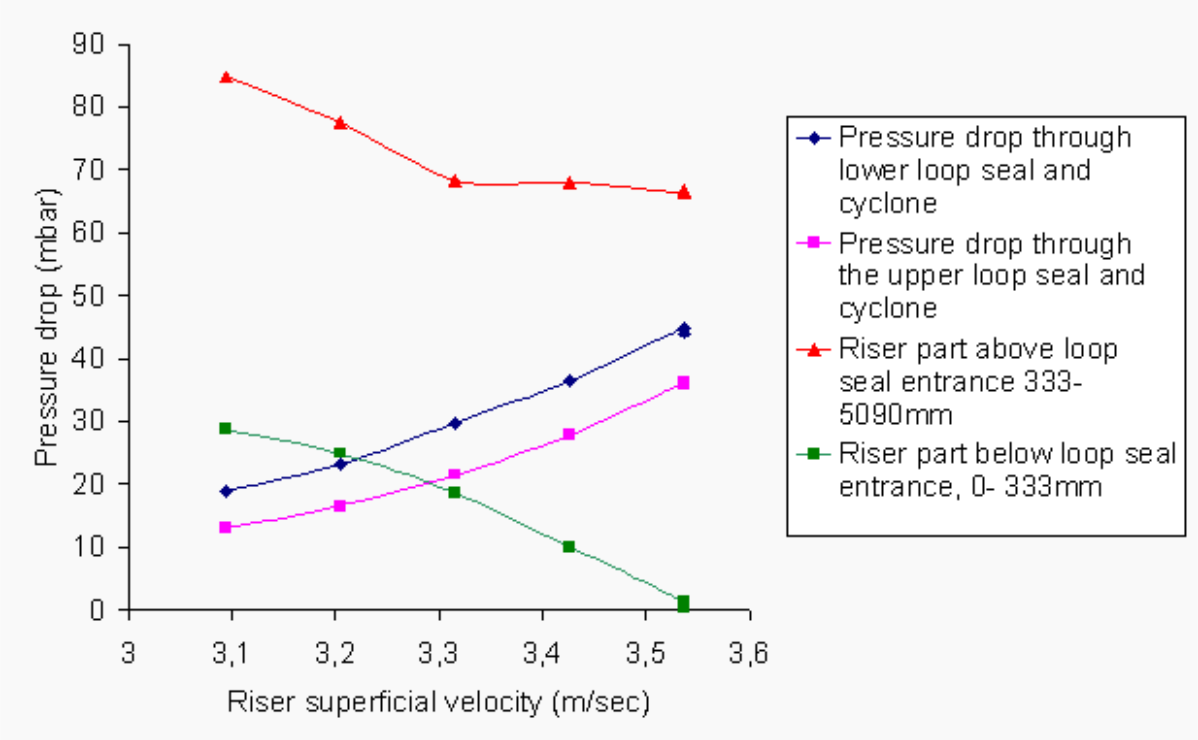

Figure 5.24: General plot of pressure drops plotted against the riser velocity

Table 5.5: Operating Conditions

Run No.	u_o	TSI	P_{BFB}	A_{cone_valve}	LSU bottom air	LSU side air	LSD bottom air	Standpipe status
	m/s	kg	mbar	mm^2	m/s	m/s	m/s	up-down
40	3.09	3.95	46.39	5.26	0.38	0	0.08	bubbling-bubbling
41	3.20	3.95	28.74	5.26	0.39	0	0.08	bubbling-bubbling
42	3.32	3.95	27.95	5.26	0.41	0	0.08	bubbling-bubbling
43	3.43	3.95	28.96	5.26	0.44	0	0.08	bubbling-bubbling
44	3.54	3.95	29.41	5.26	0.46	0	0.09	bubbling-bubbling

5.17 Effect of the particle size

One of the main objectives of this experimental work was to find, analyze and describe the particle size effect on the operational parameters of the cold model in use. as already stated. At this point it should be stated that Bidwe's work [40] provided results for a mean particle size of 142μm whilst experiments of this thesis were carried out with a mean particle size of 230μm (called in this thesis "higher particle size"). The results of this work are discussed here and they are cross-checked with the ones given by Bidwe's work [40].

5.17.1 Effect of particle size on the operating window

In both cases the cold model was ran with different TSI, so as to indentify the operating window. The main objective was to observe whereas there is an effect of the particle size in the operating window, therefore the TSI in use was kept the same, so as to have the same operational conditions. As it is stated in figure 5.25, the operational window for higher particle size moves upwards (more mass in the system results in higher total pressure drops) and to the right, meaning that for same TSIs, more air flow is needed to lift the same amount of mass. This result was expected, because it is common knowledge that higher particle size means more mass per particle. Hence, the bigger particles are heavier and need more air to be lifted according to the experimental needs. More air, means more riser velocity and therefore for same TSIs, the spectrum of the operational velocities moves to the right, whilst both minimum and maximum velocities increase. In the same time it is observed that the operational window moves upwards as well. This happens because the heavier particles are more difficult to be lifted, hence more difficult to leave the riser and accumulate in different parts of the cold model, as in the standpipes or the loop seals. As already discussed, this is the expecting behaviour from the rise of the velocity. As a result, more percentage of the mass remains in the riser, and for same TSIs, lifts its total pressure drop, making the operational window to move upwards, because the riser now operates in a higher spectrum of total riser pressure drops.

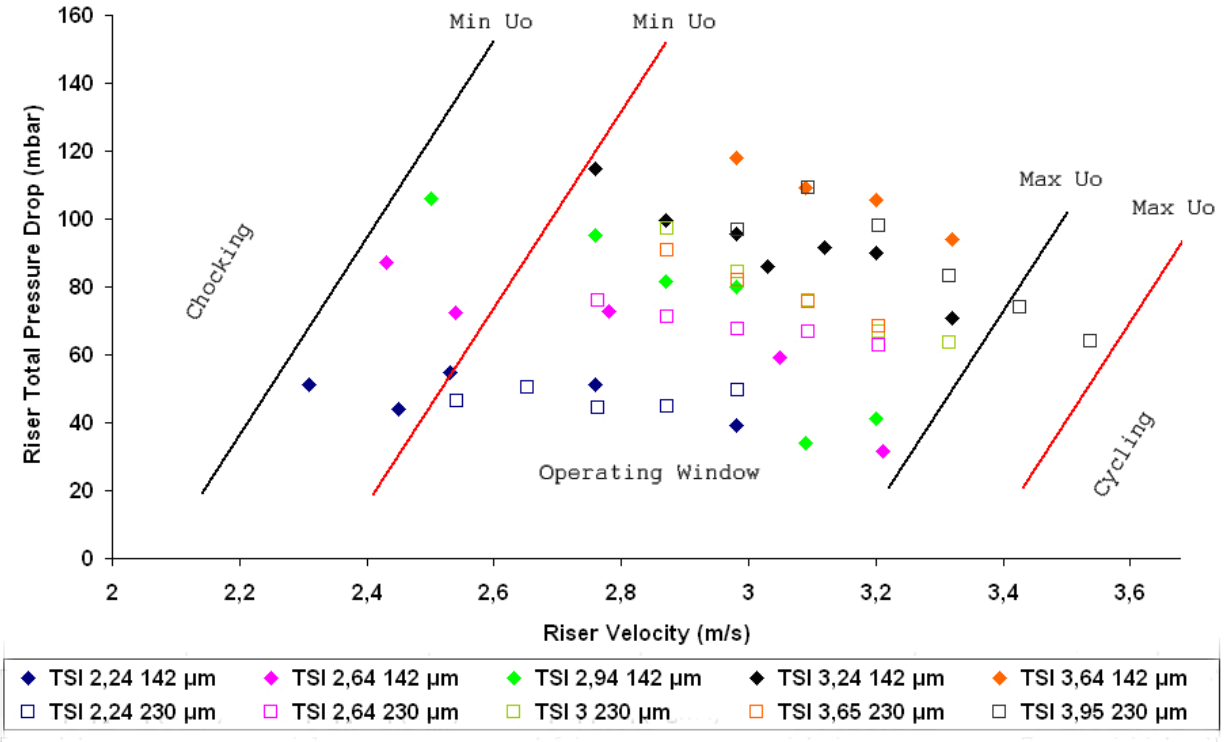

Figure 5.25: Particle size effect on operating window

5.17.2 Effect of particle size on Riser Entrainment

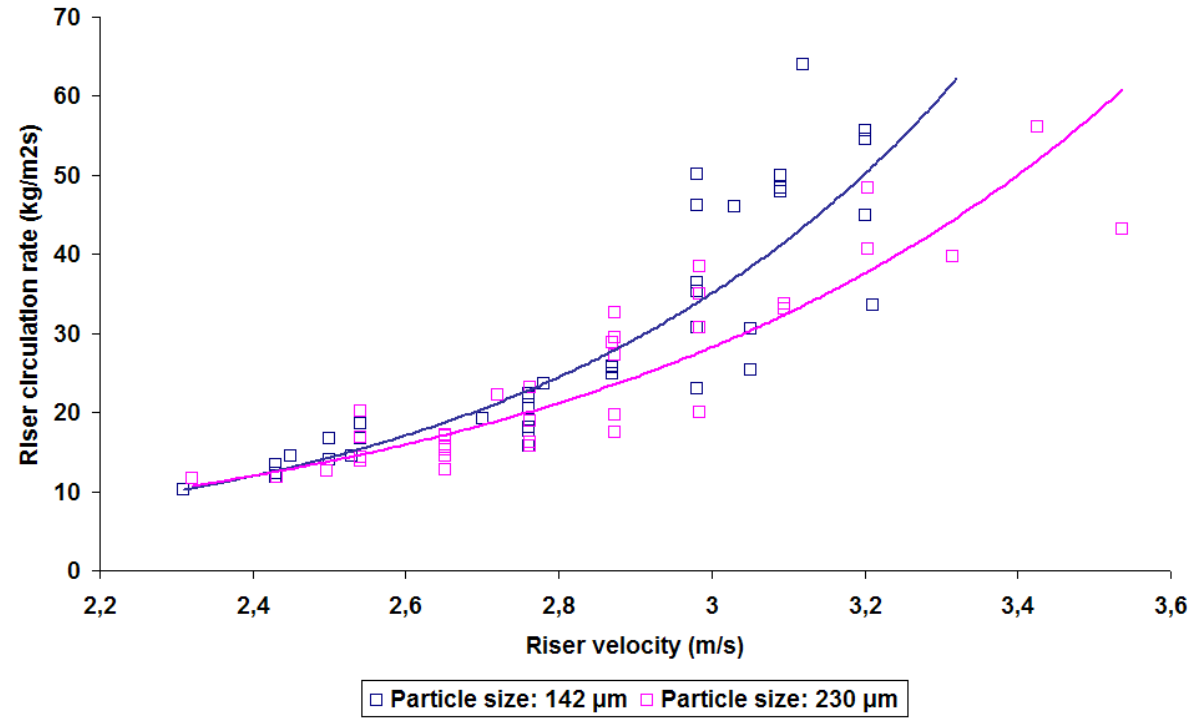

Figure 5.26: Particle size effect on riser circulation rate

The experiments with the higher particle size of 230 μm showed a similar behaviour to the ones with the lower particle size of 142 μm, meaning that as it is stated in figure 5.26, there is an exponential behaviour between riser circulation rate and riser velocity with really nice fit for both cases as shown in eq. 5.3 and 5.4. Furthermore, it is sure that for same velocities, the higher particle size experiments had less circulation rate in the riser than the one with the lower particle size. That is another effect of the particle size and this happens because higher particle size means more inertia for same velocities. This result in diminishing the ability of the riser to lift up the mass provided and hence the higher particle is more difficult to be circulated. The given equations for both particle sizes have been already noted as eq. 5.3 and eq. 5.4.

5.17.3 Effect of particle size on cone valve discharge

As it is shown in fig. 5.27, the particle size has little effect on the cone valve discharge and is related mostly with the product of the cone valve opening and the pressure drop through it. Results for both particle sizes are depicted in fig. 5.27. In both cases it is stated that there is a linear function between the cone valve discharge and the opening of the cone valve times its pressure drop. In the case of 230 μm, it is witnessed that there is a small diversion in the sense that the extension of the line does not go through point (0.0) which can be attributed to experimental errors. The equations for the figure 5.27 have been already discussed and are the eq. 5.1 and 5.2, which gave a satisfying fit.

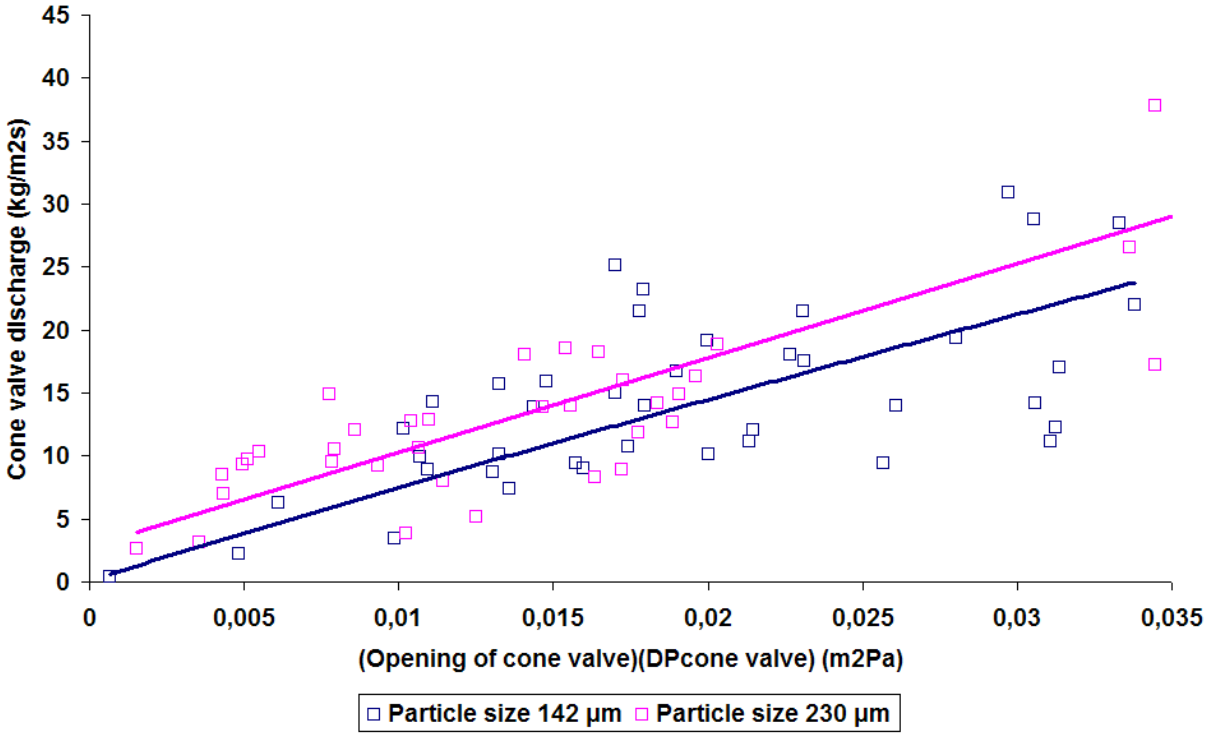

Figure 5.27: Effect of particle size in cone valve discharge

5.17.4 Effect of particle size on the pressure drop profile of the riser

In figure 5.28 different runs from both particle sizes with same total riser pressure drops were chosen so as to discuss the differences in the mass distribution within the riser. Same total riser pressure drop means that in both cases the riser contained the same weight of mass. Therefore the differences in the pressure drop in the different sections of the riser can only be attributed to the particle size.

As it is shown in figure 5.28, the higher particle size of 230 μm accumulates more mass in the lower parts of the riser (0mm-2621mm), while the lower particle size of 142 μm. has more mass distributed in the higher part and the exit of the riser (2621mm-5090mm) for the same overall pressure drop of the riser. This is easily explainable by the fact that higher particle size means heavier particles which results in more inertia for same riser inventory. Hence, the riser has more difficulties in lifting up the same mass. so in the higher particle size case more mass accumulates in the lower parts of the riser. Moreover, in the case of the 142 μm the pressure drop at the exit of the riser (4328mm- 5090mm) is always greater than the pressure drop at the same part for 230 μm particles. As already mentioned the pressure drop at the exit of the riser is linked to the riser circulation rate. As mentioned just above circulation rates are lower for bigger particle size and same velocity. Hence the measured pressure drop at the exit of the riser and the riser entrainment measurements for the two particle sizes are in accordance.

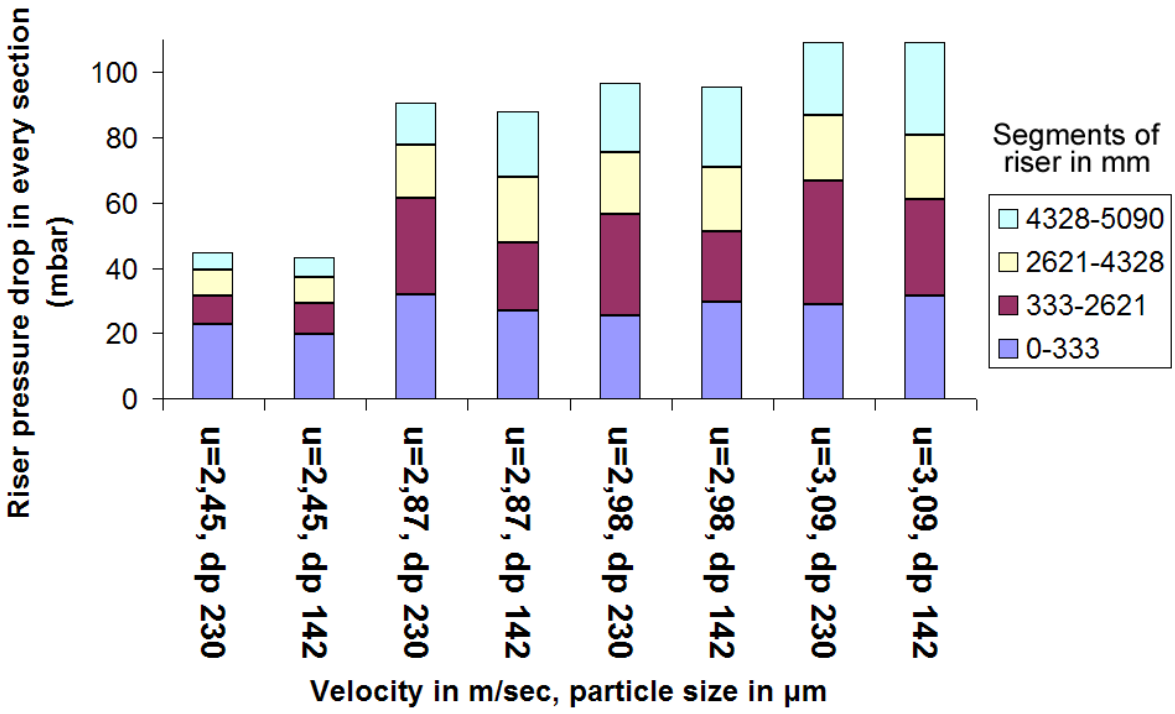

Figure 5.28: Effect of particle size in pressure drop profile of the riser

Table 5.6a: Operating Conditions of the Runs of Figure 6.31 - particle size 230 μm

Run No.	u_o	TSI	P_{BFB}	A_{cone_valve}	LSU bottom air	LSU side air	LSD bottom air	Standpipe status
	m/s	kg	mbar	mm^2	m/s	m/s	m/s	up-down

16	2.43	3	36.29	5.26	0.19	0	0.05	moving-moving
35	2.87	3.65	38.18	5.26	0.29	0	0.08	bubbling-bubbling
39	2.98	3.95	27.95	5.26	0.35	0	0.07	bubbling-moving
40	3.09	3.95	46.38	5.26	0.38	0	0.08	bubbling-bubbling

Table 5.6b: Operating Conditions of the Runs of Figure 6.31 - particle size 142 μm

Run No.	u_o	TSI	P_{BFB}	A_{cone_valve}	LSU bottom air	LSU side air	LSD bottom air	Standpipe status
	m/s	kg	mbar	mm^2	m/s	m/s	m/s	up-down
2	2.45	2.24	0	5.77	0.06	0.03	0.05	moving-moving
35	2.98	3.24	70	5.77	0.09	0	0.05	moving-moving
26	2.87	2.94	50	5.77	0.11	0	0.05	bubbling-moving
42	3.09	3.64	75	5.77	0.10	0	0.04	moving-moving

5.18 Effect of design improvement on the mass distribution

As a part of this research there is a need to discuss the effect of the use of a wider bottom part in the lower part of the riser. Therefore, the original part which had a diameter of 30 mm was replaced by another one with similar geometry, which had a diameter of 40 mm. The effects of the new part are discussed in this chapter. This has been done in an attempt to increase the inventory of the CFB riser.

As it is shown in fig. 6.33, the use of the wider bottom part has a huge effect in the mass distribution of the riser. In fig. 6.33 the mass distribution of certain runs is compared. These runs had the exactly same operating conditions, but different bottom parts.

It is clearly shown that more mass is gathered in the lower part of the riser, as shown in fig. 6.33. This results in increasing the total mass which is gathered in the riser, in each case. This more favourable distribution of the inventory due to the use of the wider bottom part is because of the increased diameter of the bottom part. Due to this a larger portion of the mass of the riser does not contribute to the pressure balance loop for same other conditions. So, lesser mass is needed in the standpipes so as to provide adequate sealing.

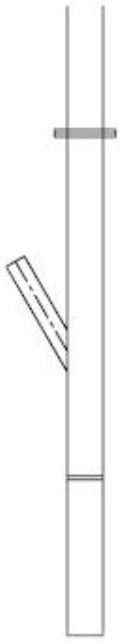

Figure 5.29: Original bottom part. diameter 30mm

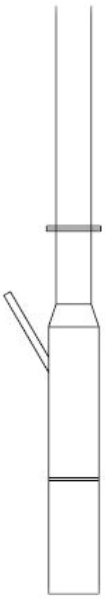

Figure 5.30: Wider bottom part. diameter 40mm. height 500mm

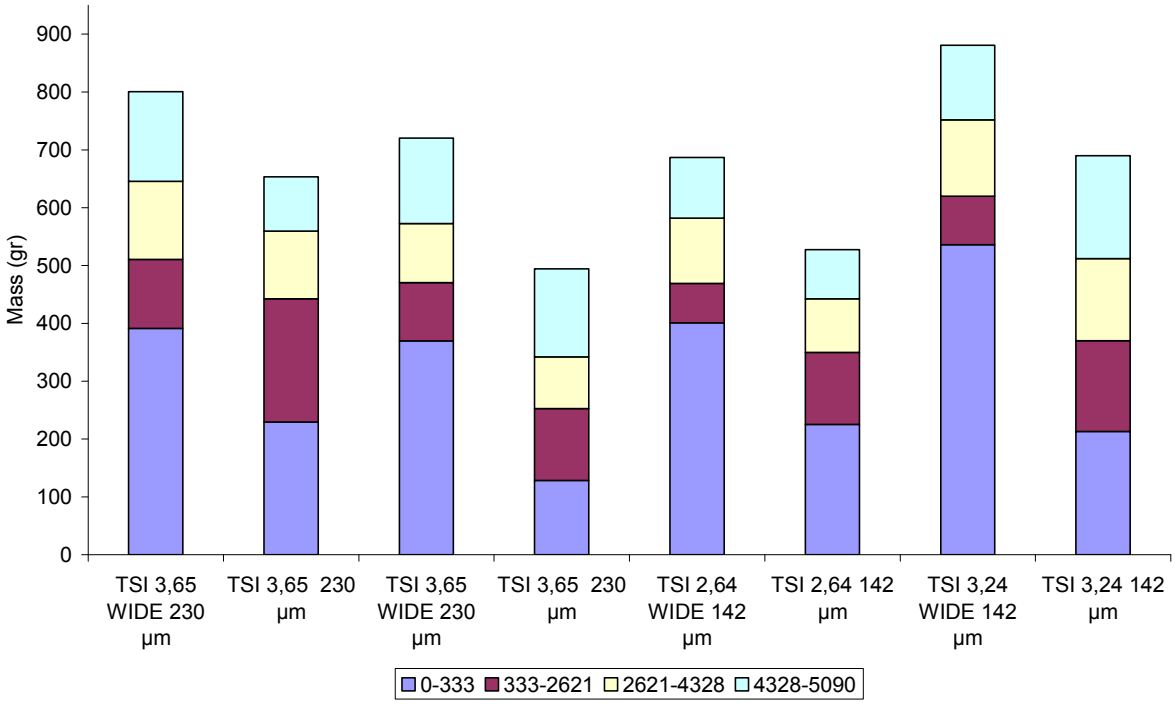

Figure 5.31: Comparison of mass distribution between the wide and the normal bottom

Table 5.7: Operating Conditions of the Runs of Figure 5.31

Run No.	u_o	TSI	P_{BFB}	A_{cone_valve}	LSU bottom air	LSU side air	LSD bottom air	Standpipe status
Particle size (µm)	m/s	kg	mbar	mm^2	m/s	m/s	m/s	up-down
35 (230)	2.87	3.65	38.18	5.26	0.29	0	0.08	bubbling-bubbling
38 (230)	3.20	3.65	39.44	5.26	0.32	0	0.07	bubbling-bubbling
65 (230-wide)	2.87	3.65	40	5.26	0.25	0	0.07	bubbling-bubbling
66 (230-wide)	3.20	3.65	40	5.26	0.28	0	0.07	bubbling-bubbling
16 (142)	2.78	2.64	40	5.77	0.09	0.01	0.01	moving-moving
35 (142)	2.98	3.24	70	5.77	0.09	0	0.05	moving-moving
68 (142-wide)	2.76	2.64	50	5.26	0.02	0.02	0.08	bubbling-moving
71 (142-wide)	2.98	3.24	50	5.26	0.13	0.02	0.05	moving-moving

6. Conclusions

The results of this work showed that high CO_2 capture efficiencies are possible in a Dual Fluidized Bed (DFB) system with CFB carbonator since the required mass loadings and pressure drops were achieved in the reactor and the circulation rate between the beds can be easily controlled with the use of a cone valve in the process range. It was stated that the cone valve discharge is a linear function of the cone valve opening and the pressure drop through the valve. The riser entrainment is mainly a function of velocity. Its high values which were measured justify the use of a cone valve. Increase of loop seal aeration increases the riser pressure drop until the standpipes reach bubbling conditions. The increase of particle size results in reducing the riser entrainment. For same velocity and total pressure drop, more mass is led in the lower parts of the riser. Greater pressure drops through the cyclone and the cyclone duct were measured. Finally, the operating window moves towards higher velocities. The increasing velocity reduces the total pressure drop of the bed, increases riser entrainment and increases the pressure drop through cyclone and loop seal.

This research showed that the increase of certain operational parameters, affect the pressure drop distribution along the riser. More specifically, the increase in upper loop seal aeration and the increase of BFB pressure, both result in increasing the amount of the mass led into the riser. This mass gets distributed along the riser with its higher percentage remaining in the lower parts of the riser.

One major goal for the research program was to find out if there would be any effect in the pressure balance and mass distribution, if a higher particle size was in use. The results of the undergone research showed that there is indeed an effect in three operational figures: the operating window, the pressure drop profile and the riser entrainment. With the higher particle size in use, the operating window moves to the right, meaning that for same TSI's, a higher spectrum of velocities is needed to operate with stability. Furthermore, the same critical velocities appeared concluding that the same limitations apply for higher particle size as well. The pressure drop profile doesn't change drastically, but it is noticed that the heavier particles are more difficult to be lifted up and as a result, more mass accumulates in the lower parts of the installation. Another notable effect is on the riser entrainment. For higher particle size and same operating velocities, the riser entrainment proved to be less, compared to the one with the mean particle size. Finally, no change in the cone valve discharge behaviour was noted.

In order to force the installation to gather more mass in the riser bottom part, a wider bottom part was used to study its results. The experiments showed that there is indeed an increase in the mass accumulated in that part and hence that can be considered a design improvement.

7. Further Work

After having completed the present series of experiments, there were a few aspects that needed further research in order to comprehend more thoroughly the hydrodynamics of the fluidized beds. In this field, the system behaviour with Geldart A particle size should be analysed. Furthermore, in order to specify exactly the direction of the flow within the system, gas leakage measurements should take place, between the system compartments. In the field of design improvements, the system behaviour should be tested with altered positions of inlet of loop seals, with a different cyclone (so as to reduce the outlet pressure drop) and further testing with the wider bottom should take place. Furthermore, an attrition model of CaO should be created if the results of all the particle sizes in use should be combined.

Bibliography

[1] Lyngfelt. A.. Thunman. H.: Construction and 100h of operational experience of a 10-kW chemical looping combustor. Carbon dioxide Capture for Storage in Deep Geological Formations—Results from the CO2 capture project (2005) 1. p.625- 645

[2] Lyngfelt. A. et al. The GRACE project. Development of oxygen carrier particles for chemical-looping combustion. Development of a 10 KW chemical-looping combustor. In the 7th International Conference on Greenhouse Gases. Vancouver. 2004

[3] Berguerand N.. Lyngfelt A.: Design and operation of a 10kWth chemical-looping combustor for soli fuels - Testing with South African coal. Fuel 87 (2008). p. 2713- 2716

[4] Berguerand N.. Lyngfelt A.: The use of petroleum coke as fuel in a 10KWth chemical-looping combustor. Int. J. Greenhouse Gas Control 2 (2008). p. 169- 179

[5] Lyngfelt A.. Johansson M.. Mattison T.: Chemical looping combustion- status of the development. In the CFB9 conference. Hamburg. 2008

[6] Johansson E.. Mattison T.. Lyngfelt A.. Thunman H.: Combustion of syngas and natural gas in a 300 W chemical looping combustor. Chem. Eng. Res. Des. 84 (2006) A9. p. 819-827

[7] Kolbitsch P.. Bolhàr-Nordenkampf J.. Pröll T.. Hofbauer H.: Design of a chemical looping combustor using a Dual Circulating Fluidized Bed (DCFB) system. In the CFB9 conference. Hamburg. 2008

[8] Pröll T.. Rupanovits K.. Kolbitsch P.. Bolhàr-Nordenkampf J.. Hofbauer H.: Cold flow model study on a Dual Circulating Fluidized Bed (DCFB) system for chemical looping processes. In the CFB9 conference. Hamburg. 2008

[9] Kronberger B.. Lyngfelt A.. Adanez J.. Hofbauer H.: Circulating Fluidized Bed Reactor Systems for chemical-looping combustion. In the 19th FBC conference. Vienna. 2006

[10] Kronberger B.. Lyngfelt A.. Löffler .. Hofbauer H.: Design of a bench-scale combustion system with CO2 separation- chemical-looping combustion. Ind. Eng. Chem. Res. 44 (2005). p. 546- 556

[11] Johansson E.. Lyngfelt A.. Mattison T.. Johnsson F.: Gas leakage measurements in a cold model of an interconnected fluidized bed for chemical-looping combustion. Powder Technology 134 (2003) p.210- 217

[12] Hofbauer H.: Scale up of fluidized bed gasifiers from laboratory scale to commercial plants: Steam gasification of solid biomass in a Dual Fluidized Bed system. In the 19th FBC conference. Vienna. 2006

[13] Pfeifer C.. Soukup G.. Kreuzeder A.. Cuadrat A.: In- situ CO2- capture in a dual fluidized bed biomass steam gasifier: Bed material and fuel variation. In the CFB9 conference. Hamburg. 2008

[14] Marquard- Moellenstedt T.. Sichler P.. Specht M.. Michel M.. Berger R.. Hein K.. Höftberger E.. Rauch R.. Hofbauer H.: New approach for biomass gasification to hydrogen. In 2nd world biomass conference. Rome. 2004

[15] Weimer T.. Berger R.. Hawthorne C.. Abanades J.C.: Lime enhanced gasification of solid fuels: Examination of a process from simultaneous hydrogrn production and CO2 capture. Fuel 87 (2008). p.1678- 1686

[16] Bolhàr-Nordenkampf M.. Bosch K.. Rauch R.. Kaiser S.. Tremmel H.. Aichering C.. Hofbauer H.: Scale-up of a 100kWth pilot FICFB-gasifier to a 8 MWth plant in Güssing (Austria). In the 1st Ukranian conference on biomass and energy. Kiew. 2002

[17] Pfeifer C.. Kreuzeder A.. Hofbauer H.: Fluid- dynamic investigations in a cold model for a dual fluidized bed biomass steam gasifier: solid circulation and fuel residence time. In the CFB9 conference. Hamburg. 2008

[18] Kotik J.. Pröll T.. Hofbauer H.: Advanced concept for a „next generation" biomass gasification CHP-plant- Basic engineering and cold flow model results. In the CFB9 conference. Hamburg. 2008

[19] Löffler G.. Kaiser S.. Bosch K.. Hofbauer H.: Hydrodynamics of a dual fluidized-bed gasifier- Part I: Simulation of a riser with injection of a gas diffuser. Chem. Eng. Sci. 58 (2003). p. 4197- 4213

[20] Kaiser S.. Löffler G.. Bosch K.. Hofbauer H.: Hydrodynamics of a dual fluidized-bed gasifier- Part II: Simulation of solid circulation rate. pressure loop and stability. Chem. Eng. Sci. 58 (2003). p. 4215- 4223

[21] Boukis I.Ph.. Grammelis P.. Bezergianni S.. Bridgwater A. V.: CFB air-blown flash pyrolysis. Part I: Engineering design and cold model performance. Fuel 86 (2007). p. 1372- 1386

[22] Haslinger W.. Kronberger B.. Hofbauer H.: Fluid dynamics of a novel CFB reactor design with converging section. In the 19th FBC conference. Vienna. 2006

[23] Kobyłecki R.. Klajny M.. Thamm J.. Zyła J.. Krupka S.. Zabłocki W.. Bis Z.: Experiences on erosion protection in CFB furnaces. 4th international workshop "operating experience with fluidized bed systems"

[24] Mirek P.. Nowak W.: Operating conditions of arrowhead nozzles and the windox in a 235 MWe boiler. In the 19th FBC conference. Vienna. 2006

[25] Qi X.-B.. Zhu H.-Y.. Zhu J.: Distinctions between circulating- turbulent fluidized beds. turbulent fluidized beds and high- density circulating fluidized beds. In the CFB9 conference. Hamburg. 2008

[26] Issangya A.S.. Bai D.. Bi H.T.. Lim K.S.. Zhu J.. Grace J.R.: Suspensions densities in a high- density circulating fluidized bed riser. Chem. Eng. Sci. 54 (1999). o. 5451- 5460

[27] Abanades J.C.. Anthony E.J.. Wang J.. Oakey J.E.: Fluidized Bed Combustion Systems Integrating CO2 Capture with CaOEnviron. Sci. Technol 39 (2005). pp. 2861- 2866

[28] Abanades J.C.. Grasa G.. Alonso M.. Rodriguez N.. Anthony E.J.. Romeo L.M.: Cost Structure of a Postcombustion CO2 Capture System Using CaOEnviron. Sci. Technol. 41 (2007). pp. 5523-5527

[29] Shimizu T.. Hirama T.. Hosoda T.. Gitano H.. Inagaki K.. Tejima M.: A twin fluid-bed reactor for removal of CO2 from combustion processes. Transactions of IChemE 77 (1999) part A. p. 62- 66

[30] Alvarez D.. Abanades J.C.: Pore-size and shape effects on the recarbonation performance of calcium oxide submitted to repeated calcination/ recarbonation cycles Energy and fuels 19 (2005). p. 270- 278

[31] Grassa G.. Abanades J.C.: CO2 capture capacity of CaO in long series of carbonation/ calcination cycles. Ind. Eng. Chem. Res. 45 (2006). p.8846- 8851

[32] Abanades. J.C.. Anthony. E.J.. Lu. D.Y.. Salvador. C.. Alvarez. D.: Capture of CO2 in a FBC of CaO. AIChE J. 50. (2004) pp. 1614-1622

[33] Lu D. Y.. Hughes R. W.. Anthony E.J.: Ca- based sorbent looping combustion for CO2 capture in pilot-scale dual fluidized beds. Fuel Processing Technology. In Press. Corrected Proof (2008)

[34] C. Hawthorne. A. Charitos. C.A Perez- Pulido. Z. Bing. G.Scheffknecht: Design of a dual fluidized bed system for the post- combustion removal of CO2 using CaO. Part I: carbonator reactor model. In the CFB9 conference. Hamburg. 2008

[35] Bhatia. S. K.. Perlmutter. D.: Effect of the prduct layer on the kinetics oft he CO2 lime reaction AIChe J. 29 (1983). pp. 79- 86

[36] Abanades J. C.: The maximum capture efficiency of CO2 using a carbonation/calcination cycle of CaO/CaCO3Chem. Eng. J. (2002). pp. 303-306

[37] Kunii D.. Levenspiel O.: Fluidized reactor models. 1. For bubbling beds of fine. intermediate. and large particles. 2. For the lean phase: freeboard and fast fluidizationInd. Eng. Chem. Res. (1990). pp. 1234-1239

[38] Pugsley T.S.. Berruti F.: A predictive hydrodynamic model for circulating fluidized bed risersPowder Technology 89 (1996). pp. 57-69

[39] A. Charitos. C. Hawthorne. A. Bidwe. L. He. G.Scheffknecht: Design of a dual fluidized bed system for the post- combustion removal of CO2 using CaO. Part II: Scaled cold model investigation. In the CFB9 conference. Hamburg. 2008

[40] Bidwe. A.: Diplome Thesis. IVD. Univarsitat Stuttgart: s.n.. 2007.

[41] Hawthrone C.. Berger R.: Hydrogen from European low rank coal: Reducing CO2 emission. Osaka. Japan. : s.n.. 2004 . Proceedings of the Twenty First Annual Ptisburgh Coal Conference in.

[42] Smyth F.H.. Adams L.H.: The system Calcium Oxide-Carbon Dioxide. Journal of American Chemical Society-Vol 45. 1923. pp. 1167-1184.

[43] Baker E.H.: The Calcium Oxide-Carbon Dioxide System in the Pressure. Journal of American Chemical Society Vol-70. 1962. p. 464.

[44] Abanades J.C.: The maximum Capture efficiency of CO2 capture using a carbonation / calcination cycle of CaO/CaCO3. Chemical Engineering Journal Vol 90. 2002. pp. 303-306.

[45] Basu P.. Cheng L.: An analysis of loop seal operations in a circulating fluidized bed. Chemical Engineering Research and Desing. October 2000 . Vol 78. pp. 991-998.

[46] Nikolopolous. A.: Diplome Thesis . IVD. Universität Stuttgart : s.n.. 2006.

[47] Knowlton. T.M.: Standpipe and Return Systems. [book auth.] Grace. Avidan Knowlton. Circulating Fluidized beds. s.l. : Chapmann & Hall. 1997. p. Chapter 7.

[48] Kim S.W.. Kim S.D.. Lee D.H.: Pressure balance model for Circulating fluidized beds witha loop seal. Industrial Engineering chemistry. 2002. 41. 4949-4956.

[49] Matsen J.M.: Scaling of Fluidised bed processes. Powder Technology. Vol 88 1996. pp. 237-244.

[50] Glicksman L.R.: Scaling Relationships for Fluidized bed . Chemical Engineering Science. Vol 39 1984. pp. 1373-1379.

[51] Glicksmann L.R.: Simplified Scaling Relationships for Fluidized bed. Powder Technology. Vol 77 1993. pp. 177-199.

[52] —. Scaling Relationships for Fluidized Bed. Chemical Engineering Science. pp. 1419-1421.

[53] Glicksmann L.R.. Hyre M.R.. Farell P.A.: Dynamic Similarity of Fluidization. International Journal of Multiphase Flow .

[54] Chang H.. Louge M.: Fluid dynamic similarity of circulating fluidized beds. Powder Technology. June Vol 70. 1992. pp. 259-270.

[55] Kehlenbeck R.: Dissertation: Scaling of 500 kw Pilot plant with integrated Circulating fluidized bed for the generation of hydrogen rich gas from biomass steam gasification and fluid dynamic investigations of a cold model. Technichen Universität Wien Fakultät für Machinenbau : s.n.. 2000.

[56] Ling H.. Zenteno L.: Cold model experiment results with Sand (Internal Report). IVD Universität Stuttgart : s.n.. 2007.

[57] Perry´s: Perry´s Chemical Engineering Handbook.

[58] O'Dea D. P.. Rudolph V. and Chong Y. O.: Gas—solids flow through the bottom restriction of an inclined standpipe . Powder Technology Volume 62. September 1990. pp. 291-297 .

ANNEX

1. Table 1

Run No.	u_o	TSI	P_{BFB}	A_{cone_valve}	LSU bottom air	LSU side air	LSD bottom air	Standpipe status
	m/sec	kg	mbar	mm^2	m/s	m/s	m/s	up-down
31	2.76	3.65	31.57	5.26	0.22	0.00	0.05	mov-mov
32	2.87	3.65	38.80	5.26	0.23	0.00	0.05	mov-mov
33	2.87	3.65	36.51	5.26	0.26	0.00	0.08	mov-bub
34	2.87	3.65	36.04	5.26	0.27	0.00	0.08	mov-bub
35	2.87	3.65	38.19	5.26	0.29	0.00	0.08	bub-bub
36	2.98	3.65	39.93	5.26	0.31	0.00	0.09	bub-bub
37	3.09	3.65	38.51	5.26	0.31	0.00	0.07	bub-bub
38	3.20	3.65	39.44	5.26	0.32	0.00	0.07	bub-bub
39	2.98	3.95	27.95	5.26	0.35	0.00	0.07	bub-mov
40	3.09	3.95	46.39	5.26	0.38	0.00	0.08	bub-bub
41	3.20	3.95	28.74	5.26	0.39	0.00	0.08	bub-bub
42	3.32	3.95	27.95	5.26	0.41	0.00	0.08	bub-bub
43	3.43	3.95	28.95	5.26	0.44	0.00	0.08	bub-bub
44	3.54	3.95	29.41	5.26	0.46	0.00	0.09	bub-bub
45	3.54	3.95	30.19	5.26	0.46	0.09	0.09	bub-bub
46	2.54	2.24	38.67	5.26	0.15	0.02	0.06	bub-bub
47	2.65	2.24	38.64	5.26	0.21	0.02	0.07	bub-bub
48	2.76	2.24	36.17	5.26	0.23	0.02	0.07	bub-bub
49	2.87	2.24	35.93	5.26	0.24	0.02	0.07	bub-bub
50	2.98	2.24	35.03	5.26	0.26	0.02	0.08	bub-bub
51	2.76	2.64	39.13	5.26	0.31	0.00	0.07	bub-bub
52	2.87	2.64	39.86	5.26	0.33	0.00	0.08	bub-bub
53	2.98	2.64	34.70	5.26	0.35	0.00	0.08	bub-bub
54	3.09	2.64	36.08	5.26	0.36	0.00	0.09	bub-bub
55	3.20	2.64	35.91	5.26	0.36	0.00	0.09	bub-bub
56	2.87	3	40.00	5.26	0.14	0.00	0.07	bub-bub
57	2.98	3	40.00	5.26	0.17	0.00	0.08	bub-bub
58	3.09	3	35.00	5.26	0.19	0.00	0.08	bub-bub
59	3.20	3	35.00	5.26	0.27	0.00	0.08	bub-bub
60	3.32	3	35.00	5.26	0.29	0.00	0.09	bub-bub

2. Figure 1

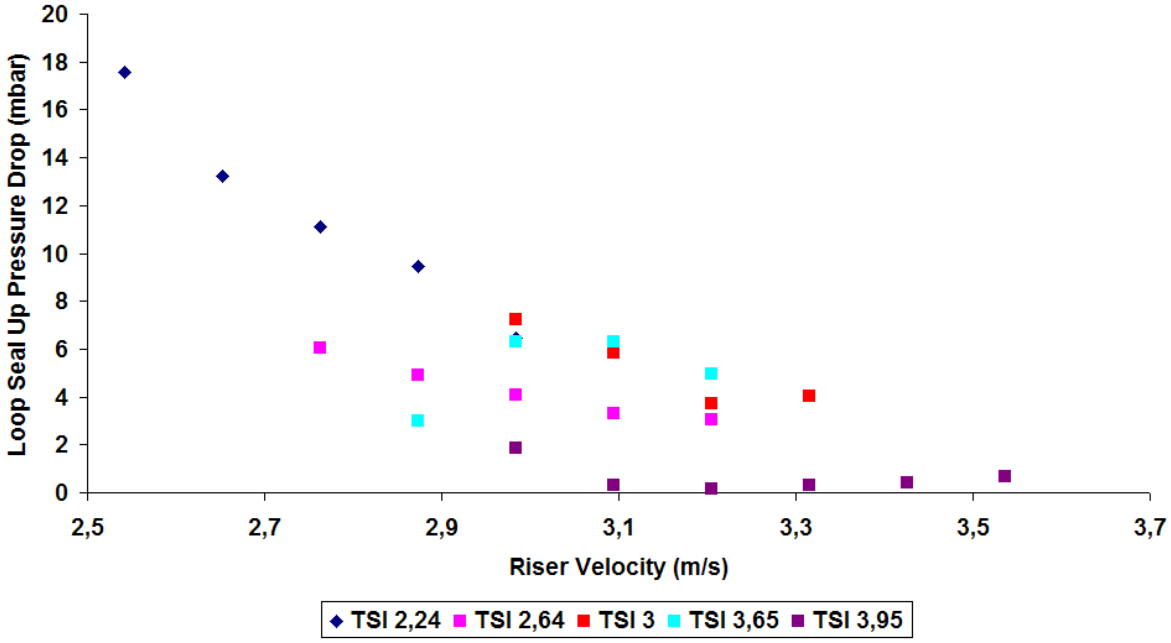

Figure 1: Upper loop seal pressure drop versus riser velocity for particle size of 230 µm

3. Figure 2

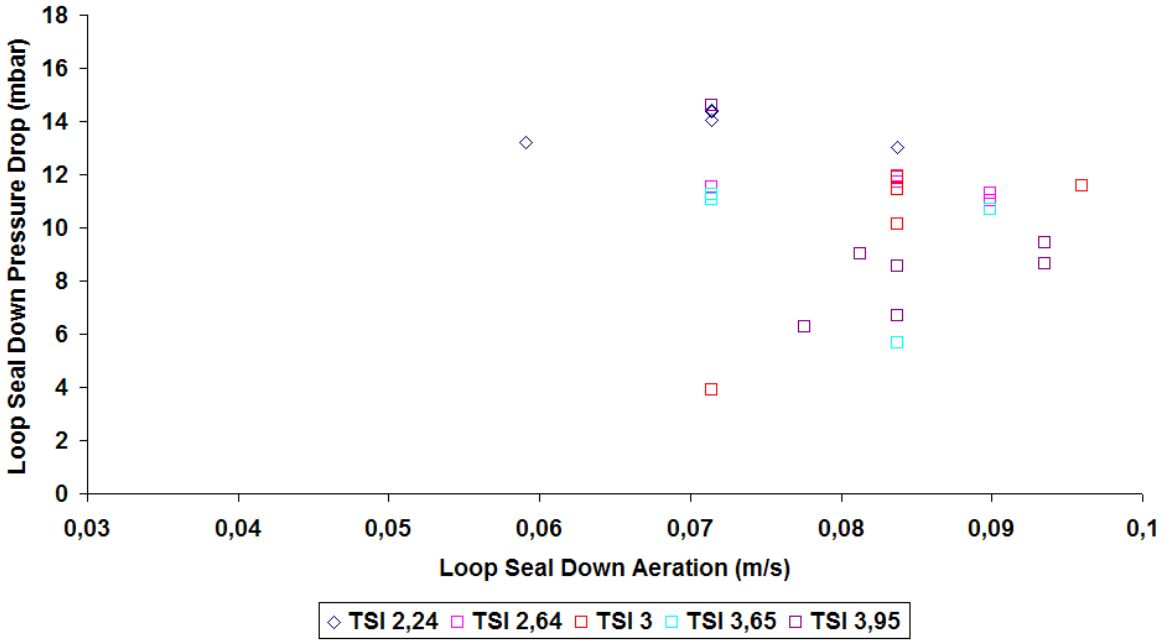

Figure 2: Lower loop seal pressure drop versus lower loop seal aeration for particle size of 230 µm

4. Figure 3

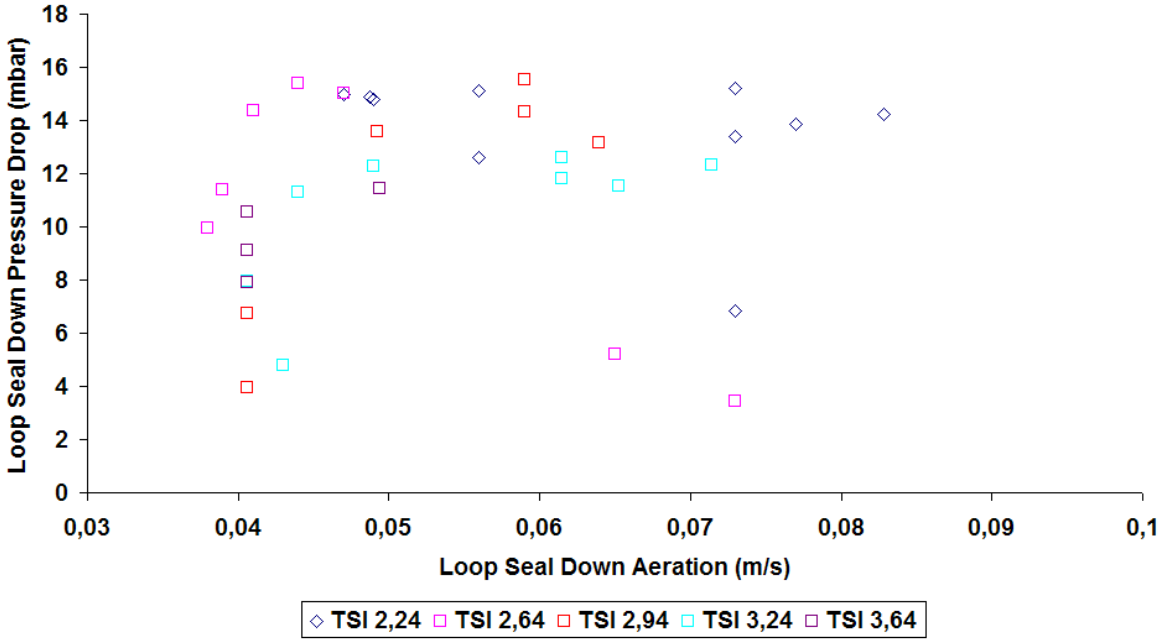

Figure 3: Lower loop seal pressure drop versus lower loop seal aeration for particle size of 142 µm

5. Figure 4

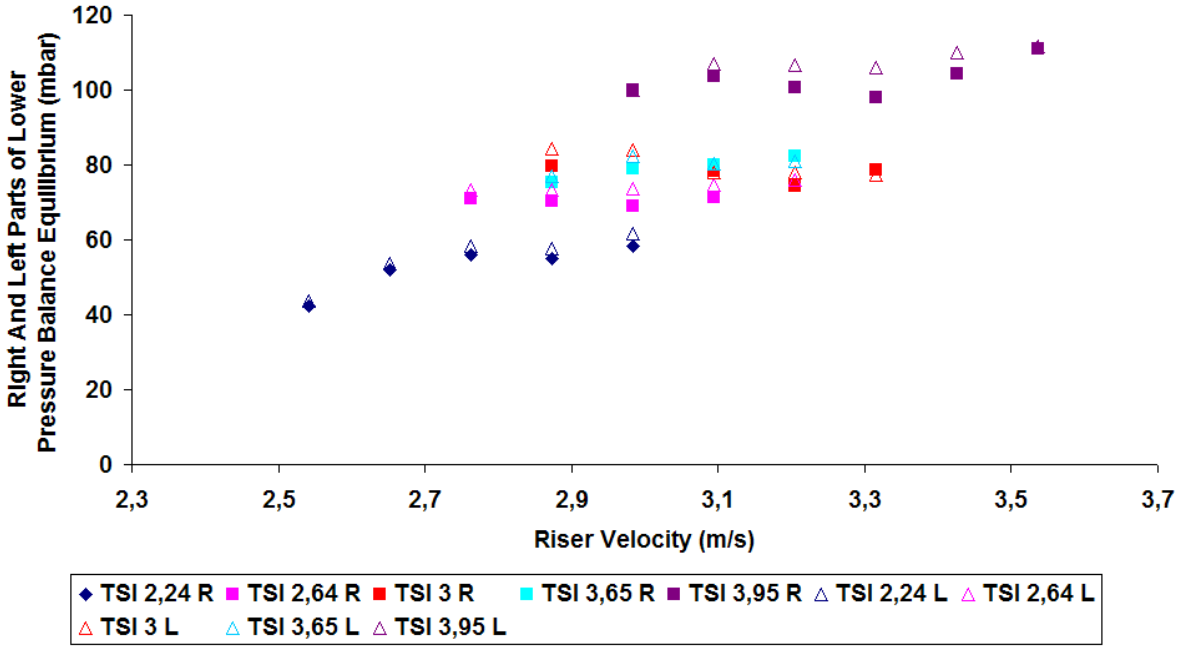

Figure 4: Lower pressure balance equilibrium for a particle size of 230 µm

6. Figure 5

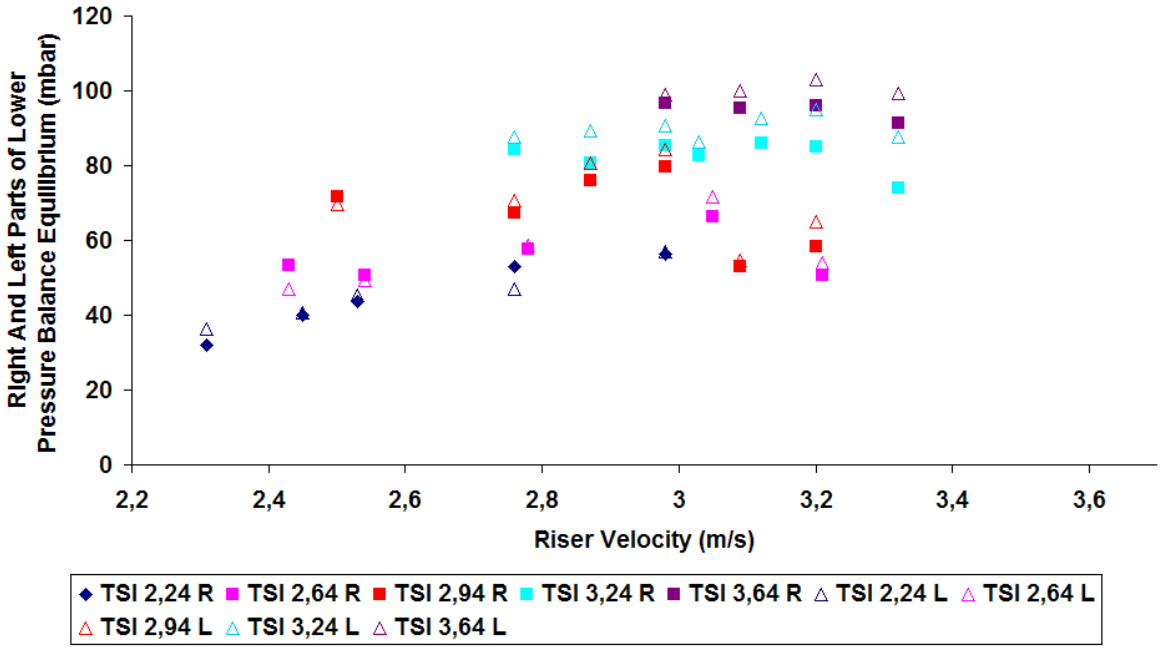

Figure 6: Upper pressure balance equilibrium for a particle size of 142 µm

7. Table 2: Upper balance loop

	Left part of upper pressure balance equation	Right part of upper pressure balance equation			
	LHS	RHS			
Run No.	Loop Seal Up Standpipe	Riser Top	Cyclone	Loop Seal Up	LHS-RHS
	(mbar)	(mbar)	(mbar)	(mbar)	
35	72.74	62.79	6.79	3.00	0.15
36	76.41	58.59	9.85	6.30	1.66
37	73.48	56.02	12.72	6.28	1.54
38	72.44	54.84	16.43	4.97	3.80
39	89.31	75.66	9.85	1.85	1.95
40	93.56	84.79	12.72	0.28	4.24
41	91.93	77.42	16.43	0.17	2.09
42	89.60	68.38	21.22	0.31	0.31
43	92.47	68.03	27.41	0.40	3.37
44	94.44	66.28	35.40	0.67	-7.91
45	96.94	66.77	35.40	0.52	5.75
46	47.52	25.88	3.12	17.54	0.98

47	51.51	33.69	4.14	13.20	0.48
48	53.47	34.48	7.13	11.12	0.73
49	50.84	32.46	8.20	9.43	0.74
50	53.14	35.90	9.36	6.47	1.39
51	66.10	52.18	7.45	6.047	0.42
52	63.73	48.95	9.37	4.90	0.51
53	62.48	47.29	9.85	4.09	1.24
54	63.22	47.42	12.72	3.32	0.25
55	63.65	46.49	16.43	3.05	-2.33
56	73.64	68.89	6.84	0.77	2.86
57	76.71	59.18	9.85	7.24	0.43
58	71.83	53.73	12.72	5.85	0.47
59	65.36	46.35	16.43	3.70	1.11
60	67.16	45.98	21.22	4.04	4.08

8. Table 3: Lower balance loop

	Left part of lower pressure balance equation	**Right part of lower pressure balance equation**				
	LHS		**RHS**			
Run No.	**BFB**	**Loop Seal Down Standpipe**	**Riser Top**	**Cyclone**	**Loop Seal Down**	**LHS-RHS**
	(mbar)	**(mbar)**	**(mbar)**	**(mbar)**	**(mbar)**	
35	38.18	38.68	62.79	6.78	5.69	1.60
36	39.92	42.41	58.59	9.85	10.69	3.20
37	38.51	41.70	56.02	12.72	11.26	0.21
38	39.44	41.40	54.84	16.43	11.07	1.50
39	27.95	72.16	75.66	9.85	14.60	0
40	46.38	60.76	84.79	12.72	6.27	3.35
41	28.73	77.81	77.42	16.43	6.71	5.98
42	27.95	78.07	68.38	21.22	8.54	7.87
43	28.95	80.90	68.03	27.40	9.03	5.38
44	29.40	82.15	66.28	35.39	9.41	0.46
45	30.18	83.58	66.77	35.39	8.66	2.93
46	38.66	4.98	25.88	3.11	13.23	1.41
47	38.64	14.86	33.69	4.13	14.05	1.62
48	36.16	22.16	34.48	7.12	14.39	2.31
49	35.92	21.77	32.46	8.19	14.39	2.65
50	35.02	26.67	35.90	9.36	13.02	3.40
51	39.13	34.31	52.18	7.44	11.52	2.29
52	39.86	33.33	48.95	9.37	11.94	2.92
53	34.70	38.82	47.29	9.85	11.70	4.67
54	36.08	38.63	47.42	12.72	11.03	3.53
55	35.90	40.06	46.49	16.43	11.30	1.73
56	36.69	44.37	68.89	6.84	3.90	1.42

57	37.95	43.88	59.18	9.85	10.12	2.67
58	37.42	43.13	53.73	12.72	11.88	2.20
59	34.23	43.04	46.35	16.43	11.43	3.06
60	36.75	42.23	45.98	21.22	11.59	0.19

9. Explanation

Loop seal up (f) - Riser loop (b): As observed values LHS- RHS values for this loop in most of the cases are near to zero. Thus above equations are validated by the experimental results.
Loop seal down (l)- Riser loop (b): As observed for this loop some times the values are close to zero as well. case that actually backs up our original statement concerning the closing of the loop seal balance.

10. Figure 6

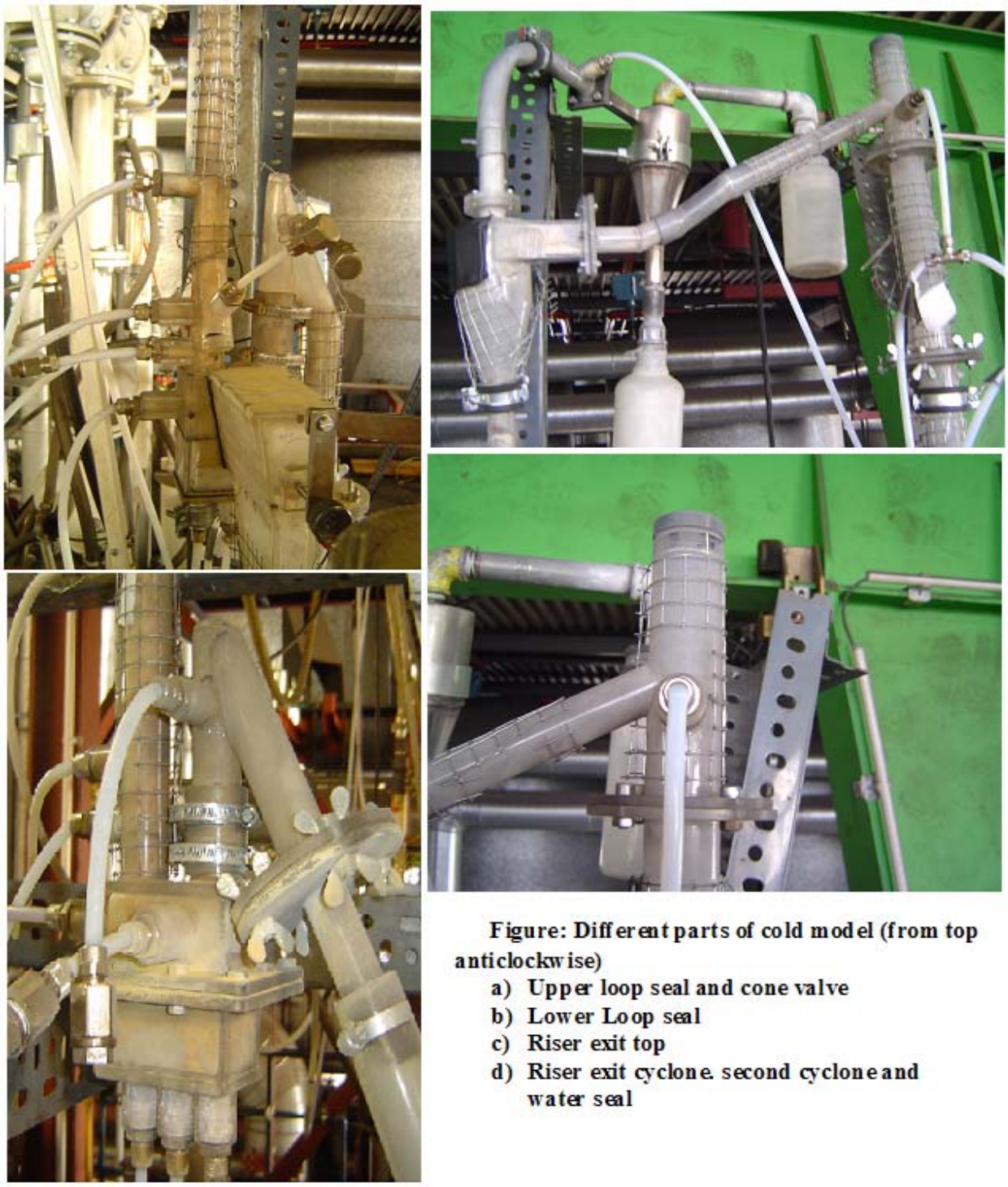

Figure: Different parts of cold model (from top anticlockwise)

a) **Upper loop seal and cone valve**
b) **Lower Loop seal**
c) **Riser exit top**
d) **Riser exit cyclone. second cyclone and water seal**

11. Figure 7

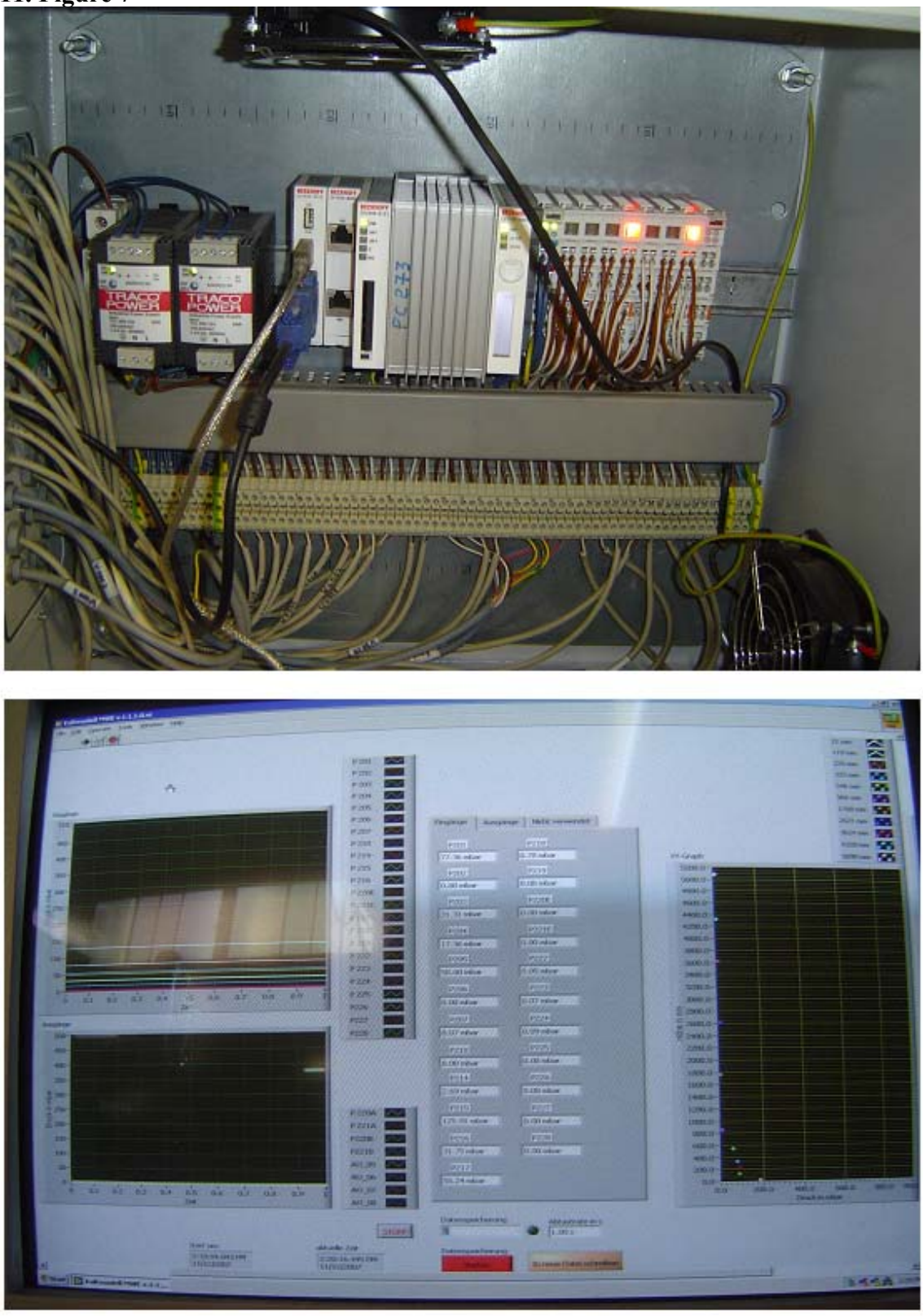

Figure: a) Hardware for pressure transducer measurement and recording
b) Lab view measurement screen